JANUS PARTICLES DESIGNED FOR CANCER IMMUNOTHERAPY

A Dissertation
Presented to
The Academic Faculty

by

Elizabeth Anne Campbell

In Partial Fulfillment
of the Requirements for the Degree
Doctor of Philosophy in the
Wallace H. Coulter Department of Biomedical Engineering

Georgia Institute of Technology
Emory University
August 2018

COPYRIGHT © 2018 BY ELIZABETH A. CAMPBELL

JANUS PARTICLES DESIGNED FOR CANCER IMMUNOTHERAPY

Approved by:

Dr. Todd Sulchek, Advisor
Woodruff School of Mechanical Engineering
Georgia Institute of Technology

Dr. Krishnendu Roy
Wallace H. Coulter Department of Biomedical Engineering
Georgia Institute of Technology

Dr. Edward Botchwey
Wallace H. Coulter Department of Biomedical Engineering
Georgia Institute of Technology

Dr. Edmund Waller
School of Medicine
Emory University

Dr. Gabriel Kwong
Wallace H. Coulter Department of Biomedical Engineering
Georgia Institute of Technology

Date Approved: [May 11, 2018]

To my family.

I have known no end to your support or love.

Thank you.

ACKNOWLEDGMENTS

First, I would like to thank Dr. Todd Sulchek. He took me into his lab when I was a second year student and handed me my thesis project idea, which has taken all sorts of twists and turns through pitfalls and occasional heights. Dr. Sulchek has always supported and challenged me through it all. Secondly, I would like to thank my committee members. Dr. Ned Waller and his lab was an invaluable resource for providing the clinical point of view on my project and collecting blood for my experiments. Dr. Ed Botchwey pushed me to think bigger about my project, and how we might complicate conditions to discover more interesting results. Dr. Gabe Kwong encouraged me to push boundaries and be creative. I would finally like to thank Dr. Krish Roy for his genuine interest in my project – he never failed to ask how things were going when we ran into each around campus. I am so grateful that all my committee members invested their valuable time and expertise in helping me develop as a researcher.

I would like to thank the many Georgia Tech technical and administrative support staff who has helped me out numerous times over the course of completing my PhD. I would especially like to thank Andrew Shaw for his invaluable microscopy expertise and also genuine enthusiasm and interest in me and my project. I would not have been able to accomplish this work without him. I would also like to thank Nadia Boguslavsky and Sommer Durham for the work they did and do in running the flow cytometry core. I would also like to thank Shannon Sullivan and Sally Gerrish who, when they were here, gave great advice and were advocates for the graduate students in the BME department.

I would like to extend a heartfelt thank you to my labmates. We've spent at least 40 hours a week together for years and I can never repay for your support and enthusiasm. I will never forget coming into lab on snow days, expecting to be the only person there, and slowly seeing the whole lab trickle in and out. You have all given invaluable feedback on presentations and never hesitated to pitch in for lab chores when necessary. The Sulchek lab has such a wonderful lab environment and I cannot thank my labmates enough for nourishing that atmosphere. I want to thank especially the Janus/Cerberus particle crew, Kathryn, Mike, and Katily. They have helped me refine conjugation protocols, given tips on getting the best images, and commiserated with me when functionalization schemes were inexplicably not working. Beyond labwork, they have been wonderful work-friends, always up for a chat or a drink after work. I'd also like to say a sincere thank you to Tom and Nick. They were always enthusiastic participants when I needed to bounce ideas off about new projects or thesis directions and were always willing to provide a sanity check for me when it came to new experiments. I would first like to thank Katie for always having a positive attitude; she never failed to ask how things were going and for the past couple of years has handled the thankless task of ordering materials with incredible patience and proficiency. Secondly, I would like to thank Anna for taking on the burden of undergraduate lab orientation. Her firm hand with undergraduates is complemented by her wit – I'll miss her puns and definitely her "pot" brownies (it was stainless steel). She also lent me some of her isolated primary T cells which have been invaluable in completing my thesis research. Although Aaron's and my research only seems to overlap in the sense that our experiments take place in the same physical space, Aaron's unfailingly generosity has benefited me in numerous ways:

extensively critiquing of presentations and PowerPoint slides, offering to look over grants or papers, and 3D printing two dog bone cookie cutters for me once. I would like to thank our newest lab member Alan for initiating lots of lab bonding through coffee corner and hot pot, and generally being a very friendly and easygoing labmate who is always willing to pitch in. Thank you also to Dr. Muhymin Islam, Dr. Bushra Tasadduq, Dan Potter, Shawn Newlan, Dr. Patricia Hernandez, Dr. Billy Wang, Dr. Kipp Schoenwald, Dr. Wenwei Xu, and Dr. Ahmad Haider for being great labmates.

In addition to having a great lab, my friends outside of lab, especially Cheryl, Candice, Claire, Giuli, and Efrain, have been the greatest support system I could ever conceive of and I truly wouldn't be here without them. I met Candice Hovell during recruitment and neither one of us thought we'd ever be friends, let alone great friends and roommates for two years. Claire always provided an aesthetic to aspire to and Efrain was always willing to talk and never turned down a boozy brunch invitation. Giuli has been so supportive, especially these past couple months as we were both finishing our theses. Finally, Cheryl San Emeterio (née Lau), whom I met on my first day of orientation, has completely changed my life for the better.

Next, I would like to thank Marc. He has offered me unending support and encouragement during our entire relationship but especially during these past few months of finishing my thesis, sometimes actually feeding and clothing me. Every day I am reminded how lucky I am to have found him.

Finally, I would like to thank my family with all my heart. My parents raised me to value hard work and pursue my passions and were always unflinchingly supportive

and loving through it all. My sisters were, and have always been, the people I can always turn to for advice, to vent, and to cry on a shoulder. I absolutely do not deserve them – but I'll keep them nonetheless. I am thankful to the core that they are my family.

TABLE OF CONTENTS

LIST OF TABLES

LIST OF FIGURES

LIST OF SYMBOLS AND ABBREVIATIONS

CTLA-4	Cytotoxic T lymphocyte associated protein 4
Fc	Fragment crystallizable
PD-L1	Programmed death ligand 1
APC	Antigen presenting cell
PFS	Progression-free survival
OS	Overall survival
NK	Natural killer
NKT	Natural killer T cell
DC	Dendritic cell
MHC	Major histocompatibility complex
CD	Cluster differentiation
TCR	T cell receptor
TNF	Tumor necrosis factor
INF-γ	Interferon-gamma
VAT	Visceral adipose tissue
TAM	Tumor-associated macrophages
Treg	Regulatory T cells
TNFR2	TNF receptor 2
CCL	CC chemokine (family) ligand
CXC	CXC chemokine (family)
LFA-1	Lymphocyte function-associated antigen-1
FR	Folate receptor

ELISA	Enzyme-linked immunosorbent assay
TAA	Tumor-associated antigens
MUC-1	Mucin-1
MSLN	Mesothelin
VEGF	Vascular endothelial growth factor
IL	Interleukin
TGF-β	Transforming growth factor beta
CAF	Cancer-associated fibroblasts
IDO	Indoleamine 2,3-dioxygenase 1
Th	CD4+ T cell, helper T cell
FDA	Food and Drug Administration
aAPC	Artificial antigen presenting cells
ICAM-1	Intercellular adhesion molecule 1
AFM	Atomic force microscopy
T-BsAb	T cell engaging bispecific antibodies
MDSC	Myeloid-derived suppressor cells

SUMMARY

Ovarian cancer is the most lethal gynecologic cancer due to its typical late stage diagnosis, after metastasis has begun. The lack of a treatment without harmful side effects and ultimately, a cure, is an increasingly significant clinical burden. Although immune cells are heavily present within ovarian cancer tumors and the surrounding microenvironment, late stage diagnoses result in less than a 25% patient 5-year survival rate. Current standard of care includes chemotherapy, radiation, and surgery but exhibits limited success and has complications due to side effects. Moreover, although over 80% of ovarian cancer patients respond favorably to treatment initially, the majority of these patients will ultimately experience cancer recurrence, which can eventually lead to chemotherapy-resistance. Consequently, there is an unmet need for innovative treatment strategies – immunotherapy is of particular interest as there is an increased understanding about the frequently immunosuppressive nature of the tumor microenvironment; advances in immunotherapeutic strategies have even yielded curative results in some patients.

Tumor microenvironments are made up of cancer cells, resident healthy tissue, supporting stromal cells, and immune cells. Cues from these cells interplay in a highly coordinated fashion to drive pro-cancer or anti-cancer immune responses and thus govern the tumor microenvironment and determines whether cancer cells proliferate or die. Notably, resident tumor cells frequently express or secrete immune-inhibitory signals that work to suppress immune cell recognition and function. Thus, understanding how to activate potential effector cells against cancerous cells within the immunosuppressive

tumor microenvironment is critical to harnessing their cytotoxic function in directing cancer cell death. To address this challenge, we developed a novel immunomodulatory particle platform that leverages the potential of resident CD8+ T cells to better elicit tumor-specific cytotoxicity.

The particles simultaneously display tumor targeting molecules and anti-CD3 molecules to activate resident immune cells. To understand the immune activation effects, we varied particle size and anti-CD3 antibody density to identify 300 nm particles with a surface conjugation density of approximately 41% lead to the greatest amount of granzyme B release from Jurkat cells, compared to 3 μm and 1 μm particles. We demonstrate that via treatment with this particle, we can elicit higher T cell activation and cytotoxicity responses, including proliferation, CD107a expression, and cancer cell death in comparison to equivalent amounts of soluble anti-CD3 antibody. Synergizing the anti-CD3 particles with anti-CD28 antibody conjugation resulted in greater T cell activation responses, by increasing the extent of cytoskeletal remodeling, driving increased immune synapse formation, cell softening, and longer and more frequent T cell binding to cancer cells. We further explore the hypothesis that employing Janus particles to separate the anti-CD3/28-T cell activating signal from the cancer cell binding signal (anti-folate receptor) could beneficially impact the cancer cell specificity of cytotoxicity. We found that delivering these molecules using the Janus particle system, compared to uniformly coating particles with all three antibodies, resulted in not only increased cancer cell specificity but increased the percentage of targeted cancer cell death. Ovarian tumor spheroid models treated with Janus particles resulted in increased cytotoxicity and T cell infiltration. Interestingly, when we included a second cancer-targeting molecule, the

degree of cytotoxicity in the targeted cancer cell line did not increase. However, cytotoxicity in the untargeted cancer cell line decreased. These findings represent an improved understanding of the cellular processes particle-based immunotherapeutic strategies must address in reestablishing anti-cancer effector immune responses within the immunosuppressive tumor microenvironment.

CHAPTER 1. INTRODUCTION AND SPECIFIC AIMS

Cancer cells evade and suppress the immune response using a variety of intrinsic and extrinsic mechanisms, including downregulating proteins recognized by immune cells and expressing or secreting molecules that suppress effector immune cell function(1-3). For example, a resident CD8+ T cell may not recognize a tumor cell if MHC expression is downregulated on the cancer cell surface. Additionally, an immune response could be rendered nonfunctional if the tumor secretes anti-inflammatory cytokines, such as IL-10 and TGF-β(4, 5). It is well understood that reestablishing a robust immune response against cancer cells within the immunosuppressive tumor microenvironment is critically important to improve patient outcomes. However, given the propensity of cancer cells to mutate, changing their expression of specific cell markers, current immunotherapeutic strategies that rely on cancer cells expressing a particular protein may sometimes only be temporarily effective(6-8). Therefore, non-antigen specific activation of immune cells should be considered as an immunotherapeutic strategy as tumor cells cannot easily escape immune recognition. We propose a novel particle platform in which T cells are activated in a non-antigen-specific manner but targeted to cancer cells through the particle, producing an artificial cancer cell-specific immune response.

The overall objective of this dissertation is to explore the anti-cancer effects of immune-activating Janus particles. Janus particles occupy a unique space within cancer immunotherapy – by displaying T cell activating molecules and cancer targeting antibodies in a spatially segregated manner, this novel particle platform acts as a hybrid of two immunotherapies: T cell engaging bispecific antibodies and artificial antigen

presenting cells. The advantages offered by both strategies (i.e. cancer cell-effector immune cell ligation following T cell engaging bispecific antibody (T-BsAb) treatment, highly concentrated and localized signal on an APC) are included in the design of our Janus particles. By targeting cancer cells using antibodies conjugated to one hemisphere of the Janus particle whilst simultaneously binding and activating T cells using anti-CD3/28 antibodies functionalized to the other hemisphere, we can kill cancer cells in a targeted manner, thereby increasing the overall amount of T cell cyotoxic response.

The purpose of this current work is to develop to a particle platform capable of activating all bystander T cells against cancer cells regardless of antigen specificity. Non-specific T cell activation within the tumor microenvironment offers the advantage of stimulating all cells present – not only effector T cells that that are specific for a tumor associated antigen. Ultimately, the *overall objective* of this work is to develop a Janus particle platform capable of eliciting a non-specific T cell activation response against specific cancer cells. The central hypothesis of this project is that concentrated molecular signals on particles will lead to sustained T cell activation in both 2D and 3D *in vitro* cancer cell cultures, leading to enhanced cancer cell targeting and cytotoxicity. This hypothesis is investigated through the following specific aims:

1.1 Specific Aim 1: Characterize the effects of anti-CD3 and anti-CD3/28 functionalized particles on T cell activation and immune synapse formation.

We *hypothesize* that anti-CD3/28 presentation affects T cell activation and cytotoxicity through variation of particle size, antibody density, and anti-CD3: anti-CD28 antibody ratios. We fabricated particles that were delivered to T cells to quantify activation and

binding activity using ELISA and flow cytometry, respectively. Cancer cell death was measured using standard live/dead flow cytometric assays. The biophysical implications of activating T cells with particles were also assessed with AFM, cytoskeleton and immune synapse imaging, and a motility assay; we found cells soften upon activation, driven by changes in cytoskeleton arrangements.

1.2 Specific Aim 2: Evaluate the effects of spatially segregating the biological signals to crosslink T cells and cancer cells and provoke downstream cytotoxicity.

A novel Janus particle fabrication protocol was established to spatially isolate and concentrate signals that stimulate T cells and target ovarian cancer cells. Multi-functionality was determined using flow cytometry and spatial segregation was confirmed using fluorescent microscopy. We *hypothesized* that Janus particle presentation of T cell activating (anti-CD3/28 antibodies) and cancer cell targeting molecules (anti-folate receptor (FR) with and without anti-e-cadherin antibody) would facilitate T cell cytotoxicity against a cognate cancer cell. Cell crosslinking will be measured using fluorescent microscopy and cytotoxicity assessed with flow cytometry. We also tested the Janus particle with a three dimensional cell spheroid as a more physiologically relevant model of ovarian cancer than tradition 2D cell cultures. Ovarian cancer cell cytotoxicity was assessed via fluorescent imaging of tumor spheroids. Confocal microscopy was also used to examine T cell infiltration.

1.3 Innovation and Significance

Conventional methods of treatment for cancer involves surgery, radiation, and/or chemotherapy, which has thus far exhibited limited success at treating more advanced stages of the disease. Cancer is one of the greatest threats to health worldwide, killing over 600,000 people in 2017. There exists an unmet clinical need for therapeutics that can improve patient outcomes and quality of life. Lack of an effective immune response plays a substantial and critical role in cancer progression and eventual patient death. Immunotherapies, such as the Janus particle treatment presented here, offer exciting possibilities for treatment as immune cells can be present in the tumor microenvironment during all cancer stages and even when in remission. We have demonstrated that T cell activation with our particles results in immune synapse formation, cell softening, and enhanced granzyme b secretion. The functional effects of stimulation of T cells include enhanced cancer cell cytotoxicity from stimulated T cells greater penetration of T cells into a solid tumor model. The work presented here represents the first time Janus particles have been used as a platform to physically crosslink T cells and cancer cells, resulting in more frequent and sustained binding, and thus enhanced specific cancer cell cytotoxicity. Taken together, we have gained an improved understanding of the necessary cell interactions to elicit endogenous anti-tumor immune responses non-specifically.

Although biological Janus particles offer the ability to perform multiple functions, they have only been used thus far to elicit a single action from a cell, such as endocytosis. While uniformly coated, multi-functional micro- and nanoparticles are commonly studied in the field of bioengineering for applications such as drug delivery, the utilization of Janus particles to perform two spatially and temporally linked biological activities, both at high potency, is highly innovative and has not yet been investigated as a potential

treatment for cancer. The flexible design is capable of multiplexing a variety of signaling and bioresponsive behaviors limited only by the signaling molecules incorporated and particle biophysical properties. By combining microfabrication and bioengineering techniques, we can leverage Janus particles to address known problems in the field of ovarian cancer immunoengineering, summarized by the following:

1) *Danger from overstimulation of the immune system*, which we address by tuning the surface density of the activating ligands so that immune cells are not excessively stimulated, causing either activation-induced cell death in T cells or systemic toxicity. Additionally, we selectively target the cancer cells such that the immune stimulatory agent is highly available only within the tumor microenvironment. We emphasize the self-limiting nature of the immune stimulation through engagement of the body's homeostatic and clearance mechanisms (e.g. phagocytosis);
2) *Likelihood of off-target effects*, while cancer antigens are ideally uniquely or highly expressed by cancer cells compared to normal tissues, it is not uncommon for healthy cells to express low levels of tumor associated antigens, which can cause off-targeting. The high avidity enabled by the particle motif can lead to improved binding characteristics. However, although this enhanced binding can result in non-specific binding, the modular nature of the particle allows a different or additional targeting molecule to be utilized with relative ease;
3) *Intratumor heterogeneity*, solid tumors are heterogeneous and not all tumor cells will express or overexpress a particular cancer associated surface marker uniformly, making complete tumor targeting difficult. Additionally, tumors

contain many non-cancerous cells that support and promote tumor growth. The nature of the Janus particle platform allows for multiple cancer or cancer-associated markers to be included for targeting purposes, so that all relevant cells may be included in this immunotherapeutic strategy;

4) *Antigen specificity*, the Janus particle motif in which targeting and immune-activating molecules are simultaneously displayed contributes to a degree of specificity (present due to the targeting molecules), despite non-antigen specific activation. Furthermore, the anti-tumor immune response would not depend on immune recognition, which cancer cells can escape via immunoediting;
5) *Difficulty in application to new diseases,* which we address through the modular nature of the particles, with targeting and cytotoxic mechanisms easily swapped with appropriate biomolecules.

The benefit of spatially segregated bifunctionality, in comparison to mixed distributions on single particles, is that a higher density of signaling ligands will increase binding and stimulative properties through multivalent interactions(9-11). This technology will provide a platform in which particle multifunctionality is possible without reducing the intensity of signal. Thus, the Janus particle platform represents a substantive depature from current approaches. Our technology is highly novel and should prove useful in providing insight into the effects spatial coordination of signaling molecules on a single particle and concurrent activation of T cells and cell targeting has in eliciting cell-specific death.

CHAPTER 2. LITERATURE REVIEW

2.1 Ovarian Cancer

Ovarian cancer is the most common gynecological malignancy and the most lethal. Over 20,000 new patients are diagnosed with ovarian cancer each year in the United States resulting in more than 14,000 deaths per year(12, 13). The exact mechanism(s) in which cells transform into malignant cells is unresolved, but spontaneous cell mutations induced via genetics or environmental factors (including diet and tobacco use) and chronic inflammation are thought to contribute (3, 14, 15).

The most immunogenic cancer cells are continually removed by the immune system until a population of tumor cells escape recognition and grow unchecked(7). Tumor cell evasion can occur by several different mechanisms, including loss of tumor antigen expression, loss of MHC-I expression, or expression of oncogenes. Once established, tumors cells will leave the primary tumor and spread either locally to nearby healthy tissue or regionally to lymph nodes or other organs and tissues. Ovarian cancer is unique in that its development and spread occurs within the peritoneal cavity – a unique environment for both tumor growth and immune responses. Ovarian cancer metastasis is understood to mostly occur via peritoneal fluid flow that carries sloughed off cancerous cells from the primary tumor elsewhere. However, recent studies suggest that ovarian cancer metastasis can also occur hematogenously(16). Regardless of mechanism, metastasis is normally localized to the greater omentum, a fatty layer of peritoneal tissue that wraps around the colon, stomach, and spleen(17, 18). Tumor cells can be shed at a

very early stage of the disease, contributing to malignant ascites formation and metastasis(15, 19).

In addition to malignant cancer cells, cancer tissues also include immune cells, fibroblasts, endothelial cells, and ECM components(20). These cells contribute to the tumor microenvironment and initially exert inhibitory effects on cancer cells; however, during tumor progression, tumor cells may circumvent these inhibitory signals or even exploit immune and stromal cells for their own growth, invasion, and metastasis(21, 22). Cancer associated fibroblasts (CAFs) have been found in omental issues of ovarian cancer patients, even without detecting cancer cell infiltration into the omentum(23). These cells may arise from local fibroblasts and fibroblasts precursors that differentiate based on growth factors and cytokines released by tumor cells(24, 25). Additionally, bone marrow cells may be recruited into the tumor niche and differentiate into CAFs or they themselves may recruit fibroblasts to adopt the CAF phenotype within the tumor milieu(24, 26, 27). Comparative gene expression profiling has revealed that CAFs are different from normal fibroblasts and may promote or inhibit cancer growth, depending on tumor milieu composition(28). The pro- and anti-tumor effects of these cells will be discussed in more detail in the following sections, but overall, the presence of CAFs contributes to tumor heterogeneity and therefore may be a possible cell to target using immunotherapeutic strategies.

Unfortunately, ovarian cancer is often detected only after metastasis, which makes it difficult to treat(12). Women diagnosed with stage III and IV ovarian cancer have less than a 25% 5-year survival rate because once metastasized, this cancer recurs in 80% of

patients(18). If ovarian cancer persists despite repeated chemotherapy treatment, patients often develop chemotherapy-resistant strains(29).

2.2 Host Immune Responses

The immune system plays at least three distinct roles in preventing cancer: 1) protecting the host against viral infection and hence suppresses virus-induced tumors; 2) preventing the establishment of an inflammatory environment that facilitates tumorigenesis by eliminating pathogens and thus resolving inflammation, and 3) eliminating tumor cells in certain tissues because transformed cells often co-express ligands for activation receptors on immune cells(7). The immune system response is accomplished by a complex system of cells and macromolecules that respond to, kill, and clear diseased and abnormal cells. Atypical proteins from cancer cells are processed and presented through multivalent forms of the MHC-I/II on APCs (30) and are recognized by CD8+ or CD4+ T cells, respectively, through their TCRs, inducing their initial activation. Subsequent activation of CD4+ and CD8+ T cells produces startlingly different results between T cell subsets. CD8+ T cells – also known as cytotoxic T cells – release cytolytic granules. These granules cross the immunological synapse and induce target cells to undergo apoptosis within hours of release(31). CD4+ T cells – also known as helper T cells – instead release immunosuppressive cytokines, like TNF-α and INF-γ, cytokines that are necessary for the differentiation of B cells, activation of macrophages and DCs, and the recruitment of inflammatory cells. NK cells are also important for the recognition and cytotoxic elimination of tumor cells.

Tumor infiltrating lymphocytes (TILs) are especially important in prolonging overall survival (OS) in ovarian cancer patients(32-34). In particular, the presence of CD8+ T cells is positively correlated with median survival and the ability of CD8+ T cells to form memory cells is critical(35). The presence of MHC on ovarian cancer cells is associated with not only increased numbers of CD8+ T cells but also increased infiltration and proliferation of these lymphocytes(36, 37).

There is also evidence that the presence of CD20+ B cells correlate with positive patient survival in ovarian cancer patients(38). CD20+ B cells have shown to co-localize with activated CD8+ T cells, express markers of antigen presentation, and, with CD8+ T cells, correlate with increased patient survival(39). Since B cells are not directly responsible for tumoricide, it is possible that B cells contribute to a pro-immunogenic immunophenotype by secreting cytokines that support CD8+ T cell function and infiltration(40).

Supporting cells can also play a role in the inhibition or propagation of ovarian cancer. TAMs are a major stromal component in solid tumors. In the ovarian tumor microenvironment, TAMs are the most abundant subset of infiltrating immune cells(41). Classical, M1-polarized, macrophages are activated by INF-γ and characterized by the production of pro-inflammatory and immunostimulatory cytokines. M1 macrophages express high levels of MHC-1 and II and thus play a critical role in tumor antigen presentation. However, M2 macrophages are activated by CD4+ T cell cytokines and thus exert anti-inflammatory effects. Recent work shows a correlation between improved 5-year prognosis and elevated M1:M2 TAMs in patients with ovarian cancer(42).

As the omentum is the most common site of ovarian cancer metastasis, we need to consider the immune microenvironment of this organ. Like other fatty tissue, the omentum is filled with macrophages and a variety of innate or innate-like cells, including NK cells(43), NKT cells(44), B cells(45, 46), and DCs(47). These immune cells can be induced to act in either a pro- or anti-inflammatory manner, depending on whether the net environment is pro- or anti-immunogenic.

2.3 Immunosuppressive Tumor Microenvironment

Spontaneous anti-tumor immune responses have only been observed in ~55% of ovarian cancer patients, giving rise to the hypothesis that robust immunosuppressive mechanisms are employed by these solid tumors(48). In fact, tumor-associated immune responses are more likely to facilitate immunosuppression than they are to establish effective antitumor responses(3, 21). Broadly, tumors may evade immune system recognition through immunoediting and immunoselection or actively suppress antitumor immune responses by secreting immunosuppressive signals and recruiting regulatory immune cells. Immunosuppressive signals are produced by tumor cells or by other cells located within the tumor microenvironment, including stromal and immune cells. New and efficient targets for immunotherapeutic that counteract immune system failure could help to eradicate tumors and the supporting network of cells that facilitate tumor formation and growth.

An essential tenet of cancer immunosurveillance is that cancer cells express antigens different from non-cancerous cells, allowing for specific recognition by immune cells. The existence of tumor associated antigens (TAAs) was first demonstrated when

researchers found that mice could be immunized against certain tumors and were protected upon re-challenge of the same tumor(49). Subsequent studies have revealed that such antigens reflect differences in expression levels, mutations, and differentiation between cancerous cells and non-transformed cells(7, 50, 51). These TAAs may then be recognized by the immune system so that tumor cells can be eliminated through the innate and adaptive immune processes. However, tumor cells expressing few or none of these TAAs survive to grow and proliferate without immune system recognition(7). Additionally tumors can escape recognition by downregulating the expression of MHC-I on cancer cell surfaces and/or upregulating the anti-apoptotic molecules FLIP and Bcl-XL (52-54), driven by a combination of genetic instability and immunoselection(6, 55). Additional resistance can occur when tumor cells express mutated, inactive forms of death receptors, including DR5 and Fas(56, 57). Such immunoediting results in a tumor of poorly immunogenic cell variants that are no longer recognized as dangerous by the immune system and can therefore grow progressively(7). This phenomenon is also important when considering ovarian cancer recurrence. In one study, ovarian cancer patients had their tumor-associated T cells evaluated for recognition of cancer cell mutations. In one case, the expression of the mutated gene antigen resulted in an antigen-specific T cells response; however, the second recurrence showed a loss of T cell response despite no change in the expression of the mutated gene, demonstrating immune escape between recurrences(8).

Alternatively, the tumor microenvironment can establish a network of cells and proteins that inhibit spontaneous immune processes using a variety of immunosuppressive molecules. Tumors often express inhibitory ligands, including PD-

L1, which inhibit T cell proliferation and effector function and also lead to recruitment of Treg cells(58, 59). Research using several cancer systems has shown that cell expression of inhibitory immune checkpoint molecules is associated with and contributes to the immunosuppressive state of the ovarian cancer tumor microenvironment. Ligation of PD1 suppresses the lytic activity of immune effector subsets and its expression on monocytes in ascites and blood is correlated with poor clinical outcome(60). The expression of the enzyme IDO by tumor cells is associated with advanced stage ovarian cancer and impaired patient survival(61). This immunosuppression works to inhibit CD8+ T cell proliferation, promote CD4+ T cell apoptosis, and suppress NK cells(62). Tumor cells will also secrete anti-inflammatory cytokines, most notably TGF-β and IL-10, which inhibit the function and infiltration of CD8+ T cells, DCs, and NK cells(5, 52, 63, 64). Additionally, TGF-β has been implicated in the transformation of effectors T cells into Treg cells(65). The TNF network – consisting of TNF-α, IL-6, and CXCL12 – is an integrated cytokine network that has been implicated in ovarian tumor establishment, growth, and metastasis(14). TNF-α expression is highly correlated with increased CXCL12 and IL-6 expression and in one study, ovarian cancer cell exposure to TNF-α resulted in proliferation, disrupted cellular organization, and functional loss of the basement membrane(66, 67). CXCL12 is found in high levels of malignant ascites and significantly, blockade of this chemokine ligand and its receptor, CXCR4, resulted in increased patient survival and tumor cell apoptosis, perhaps due decreased recruitment of Treg cells(68-70). Tumor cells, infiltrating T cells, and macrophages are the primary sources of IL-6. High levels of IL-6 are often detected in ascites and, when found in the serum of ovarian cancer patients, are associated with shorter patient survival(71). This is

unsurprising, given that IL-6 increases proliferation and angiogenesis and decreases sensitivity to apoptotic signals from immune cells, directly contributing to ovarian cancer growth and progression(72, 73). Many cancer cells produce VEGF, which is critical for establishing a blood supply for the tumor, but also inhibits DC function and NKT cell activation(2, 74, 75). It has also been shown that VEGF significantly reduces T cell proliferation via VEGFR-2(76).

Regulatory T cells, myeloid-derived suppressor cells, and tumor associated macrophages are the three major immune cell subsets that play key roles in inhibiting host immune responses. Treg cells are CD4+ T cells that express CD25 and Foxp3 and, when stimulated, inhibit the functions of CD8+ T cells by secreting IL-10 and TGF-β, expressing CTLA-4 and PD-L1, and consuming IL-2(77). Treg cells may be recruited to the tumor and their presence is associated with reduced patient survival(33, 78, 79). Treg cells expressing TNFR2 are a particularly suppressive subpopulation that is found in high levels in ascites, thus supporting further cancer growth(80). Specialized Treg cells, known as VAT-associated Treg cells, are found in abdominal fat, including the omentum, and may accompany cancer cells in malignant ascites. VAT-associated Treg cells support cancer cell survival and proliferation and immune evasion by producing cytokines, chemokines, and growth factors, such as IL-10, VEGF, and TGF-β(81). Overall, Treg cells are critical for tumor progression; experimental tumor models that eliminate Treg cells show robust antitumor immune responses(82). Furthermore, accumulation of Treg cells in the tumor microenvironment is associated with limited antitumor immunity(83). MDSCs are a heterogeneous population of mostly progenitor and immature myeloid cells that induce Treg cell differentiation and produce TGF-β. MDSCs have been shown to

inhibit T cell activation in ovarian tumors, enhance metastatic and tumorigenic potential, and decreased patient survival(84). In the ovarian tumor microenvironment, TAMs are the most dominant subset of immune cells(41). In ovarian tumors, M2 macrophages contribute to multiple mechanisms of TAM-mediated immunosuppression, mostly by upregulating B7-H4 and secreting CCL22. CCL22 produced by tumor cells and TAMs direct Tregs to home to the tumor tissue(85). B7-H4 is a member of the B7 family of APC regulatory molecules and B7-HA^{+} macrophages significantly decrease T cell proliferation and activation(42). TAMs also support ovarian cancer cell adhesion, proliferation and metastasis by secreting IL-6, IL-10, CCL18, and TNF-α, among other cytokines(14, 65, 86-88). Additional subsets of NKT cells, B cells, and CD8+ T cells have shown to exert immunosuppressive effects, although these subtypes are less well characterized(89-91).

Cancer-associated fibroblasts play a significant role in ovarian cancer. Although it remains unresolved whether CAFs themselves can induce oncogenic mutations, it is evident that CAFs promote tumorigenic activity by supporting cancer cell proliferation(92), metastasis(25), and EMT induction(93). Furthermore, CAFs have also been shown to facilitate ovarian tumor implantation or metastasis by developing special niches within the omentum tissue(25). CAF-derived signals can promote the polarization of CD4+ T cells to adoptive a tumor-supportive Th2 phenotype that is associated with enhanced infiltration of TAMs and Treg cells(94). Additionally, CAFs secrete IL-6 and CCL2 thereby promoting the development of TAMs(95). In general, CAFs contribute to the complexity of the tumor microenvironment, suppress immune cell function, and

facilitate cancer progression. Addressing the role of these cells is critical in assessing immunotherapeutic strategies.

Collectively, the immunosuppressive mechanisms described are difficult to circumvent and facilitate tumor progression by actively restraining endogenous anti-tumor immunity. As a result of these mechanisms, non-immunogenic tumor cells are immunoselected and allowed to grow and proliferate. These tumor and their supporting cells then secrete immunosuppression signals that further suppress the immune system through a variety of intrinsic and extrinsic mechanisms. As a result of these mechanisms, resident effector immune cells, including CD8+ T cells, are unresponsive to cancer cells in spite of the presence of signals conventionally triggering activation.

2.4 Current Immunotherapeutic Approaches

The FDA has approved immunotherapies for prostate cancer, advanced kidney cancer(96), lymphoma, and metastatic melanoma, but have only recently have allowed immunotherapies targeting ovarian cancer to enter clinical testing(97). However, studies of ovarian cancer patients have implicated immune system suppression is strongly associated with negative patient outcomes(12). Thus, ovarian cancer treatment strategies should integrate the immune response in order to achieve durable clinical outcomes(98). Additionally, as ovarian cancer is largely confined to the abdominal cavity, systemic administration of immunotherapeutics may not be necessary; some treatments are already delivered into the peritoneum(99, 100). However, overcoming immune suppression is a particular challenge in ovarian cancer, as immunosuppressive cells and cytokines have been observed in the tumor niche even during remission(101, 102). The two major thrusts

of ovarian cancer immunoengineering research are focused on either reversing tumor immunosuppression mechanisms or restoring T cell immunological function within the tumor environment. To restore immune functionality, researchers are currently investigating cancer vaccines that use either proteins or cells to prime T cell responses to ovarian cancer antigens(103-106) or adoptive T cell therapy to introduce and increase cancer antigen-specific T cells against ovarian cancer cells(107-110). Monoclonal antibody therapy is used to both block cancer immunosuppressive strategies and reestablish antitumor immunity by targeting cancer cells with blocking agents, anti-TAA antibodies, or chemotherapeutic conjugates (111-113). Additionally, pre-clinical studies demonstrate that biomaterial immunoengineering approaches offer an exciting alternative to better control of molecule presentation and enable tunable immune cell responses with increased specificity due to multivalent binding between the targeted cell and the biomaterial surface(114, 115).

2.4.1 Monoclonal Antibody Therapy

Antibodies, also known as immunoglobulins, are "Y"-shaped proteins composed of a consistent Fc stem and a highly variable $F(ab)_2$ portion that recognize antigens. Monoclonal antibodies have a high specificity for their antigens and thus can be optimal for targeting cancer cells that overexpress certain surface proteins with limited off target effects. In the past 20 years, antibody-based therapies for cancers have become a viable and well-established therapeutic strategy(98). Antibodies can induce tumor cell apoptosis via a variety of mechanisms: complement-dependent cytotoxicity, in which the Fc region of the antibody triggers the assembly of the membrane attack complex via the complement system to cause cell lysis; antibody-dependent cellular cytotoxicity, a

process that involves the Fc region of the antibody binding to Fc receptors on NK cells, prompting the release of cytolytic granules to kill cancer cells; immune checkpoint inhibition, which works by blocking immunosuppressive molecules, such as CTLA-4 and PD-L1; blocking certain metabolism or growth pathways, thereby interfering with the ability of cancer cells to grow and survive; and antibody-drug conjugates(116).

A promising and actively researched strategy includes checkpoint inhibitors which are used to bind and block surface molecules on cancer cells and T cells that render cytotoxic T cells anergic or apoptotic (101, 117-119). Checkpoint inhibition can be achieved using two general strategies: 1) inhibition of immunosuppressive receptors expressed by activated T cells, 2) inhibition of ligands of these receptors expressed on cancer cell surfaces. CTLA-4, an inhibitory receptor on T cells that prevents T cell activation and proliferation but enhances Treg suppression, is being investigated for clinical use. Ipilimumab has been used to treat ovarian cancer in a post-vaccine context, which elicited modest clinical benefits(120). Although these therapies have shown some success, anti-CTLA-4 therapies are associated with more significant immune-related toxicities compared with PD-1 blockade(121). PD-1 and PD-L1 blocking antibodies have also been studied against a broad range of solid tumors, including ovarian cancer, producing variable responses – from no response to complete remission(122-124). PD-1 antagonists nivolumab and pembrolizumab elicited a disease control rate of 44% and 34.6%, respectively, in ovarian cancer patients(123, 125). Antagonists to PD-L1 tested in ovarian cancer patients include avelumab and BMS-936559; both elicited more successful patient outcomes than the non-treatment control group(124, 126). While initial results of checkpoint inhibitors in ovarian cancer are promising (~18% progression-free

survival after 24 months), they are modest compared to the remarkable results reported for melanoma (~27%), renal cell (~53%), non-small cell lung (~32%)(127, 128).

Solid tumor growth and progression is reliant on neovascularization – the ovarian cancer tumor and subsequent formation of ascites depends on the formation of new blood vessels to support the abnormally high cellular growth and proliferation present in cancer(129, 130). These new blood vessels are rapidly formed and often leaky, due to defective basement membranes, and generally tortuous with poor flow(131, 132). The endothelial cells within these vessels are more dependent on pro-angiogenic signals than more mature vessels found elsewhere in the body. Thus by targeting the receptors for these growth factors – such as VEGFR – or targeting the actual protein itself, it is possible to disrupt the interaction between growth factor and its receptor, effectively limiting tumor growth. Clinicians found that women treated with these antibody therapies showed an increase in time of the median progression-free survival (PFS) or recurrence of other symptoms but only sometimes increased the median OS(133-139). Tumors also may be treated by targeting upregulated proteins involved in metabolism and/or DNA repair mechanisms, such as folate receptor, as these proteins are markedly increased in cancer cells(140-142). Such antibody therapies have shown to be moderately successful(143-145).

While monoclonal antibody therapy has demonstrated success, particularly immune check point therapy, inconsistent outcomes and sometimes only modest benefits have been observed. Potential mechanisms underpinning the limited antitumor efficacy of monoclonal antibody therapy in ovarian cancer include (1) low intrinsic tumor immunogenicity and mutational burden in ovarian cancer compared to other cancers; (2)

expression of multiple co-inhibitory receptors on T cells infiltrating ovarian cancer(146); (3) compensatory upregulation of multiple immune checkpoints when one is blocked; (4) redundant immune suppressive mechanisms. Continued research in this area of immunoengineering will hopefully address these concerns by introducing a therapy that exhibits multivalency and targeting flexibility.

2.4.2.1 Bispecific Antibodies

Another promising approach is bispecific antibodies (i.e. diabodies), which crosslink cancer-targeting moieties with T cell-stimulating antibodies using a short peptide linker (147-149). For example, Catumaxomab is a trifunctional antibody that specifically targets EpCAM on tumor cells and CD3 antigen on T cells and contains an Fc antibody region to engage with macrophages, NK cells, and DCs(150). This drug has been approved in Europe since 2009 and tested in the United States as a new therapeutic for ovarian cancer patients with malignant ascites, increasing PFS and decreasing ascites production(99, 100, 151). Most significantly, catumaxomab decreased EpCAM+ tumor cells and increased CD45+ leukocytes in ascites(100).

In general, bispecific antibodies (T-BsAbs) have targeted and activated cytotoxic T cells using only anti-CD3 antibody (although anti-CD28 antibody is being increasingly investigated in tandem with anti-CD3 antibody as well) to circumvent the antigen specificity restriction(152). Thus, polyclonal T cells can be stimulated and these responses can be directed against cancer cells. However, the design intent behind non-specific CD8+ T cell activation has had unforeseen consequences – namely the activation of other T cell subtypes, including CD4+ T cells, NKT cells, and γδ T cells(153-156).

This unintended effect is not entirely unwanted; activation of these effector T cells will only enhance immunogenicity. However crosslinking with cancer cells has limited utility with these T cell subsets given their inability to directly kill cancer cells (CD4+ T cells) or their rarity (NKT cells and γδT cells). Overall, pre-clinical studies of T-BsAbs demonstrate robust immunogenic responses – inducing and directing T cells activation against tumor cells – and have been tested against over 40 tumor cell antigens, including EGFR, EpCAM, HER2, and FR(152, 157, 158). Clinical investigations of anti-CD3 T-BsAb therapy for numerous cancer types, including acute myeloid leukemia(159) and hepatocellular carcinoma(160) are ongoing. However, while more efficacious than other antibody therapies(101), the lack of avidity between T-BsAbs and cancer cell or immunological synaptic receptors (i.e. TCR, CD3, CD8, and CD28) could limit the degree of cytotoxicity of this strategy(98, 101, 116, 161, 162). Nonetheless, the technique employed by bispecific antibodies – crosslinking cancer cells with activated T cells cancer cell – is clinically significant, effective, and impactful.

2.4.2 APC Therapy

By increasing TAA presentation, tumor-specific immune responses are possible – including the generation of tumor-antigen specific CD8+ T cells and memory cells. An effective APC therapy-induced immune response is superior to any of the other commonly used methods of cancer treatment such as chemotherapy, radiation, surgery, or even antibody therapy, by inducing an immunologic memory that lingers long after the tumor has been cleared away(98). In ovarian cancer patients, MUC-1 treatments have shown to be successful, with an increase in in PFS and OS(163). In vivo DC stimulation with TAAs has also demonstrated preclinical success using the MSLN-Hsp70 fusion

protein – administration to mouse models significantly increased survival, slowed tumor progression, and augmented tumor-specific CD8+ T cells responses(164). APC therapy also offers the possibility of priming immune responses against multiple tumor antigens, thereby reducing the potential for tumor escape(98). This strategy has already shown preclinical and clinical success, overall demonstrating an increase in PFS(165).

2.4.3 Artificial Antigen Presenting Cells

Studies have shown that cells respond more intensely when presented with highly concentrated multivalent signals(166, 167). Thus a particle platform that offers high density of activating signal can lead to improved binding and enhanced immune cell activation. Freely soluble antibodies, alternatively, do not always provide adequate receptor cross-linking to initiate highly active cell responses, especially in cytotoxic T cells(115, 168-170). Particle-based T cell activation platforms have been studied to both maximize activation responses and better understand the effect particle properties have on immune cell activation signaling. Researchers have investigated how particle shape(115, 171), molecular density(167, 172), spatial distribution(173), antibody orientation(174), and activating molecule(s)(175), and dosing regimens of commercial beads and soluble antibody affect immune cell responses. Likely, different particle properties are synergistic and few studies isolate particle design parameters or investigate the mechanisms behind increased or decreased T cell responses. Because antibodies are immobilized, particles provide better control over the spatial presentation of activating and targeting antibodies enabling tunable responses for maximal immunotherapeutic effect, compared to soluble protein therapies.

Artificial APCs are a particular kind of particle-based immunomodulatory biomaterial that occupies a unique space between adoptive cell therapy and monoclonal antibody therapy in the sense that often, these particles display monoclonal antibodies on their surface in order to mimic APC function(161). As endogenous APC activity can be tempered by the immunosuppressive tumor microenvironment or by inconsistent/ unrecognized cancer antigens (factors which most likely contributed to inconsistent clinical trial outcomes), aAPCs are an alternative approach that cannot be influenced by immunosuppressive signals and allow for controlled signal presentation of T cell activating proteins, traditionally, either anti-CD3 antibody or antigen peptide-MHC complex and anti-CD28 antibody(115).

In general, aAPC research has been conducted *in vitro* using a variety of platforms, including carbon nanotubes(176), liposomes(177), polystyrene spheres(178), and ellipsoid PLGA microparticles(179). All these platforms have demonstrated success in eliciting T cell activation in vitro and in vivo against cancer cells(161). Thus far, no *in vivo* toxicities have been observed; however, the typical aAPC – large, rigid, and usually non-biodegradable – has led to fears about possible embolisms, making FDA approval of these particles difficult(180). Newer studies have focused on nano-size aAPC to promote trafficking and reduce possible side effects(162, 173, 175).

2.4.4.1 Janus Particles

As Janus particles are multifunctional yet maintain dense molecular presentation through spatially segregation, there is potential for how these particles to be used as therapeutic agents. However, while Janus particles have been investigated for stimulation of T

cells(173, 181, 182) and uptake by macrophages(183, 184) or cancer cells(185), researchers have focused on interrogating the effects asymmetry has on cellular response, not on prompting a cellular response for a specific downstream outcome. Different T cell activation was observed as a result of different molecular patterning with more intense and sustained activation triggered by particles with an increased surface coverage of anti-CD3 antibody(181). However, T cell activation responses displayed higher variability than expected, leading the study authors to postulate that cellular response heavily depended on particle orientation. A follow-up study(182) in which particle orientation was controlled by coating one hemisphere with aluminum and the other with anti-CD3 antibody revealed distinct differences in T cell activation response. Once the anti-CD3 antibody functionalized region of the particle was oriented to interact with the T cell, a rapid transformation to an activated phenotype was observed. Lee and Yu further determined that T cell activation is most effective when stimulated with densely packed anti-CD3 antibody and is further enhanced with the presence of anti-CD28 antibody(173). Gao and Yu also investigated how Janus anti-CD3 antibody/silica particles are endocytosed by T cells(186). They found that the asymmetrical nature of Janus particles heavily influences cell membrane dynamics and reduced overall particle internalization, for all sizes investigated, in comparison to uniformly functionalized particles. Taken together, this research establishes the ability of Janus particles to activate T cells and prevent internalization, supporting the rationale that the Janus particle platform is uniquely suited for cancer immunoengineering purposes.

CHAPTER 3. CHARACTERIZE THE EFFECTS OF ANTI-CD3 AND ANTI-CD3/28 ON T CELL ACTIVATION

3.1 Introduction

The stimulation of cytotoxic T cells is a powerful pre-clinical and clinical technique(159, 160, 169, 173, 175, 177, 187-190) to directly kill cancer cells. Since cytotoxic t cells are a major immune cell type present in certain tumor microenvironments(187, 191), proper immunoengineering of their response lessens the need to recruit additional immune cell types to the tumor. Classically, cytotoxic T cells are activated in a series of discrete signals(115, 189, 192) by TCR signaling initially(177, 193) and then additionally through the co-stimulatory molecule CD28 and various cytokines. While these additional signaling molecules are required for phenotype stabilization(188, 192), it is possible to activate T cells using only anti-CD3 monoclonal antibody to induce T cell activation, which includes T cell proliferation, IFN-γ and TNF-α production, cytolytic degranulation, and surface expression of activation markers(115, 169, 187, 188, 193). The utility of activating effector T cells using anti-CD3 antibody is demonstrated through numerous successful clinical investigations of anti-CD3 bispecific antibody therapy for cancers, including acute myeloid leukemia(159) and hepatocellular carcinoma(160).

Cells respond more intensely when presented with highly concentrated multivalent signals(114, 166, 167). Thus a particle platform that presents dense activating signals can lead to sustained cell binding and enhanced activation. T cell death can also occur following this activation, if stimulating antibodies are presented overly concentrated or if co-stimulatory molecules are missing. Freely soluble antibodies,

alternatively, do not always provide adequate receptor cross-linking to initiate highly active cytotoxic T cell response due to monovalent binding behavior(115, 168-170). Furthermore, although not investigated in this study, immobilizing anti-CD3 antibody results in a more consistent effector phenotype(187), prolonged T cell stimulation, and amplified cytokine secretion upon stimulation, compared to soluble anti-CD3 antibody(168).

Particle-based T cell activation platforms have been studied to both maximize activation responses and better understand the effect particle properties have on immune cell activation signaling. Researchers have investigated how particle shape(115, 171), molecular density(167, 172), spatial distribution(173), antibody orientation(174), activating molecule(s)(175), and dosing regimens of commercial beads or soluble antibody affect immune cell responses. However, a lack of complete understanding about how to optimize these variables for ideal signal presentation for maximum T cell activation and cytotoxicity remains. Likely, different particle properties are synergistic but few studies isolate particle design parameters or investigate the mechanisms behind altered T cell responses. We and others have established that cellular responses depend on how their molecular signals are presented (16, 17, 22). Understanding how activating signal presentation affects T cell behavior, from initial activation to downstream cytotoxicity, is of critical importance to develop potent biomaterials for immunomodulation. Considering the particle and molecular properties that promote T cell activation, we investigated the effect of particle size and surface coverage of anti-CD3 and anti-CD3/28 antibodies on T cell activation responses, including GrB release, downstream T cell binding, cancer cell cytotoxicity.

Relevant commercial comparisons, including equivalent amounts of soluble anti-CD3 antibody and commercial activating beads (anti-CD3/28 Dynabeads), were made. We evaluated T cell cytotoxicity against cancer cells and determined effector cell-target cell interactions were vital for more effective cancer cell death. Furthermore, particle-elicited cytotoxic death was highly depended on a localized release of cytolytic granules. Designing particles for T cell activation and cytotoxicity has far reaching consequences to *in vitro* expansion of certain T cell populations and the modulation of the immune response within the tumor microenvironment for immunotherapeutic purposes.

3.2 Materials and Methods

3.2.1 Cell Culture

T cells – Jurkat (ATCC; Manassas, VA), a human cancer T cell line, and primary human T cells were cultured in RPMI 1640 cell culture media (ATCC, Manassas, VA) supplemented with 10% fetal bovine serum (FBS; Atlanta Biologicals; Norcross, GA) and 1% penicillin-streptomycin (Sigma Aldrich, St. Louis, MO) and maintained between 1×10^5 and 1×10^6 cells/mL. Primary human T cells were isolated from peripheral human blood using EasySep T cell Isolation Kit (Stem Cell Technologies; Vancouver, Canada). The human ovarian cancer cell line HeyA8 was gifted from the McDonald laboratory (Georgia Institute of Technology, Atlanta, GA). HeyA8 monolayers were cultured using the same cell growth medium as the T cells. All cells were maintained at 37 °C with 5% CO_2. All cells used were below passage 30 with viability assessed using trypan blue.

3.2.2 Particle Functionalization and Characterization

Carboxylated polystyrene particles with 0.3 μm, 1.0 μm, and 3.0 μm diameters were purchased from Bangs Laboratories (Fishers, IN). Mouse anti-human CD3 antibody alone or with mouse anti-human CD28 antibody (Biolegend; San Diego, CA) was conjugated to particles using standard 1-ethyl-3-(3-dimethylaminopropyl)-carbodiimide (EDC) crosslinking via a PolyLink Protein Coupling Kit for COOH Microspheres (Bangs Laboratories, Fishers, IN). Briefly, particles were washed through centrifugation and buffer exchange and incubated with 200 mg/mL EDC for 15 minutes at room temperature to activate surface carboxylic acid functional groups and then incubated with anti-CD3 antibody at room temperature for 1 hour on an end-over-end spinner. Particles were washed twice to remove unbound linker and unconjugated antibody. A schematic illustrating the particle functionalization process is shown in Figure 1. Antibody was conjugated to particles at different amounts (0 μg, 6.25 μg, 12.5 μg, 25 μg, 50 μg, and 100 μg) (Figure 1, Table 1), such that antibody labeling density was kept consistent on different particle sizes by normalizing the conjugation reaction to total surface area. 0.3 μm particles conjugated with 25 μg bovine serum albumin (BSA; Sigma Aldrich) were also created using this method. Anti-CD3/28 particles were conjugated using EDC at the following conditions: 25μg anti-CD3 with 6.25 μg, 12.5 μg, 25 μg, 50 μg and 100 μg anti-CD28 antibody.

Table 1: Surface Saturation.

Conjugated Antibody (μg)	Theoretical Surface Saturation(%)
0	0
6.25	10
12.5	21
25	41
50	83
100	>100

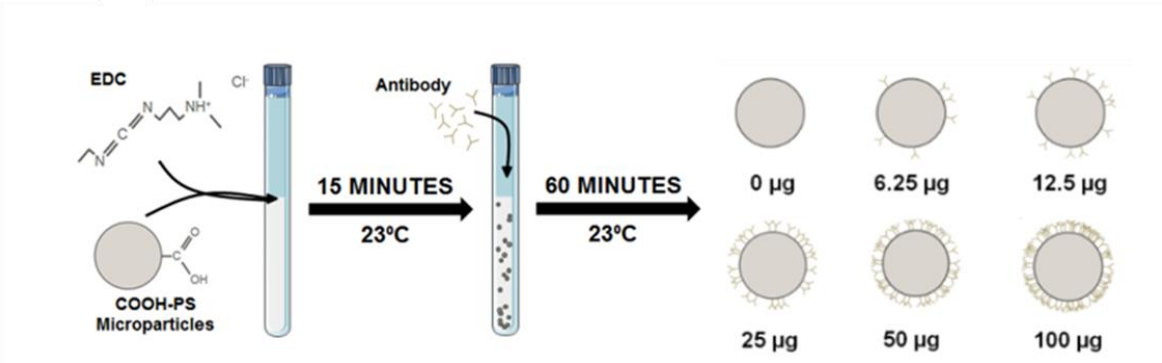

Figure 1: Particle Conjugation Schematic. Schematic of anti-CD3 antibody functionalization of three sizes of carboxylated polystyrene particles at varying labeling densities using EDC.

Batch conjugation uniformity was investigated using dynamic light scattering (DLS). A 90 Plus Particle Size Analyzer (Brookhaven Instruments Corporation, Holtsville, NY) was used to measure the dispersity index of each particle condition. The particle population was analyzed by averaging ten particle measurements taken during each run. To evaluate varying antibody conjugation to the particles, the post-conjugation supernatant was evaluated for protein content at 280nm wavelength using a BioTek Synergy H4 Hybrid plate reader (Biotek Instruments, Winooski, VT), which was quantified from standard curve measurements. FITC goat anti-mouse IgG, Fcγ fragment specific and Alexa Fluor® 647 goat anti-mouse IgG, $F(ab')_2$ fragment specific (Jackson ImmunoResearch Laboratories, West Grove PA) were used to label the respective Fc and $F(ab)_2$ portions of the primary anti-CD3 antibody. Briefly, each antibody was diluted in blocking solution (phosphate buffered saline (PBS; Invitrogen, Grand Island, NY) containing 0.02% FBS and incubated with the anti-CD3 antibody functionalized particles on ice in the dark for 1 hour. Each sample was washed and resuspended in PBS. The

fluorescent F(ab')$_2$ fragment specific secondary antibody was incubated at 1:200 and the fluorescent Fcγ fragment specific secondary antibody was incubated and 1:50. The MFI of these fluorescently tagged particles was measured using flow cytometry. Surface saturation values were calculated at each particle size and conjugation density, using the following equation provided by Bangs Laboratories,

$$S = \frac{6}{\rho_S * d} * C \quad (1)$$

in which S is the amount of protein on the particle surface, ρ_S is the density of the particle sphere, d is the particle diameter, and C is the capacity of the particle surface for the protein of interest. For human IgG, we assumed C ≈ 2.5 mg/m^2.

3.2.3 T Cell Activation

A granzyme B ELISA assay (Biolegend, San Diego, CA) was used to evaluate the magnitude of T cell activation as a result of treating Jurkat cells with our anti-CD3 particles *in vitro*. This kit measures the concentration of GrB secreted into the cell media following T cell stimulation thereby measuring the extent of T cell activation. Jurkat cells were seeded at 0.2 x 10^6 cells/mL in a 96 well plate (Corning) and treated with approximately 2 x 10^6 particles; each size and antibody labeling density was tested. Following 24 hours of cell incubation with the particles, the contents of the well were collected and the stimulated T cell supernatant was isolated by centrifugation. GrB secretion was measured in the supernatant using sandwich ELISA according to the manufacturer's specifications. When we examined particle size only, an equivalent amount of antibody was delivered between conditions (equal to 3.0 μm particles), as

opposed to number of particles. Our selected particle was compared to reagents currently in use – commercially available T cell activation particles, Dynabeads® labeled with anti-CD3 and -CD28 antibodies (Life Technologies; Grand Island, NY), and soluble anti-CD3 antibody. Unlabeled particles were used as negative controls. Dynabeads were delivered per the manufacturer's protocol. To perform time-course studies, separate wells were utilized. Once the cell supernatant was harvested, it was flash-frozen in liquid nitrogen and stored at -80 °C until all samples were collected. Frozen cell supernatant was thawed in a 37 °C water bath before analysis with ELISA.

Primary human T cell proliferation was also measured as a marker of T cell activation using Vybrant® CFDA SE (CFSE, Thermo Fisher Scientific, Waltham, MA) and stimulated with the optimized anti-CD3 particle, anti-CD3/28 particle formulations, or BSA-labeled particle. Primary human T cells were plated at 1 x 10^6 cells/mL in a 12 well tissue culture plate, stained according to the manufacturer's specifications, and monitored with the particle treatments for 10 days. On days 4 and 7, 150 μL from each sample was collected, washed, resuspended in PBS and analyzed using flow cytometry. On day 10, the fluorescent intensity of all remaining cells was measured. Cells were cultured as usual for the duration of the assay, in the dark.

3.2.4 T cell Cytotoxicity

The ability of our anti-CD3 and anti-CD3/28 particles to induce cancer cell death was evaluated using a direct co-culture. HEYA8 cells, an ovarian cancer cell line, were plated at 0.1 x 10^6 cells/mL in 12-well cell culture plates and allowed to reach homeostasis. After 24 hours, Jurkat cells were added at an identical concentration and dosed with 0.3 μm particles (~20 x 10^{12} particles/μL) functionalized with anti-CD3 or anti-CD3/28

antibody. Following 24 hour incubation, the contents of the entire well were collected to analyze viability using a live/dead stain (Invitrogen; Eugene, OR). Calcein AM identified viable cells and ethidium homodimer-1 (EthD-1) stained dead cells. Flow cytometry was used to identify non-viable cancer cells. At least 25,000 events were recorded for each sample. To generate a positive control of dead cells, both HEYA8 and Jurkat cells were incubated in a 60ºC water bath for 30 minutes. When considering our anti-CD3/28 particles, primary human T cells were used to evaluate cytotoxicity. T cell viability following particle treatment was assessed by staining T cells for with APC anti-human CD3 (Biolegend).

Additional cytotoxicity experiments were carried out with conditioned media and with transwell assays. Conditioned media was generated by seeding 0.1 x 10^6 cells/mL in 12-well cell culture plates and then dosing with our optimized particle for 24 hours. The activated Jurkat-conditioned media was harvested and used to treat an equivalent number HEYA8 cells for 24 hours. Transwell experiments were performed by seeding 0.1 x 10^6 HeyA8 cells/mL in 12-well cell culture plates and an equivalent number of Jurkat cells in the transwell. The transwell compartment further contained the optimized particle. Cancer cell cytotoxicity was assessed using the method described above.

HeyA8 cells grown on coverslips and dosed with our particle treatments were imaged using fluorescent microscopy. Cells remaining on the coverslip were stained with the live/dead staining cocktail and imaged at 20x magnification using fluorescence microscopy. 20 images per sample were taken.

Cytotoxicity was also measured by fluorescently staining for the presence of CD107a, a marker of degranulation. Briefly, primary human T cells were dosed with the

relevant treatment groups, incubated for 24 hours, and then assessed for FITC mouse anti-human CD107a (Biolegend) using flow cytometry.

3.2.5 Cytotoxic Co-Culture Interactions

The effect of our particle treatment on T cell and cancer cell interactions was assessed by time-lapse live cell imaging. We plated 1.0 x 10^4 cells/mL HeyA8 cells into 24 well culture plates, allowed them to adhere for 24 hours, and then seeded an equivalent number of Jurkat cells and dosed with our anti-CD3 particles, soluble anti-CD3, anti-CD3/28 Dynabeads, BSA particles, or left untreated. Co-cultures were allowed to incubate for one hour and then the plate was transferred to the BioTek Cytation 3 Imaging plate reader (BioTek Instruments). Bright field images of each well were taken at 10x magnification every three minutes for four hours using the Gen5 software (BioTek Instruments). The plate was shaken after each cycle of imaging to displace non-bound T cells. During this time, cells were maintained at 37 ºC and 5% CO_2. Binding events and duration was quantified by observing differences between frames. A cell was evaluated as bound if the Jurkat cell moved less than 5 μm and the interaction lasted for two or more frames.

3.2.6 Statistical Analysis

Statistical analysis was conducted in Graphpad Prism (La Jolla, CA) using one way or two-way ANOVA to determine significance of variables. Post-hoc Tukey-Kramer HSD testing was performed to determine significance. Data are represented using mean ± SEM.

3.3 Results

3.3.1 Anti-CD3 Particle Functionalization

Anti-CD3 antibody was conjugated onto 0.3 μm, 1.0 μm, and 3.0 μm carboxylated polystyrene particles, as depicted in Figure 1 and described in the methods section, such that all particle sizes displayed equivalent surface saturations at six different labeling densities (Table 1). As shown in Figure 2A, increasing the amount of soluble anti-CD3 antibody in the conjugation reaction resulted in increased protein conjugated to the particle surfaces. The dispersity index of the particles, a measure of particle size uniformity, was assessed by dynamic light scattering (DLS) and all particles exhibited size uniformity post-conjugation (Figure 2B).

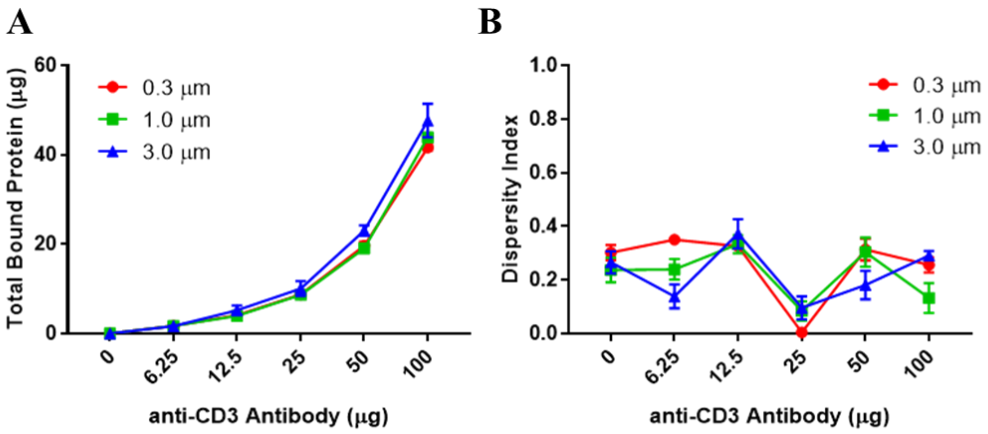

Figure 2: Particle Characterization. (A) Antibody content on particles was calculated by measuring the absorbance of particle supernatants post-conjugation at 280 nm. Data are represented as mean ± SEM, n=4. (B) Anti-CD3 particles were analyzed using DLS to calculate the size heterogeneity of the particle population, n=10.

3.3.2 Anti-CD3 Particles Triggers Granzyme B Secretion

Following conjugation, the effect of anti-CD3 surface density on T cell activation was characterized. We incubated T cells with equal moles anti-CD3 particles at all conjugation densities and found that, in general, delivering particles with increased anti-CD3 surface density resulted in increased GrB release, indicating a higher degree of T cell activation (**Figure 3**). Between the 0 μg anti-CD3 control and the best-performing anti-CD3 surface coverage, we observed nearly a three-fold increase in GrB release for 3.0 ($p<0.05$) and 1.0 μm particles, and a two-fold increase for 0.3 μm particles. However, in all three particle sizes, the particle condition with the highest amount of anti-CD3 antibody did not elicit the greatest amount of GrB secretion. We investigated this observation by characterizing the $F(ab)_2$ region accessibility (the antibody region associated with TCR binding and subsequent T cell activation) using a region-specific fluorescent antibody. As shown in **Figure 3**A, the fluorescent intensity of both region-specific markers increase as the antibody labeling density also increases, until the highest or second-highest conjugation density – 100 μg or 50 μg. This matches the trend observed in the GrB release data. At these high densities, $F(ab)_2$ region availability is reduced; Fc region availability, however, continues to increase at these high functionalization amounts. We determined GrB secretion is positively correlated with F(ab) regions accessibility (Table 2); greater $F(ab)_2$ region availability should elicit increased T cell binding and thus, greater T cell activation. Fc region accessibility is less correlated than the $F(ab)_2$ region. At each particle size investigated, the antibody conjugation density resulting in peak GrB release, similarly resulted in maximal $F(ab)_2$ region availability (**Figure 3**A). This result indicates that T cell activation is dependent on anti-CD3 $F(ab)_2$ region accessibility.

Table 2: Pearson's Correlation Coefficient.

Particle Size (μm)	$F(ab)_2$	Fc
3.0	0.965	0.006
1.0	0.82	0.563
0.3	0.827	0.751

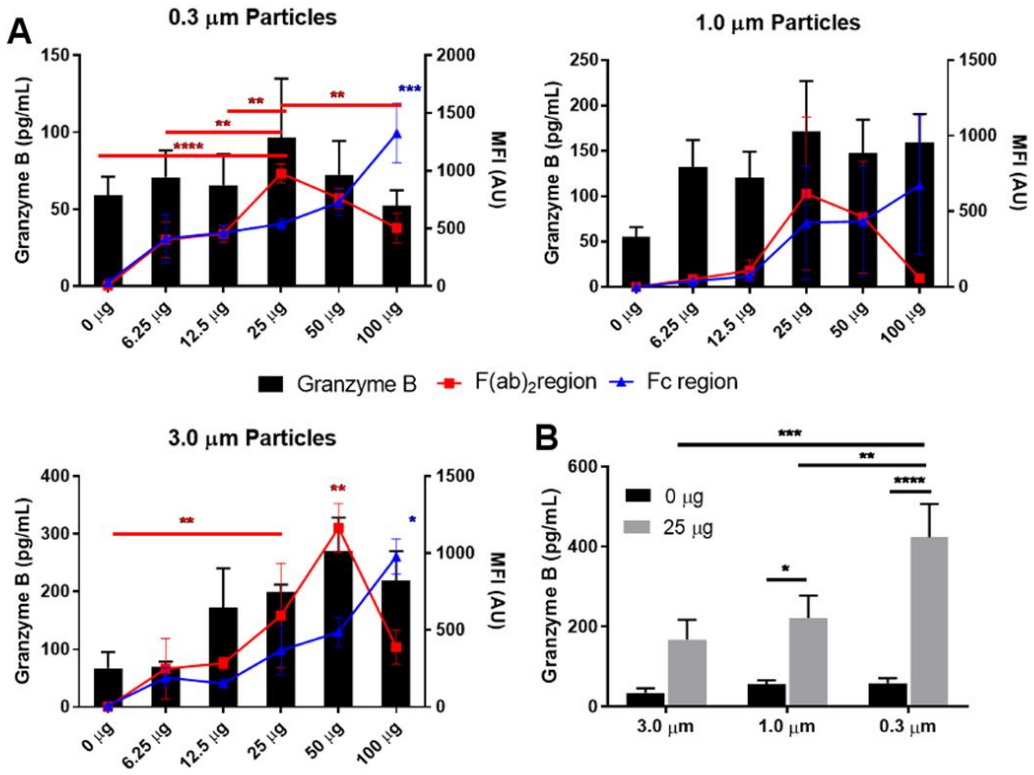

Figure 3: Particle Size and Conjugation Density Effect on Granzyme B Secretion. (A, B) Quantification of granzyme B secretion of 3.0 μm, 1.0 μm, and 0.3 μm particle sizes (A) and at 25 μg anti-CD3 antibody (B). Cells and particles were incubated together for 24 hours before isolating the supernatant and performing ELISA analysis. Data are represented as mean ± SEM, n=6(a), n=5; *p<0.05, **p<0.01, ***p<0.001, ****p<0.0001 (B). Anti-CD3 particles labeled with $F(ab)_2$-specific (■) or Fc-specific (▲) fluorescent secondary antibodies were measured for intensity using flow cytometry. n=3.

In order to de-couple the amount of anti-CD3 antibody delivered via particle from the particle size (as larger particles will present more T cell-activating antibodies than smaller particles, resulting in greater GrB secretion as shown in **Figure 3**A), we treated T cells with an equivalent amount of antibody using 25 μg conjugation densities at all particle sizes. Particle surface area was scaled so that we delivered the same dose originally administered with 3.0 μm particles. When equal amounts of total antibody were delivered, the 0.3 μm particles induced significantly greater GrB secretion than its 0 μg negative control ($p<0.0001$) and also the 3.0 μm and 1.0 μm particle sizes (**Figure 3**B, ***$p<0.001$ and **$p<0.01$, respectively), signifying that particle-elicited T cell activation is size-dependent. The fact that 0.3 μm particles did not elicit significantly greater GrB secretion than its 0 μg negative control until the anti-CD3 antibody dose increased ($p<0.0001$) also demonstrates the dose-sensitivity of T cell activation.

3.3.3 Anti-CD3 Antibody Immobilized on Particles Increase T cell Activation

Based on the above results, 0.3 μm particles emerged as the best performing particles to maximize T cell GrB secretion. The 25 μg condition (approximately 41% surface coverage, as calculated in Table 1) was further selected for continued investigation as the highest anti-CD3 F(ab)-region accessibility was observed for this conjugation density. We hypothesized that anti-CD3 particles would initiate stronger T cell activation responses than soluble antibody due to the multivalent activation signal presented by our particles. Further comparison of commercially available anti-CD3/28 Dynabeads was investigated. The proliferative effect of anti-CD3 particles on T cells was determined by measuring the depletion of CSFE – a tracer molecule that covalently binds inside cells and decreases in fluorescent intensity with each subsequent cell division. After incubating

primary human T cells with particles for five days, treatment with anti-CD3 particles results in significantly higher proliferation than untreated, BSA particle-, and soluble anti-CD3 antibody- treated T cells, as represented in **Figure 4**A. The higher proliferation is reflected by the significantly lower percentage of first generation cells (*p<0.05, ***p<0.001) and greater percentage of third generation cells (#p<0.001, ****p<0.0001). Anti-CD3/28 Dynabeads elicited similar proliferative responses to anti-CD3 particles with no significant differences.

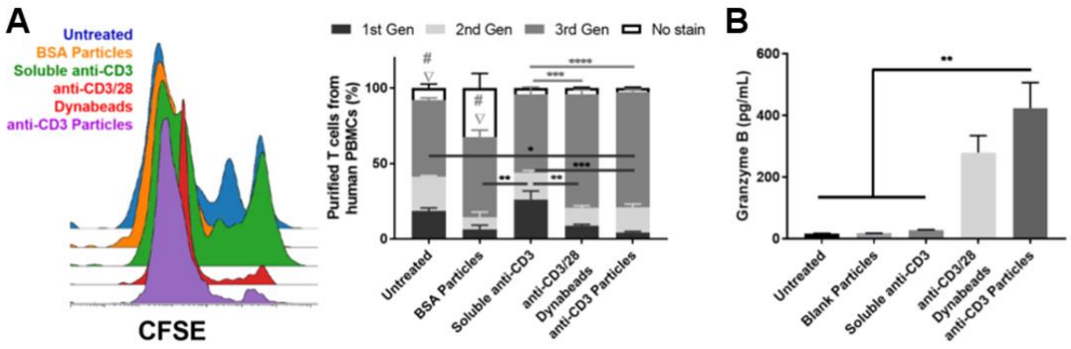

Figure 4: T cell Activation Responses by Particles. (A) Human primary T cell proliferation following incubation with anti-CD3 particles, commercial antibody activators, or negative controls for 5 days. Data are mean ± SEM, n=3; *p<0.05, **p<0.01, ***p<0.001, ****p<0.0001, ∇ = p<0.001 to anti-CD3/28 Dynabeads, # = p<0.001 to anti-CD3 particles. (B) anti-CD3 particle-elicited granzyme b secretion was compared to soluble antibody and commercially standard activation particles, n=3.

We then investigated the ability of our anti-CD3 particles to trigger GrB release compared to soluble antibody and commercial anti-CD3/28 Dynabeads. Activation from the anti-CD3 particles were determined by quantifying the concentration of GrB secreted using an ELISA immunoassay, and unconjugated particles and untreated cells were used as negative controls (**Figure 4**B). The results indicate that anti-CD3 particles and commercial anti-CD3/28 beads caused significant T cell activation (p<0.01); in contrast, an equivalent dose of soluble anti-CD3 antibody elicited substantially reduced GrB

release. These results indicate that immobilization of activating molecules enhances their effect, likely due to multivalent interactions between the particles and cells.

3.3.4 Anti-CD3 Functionalized Particles Provoke Significant T cell Cytotoxicity to Cancer Cells

Cytotoxic death of cancer cells via cytolytic granule release relies on the strength of the T cell activation response, so ensuring particle-elicited cytolytic granule secretion from T cells was deadly to cancer cells was critical. Cancer cells and Jurkat cells were incubated together and cancer cell death assessed after treatment. The results in Figure 5A show that anti-CD3 particles caused a doubling of percentage of cancer cell death ($p<0.0001$) – approximately 60% cytotoxicity—as opposed to less than 30% observed following treatment with negative controls. Lower levels of T cell mediated cancer cell cytotoxicity was also observed for the commercial anti-CD3/28 particles and the equivalent dosage of soluble anti-CD3 antibody, compared to anti-CD3 particles. Images of cancer cells exposed to T cells and treatments are shown in Figure 5B. We observed extensive detachment, altered morphology, and dramatically fewer alive-stained cells compared to soluble antibody and negative controls, which strongly indicates that anti-CD3 particles can elicit a powerful cytotoxic effect against cells. We calculated the correlation between cancer cell cytotoxicity and the previously quantified GrB secretion data and found these two data sets displayed a positive correlation, demonstrating an association between the extent of T cell activation and the degree of cytotoxicity (Figure 6).

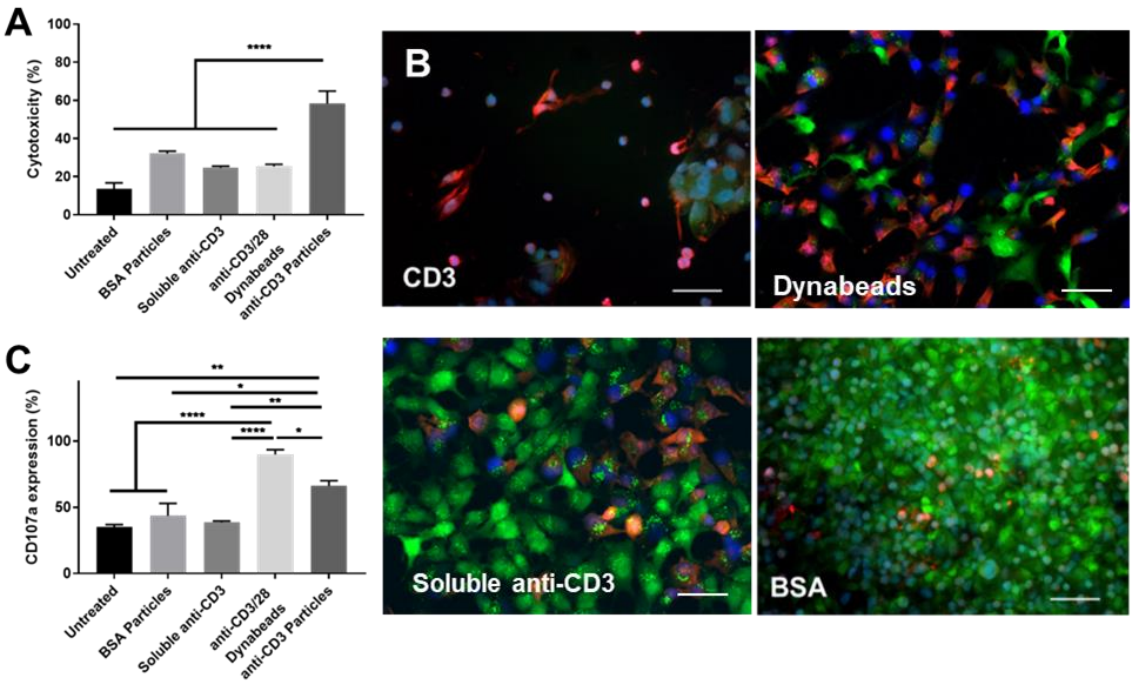

Figure 5: T Cell Cytotoxicity. (A) Co-cultures were treated with T cells and various treatments. Cancer cell death from T cell cytotoxicity was assessed by measuring live/dead fluorescent stain with flow cytometry. n=6. (B) Cancer cells were seeded onto coverslips before co-incubation with particles and T cells. Following 24 hours, cells were fluorescently labelled with live/dead stain. Representative images of each condition are shown. n=4, scale bar = 200 μm. (C) CD107a expression was quantified in human primary T cells isolated from peripheral blood using flow cytometry to measure degranulation. Data are represented as mean ± SEM, n=4; *p<0.05, **p<0.01, ***p<0.001, ****p<0.0001.

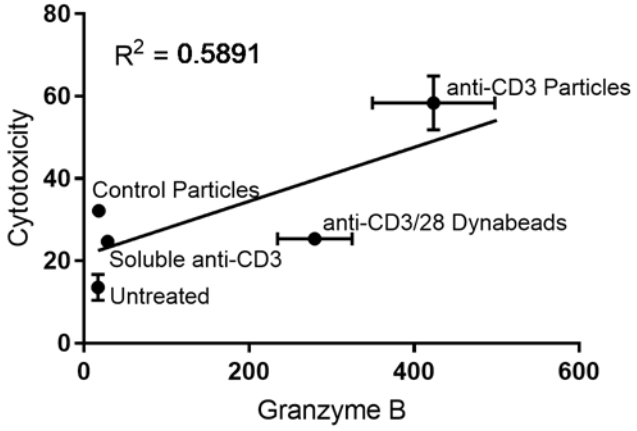

Figure 6: Correlation between Granzyme B Secretion and Cytotoxicity. Values of cytotoxicity (%) and Granzyme B (pg/mL) were plotted against each other for each condition tested for 3.0 μm particles.

We measured the expression of CD107a using primary human T cells. Soluble anti-CD3 antibody did not elicit a greater percentage of cell degranulation than our negative controls (Untreated and BSA particles) but were significantly less than anti-CD3/28 Dynabeads ($p<0.0001$) and our anti-CD3 particles ($p<0.01$). Our anti-CD3 particles and commercially available Dynabead treatment also resulted in significantly greater degranulation than negative controls; however, the percentage of cell degranulation was higher post-treatment with Dynabeads in comparison to our anti-CD3 particles ($p<0.01$). This result suggests that that although our anti-CD3 particles are eliciting fewer cytotoxic responses from T cells compared to anti-CD3/28 Dynabeads (Figure 5C), the resulting cytotoxicity is greater in intensity, causing higher cancer cell death (Figure 5A-B).

While the effectiveness of this treatment is evident, there is no specificity in regards to the cells killed by anti-CD3 particles, as shown in Figure 7. Anti-CD3 particles

elicited significantly higher cytotoxicity than no particles or the BSA particle control for all cell lines tested, including the "healthy" hDF cell line ($p<0.001$). These results suggest that the T cell activation response generated by our anti-CD3 particles is sufficiently robust and may be used ubiquitously to treat any cancer. However, these data also indicate that off target effects would be a major limitation of this approach.

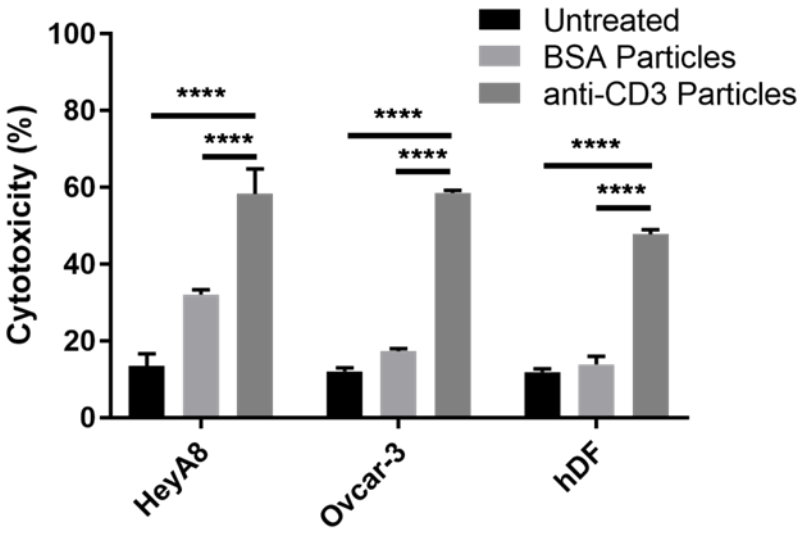

Figure 7: Anti-CD3 Particle elicits Non-Specific Cell Death. Three different cells lines, two ovarian cancer (HeyA8 and Ovcar-3) and one immortalized cell line from healthy dermal fibroblasts were dosed with anti-CD3 particles using identical conditions. Data are represented as mean ± SEM; n=6; ****$p<0.0001$.

Increased cytotoxicity is not exclusive to cancer cells. When we evaluated T cell viability following particle activation and incubation with cancer cells, T cells were significantly less viable after anti-CD3 particle stimulation, compared to Dynabeads, soluble anti-CD3 antibody, and negative controls ($p<0.0001$). Dynabeads elicited a slight decrease in viability compared to untreated T cell co-cultures ($p<0.05$). The increase in T cell death following activation, particularly after treatment with anti-CD3 particles, is likely two-fold: 1) activation-induced cell death due to repeated stimulation, and 2) the

release of cytolytic granules that caused cancer cell death (**Error! Reference source not ound.**), also lead to T cell death. The magnitude of T cell death following anti-CD3 particle treatment is undeniably tied to the stronger activation responses we observed in Figure 1F, in comparison to Dynabeads.

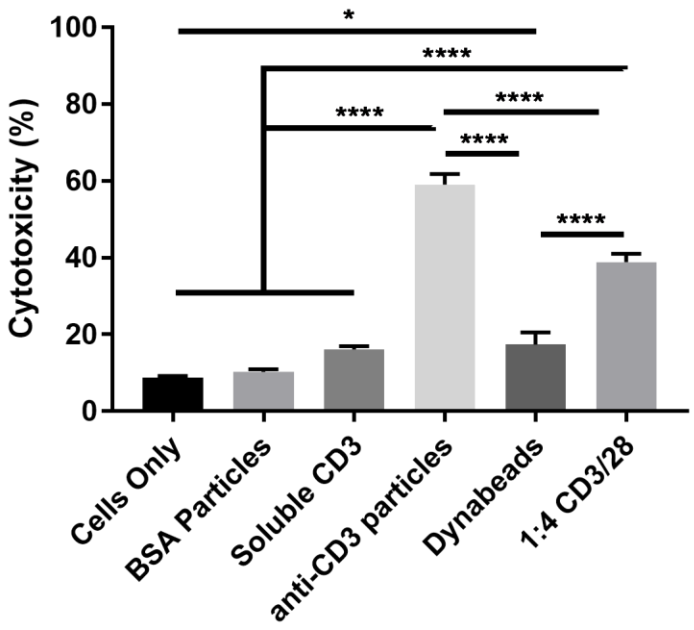

Figure 8: Jurkat cell viability. Co-cultures were treated with T cells and various treatments. T cell death from cytolytic granule release was assessed by measuring live/dead fluorescent stain with flow cytometry. Data are represented as mean ± SEM, *p<0.05, ****p<0.0001, n=6.

3.3.5 Unencumbered Interaction of T cells with Cancer Cells is Critical for Cytotoxicity

As T cells typically kill cancer cells by directly engaging via TCR—MHC-I interactions, we examined both the necessity of T cell and cancer cell interactions and whether our anti-CD3 particles promote them. The extent to which we restrict T cell-cancer cell interactions, and its effect on cytotoxicity, was investigated using three different cytotoxic experimental designs: conditioned media, transwell, and direct co-culture as

described in Figure 9. This result shows that direct co-culture elicited higher levels of cytotoxicity than both the conditioned media ($p<0.001$) and transwell ($p<0.01$) conditions, demonstrating that the ability of Jurkat cells to freely interact and come into close proximity with cancer cells is critical for significant cytotoxicity. Additionally, a delayed exposure to cytolytic granules reduced cancer cell death, although not significantly, as shown in Figure 10. This is unsurprising; the T cell cytotoxic milieu is dynamic, with unsteady secretion of activation products (Figure 10).

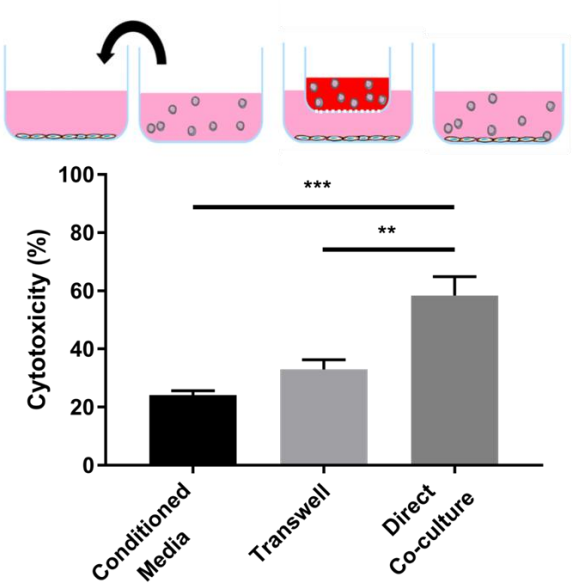

Figure 9: Experimental Design effects on Cytotoxicity. Three experimental design conditions–conditioned media, transwell, and direct co-culture–were assessed for effective cytotoxicity. Schematics of the set-ups are depicted above the graph. Data are represented as mean ± SEM, n=5; **p<0.01, ***p<0.001.

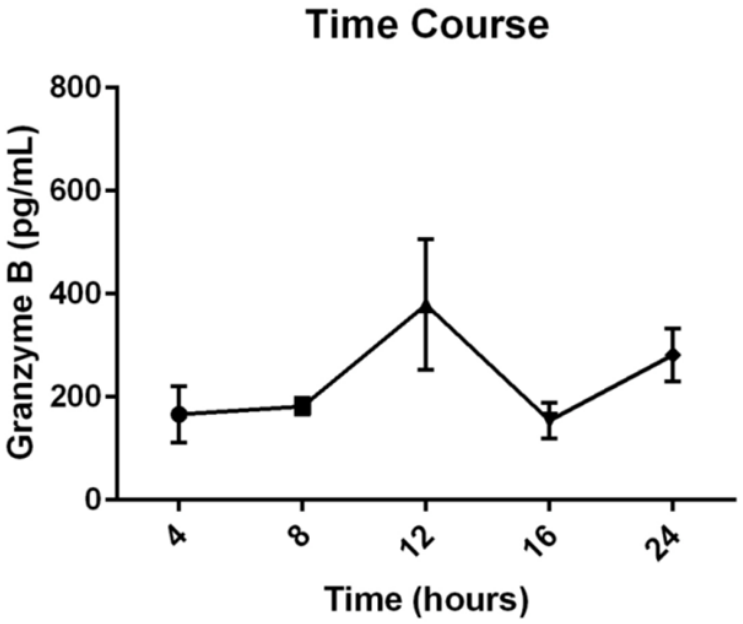

Figure 10: Granzyme B Secretion varies over 24 hours. Jurkat cells were activated using anti-CD3 particles and, over the course of 24 hours, conditioned cell media samples were taken, flash frozen, and then measured for GrB content at the end of the experiment. Data are represented as mean ± SEM, n=5; data not significant.

3.3.6 Inclusion of anti-CD28 onto anti-CD3 Functionalized Particles Amplifies T cell Activation

We tested the effect of adding co-stimulation by functionalizing particles with anti-CD3 and anti-CD28 antibody on T cell activation. We investigated five different particle conditions: 1:4 anti-CD3/28, 1:2 anti-CD3/28, 1:1 anti-CD3/28, 2:1 anti-CD3/28 and 4:1 anti-CD3/28 antibodies, and assessed the effect on cell targeting and proliferation on primary human T cells. Figure 11A shows that 1:2 anti-CD3/28 particles bound to significantly fewer particles than any other condition ($p<0.01$ at least). Additionally, following five day incubation with all particle conditions, 1:2 anti-CD3/28 ($p<0.01$) and

1:4 anti-CD3/28 particles ($p<0.05$) elicited higher proliferation than 1:1 anti-CD3/28 particles (Figure 11B).

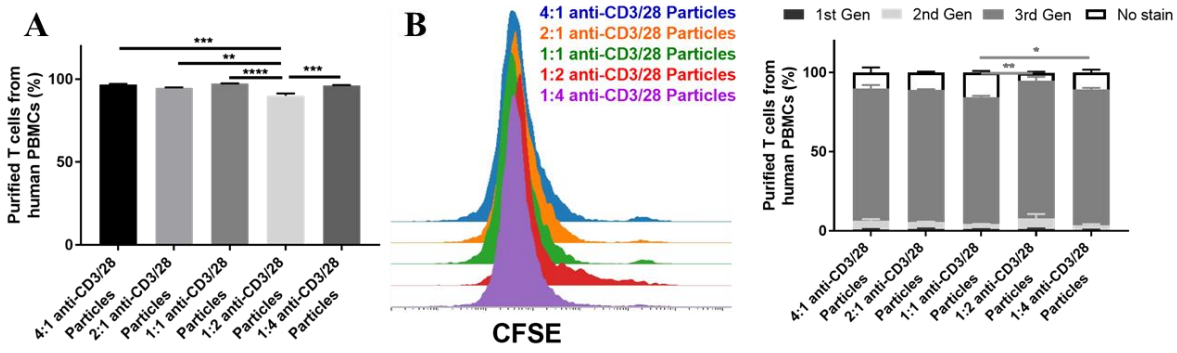

Figure 11: Effect of anti-CD3: anti-CD28 Antibody Ratios on T cell Binding and Proliferation. (A) Primary human T cells were incubated with various formulations of CD3/28 particles and the percentage of cells with particles bound was measured using flow cytometry. Data are mean ± SEM, n=3; **$p<0.01$, ***$p<0.001$, ****$p<0.0001$. (B) T cells were stained with CFSE and incubated with functionalized particles for five days before analyzing using flow cytometer. n=4; *$p<0.05$.

Based on our findings presented in **Figure 4**, we hypothesized that increased proliferation response was a result of increased particle interactions with T cells. As shown in Figure 12A, incubating primary human T cells with our particles (anti-CD3, anti-CD28, and 1:4 anti-CD3/28) led to significantly increased binding compared to anti-CD3/28 Dynabeads ($p<0.0001$) or our negative controls ($p<0.0001$). The effect of these interactions was further examined by measuring cell proliferation following five day incubation (Figure 12B). 1:4 anti-CD3/28 particles elicited greater proliferation than anti-CD3/28 Dynabeads ($p<0.01$) and anti-CD3 particles ($p<0.001$). Unexpectedly, there were no differences between anti-CD28 particles and 1:4 anti-CD3/28 particles.

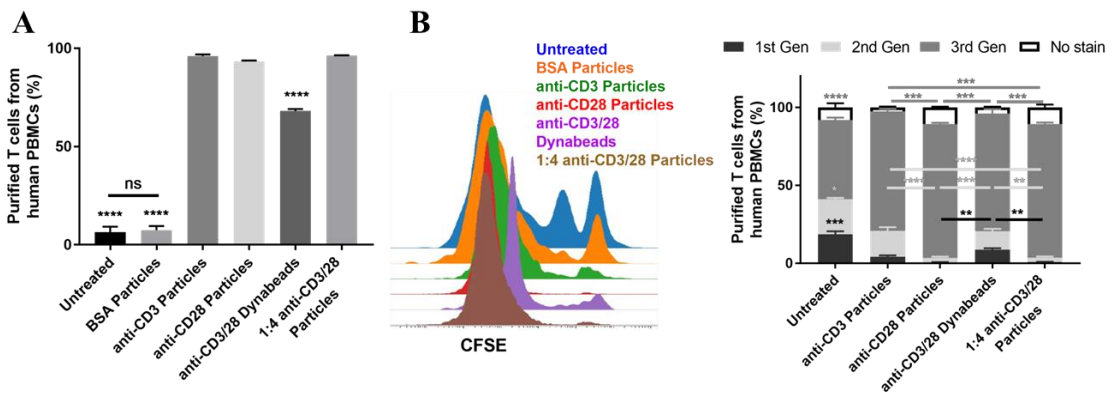

Figure 12: T cell Activation from anti-CD3/28 Particles. (A) T cells were incubated with anti-CD3, anti-CD28, 1:4 anti-CD3/28 particles and anti-CD3/28 Dynabeads and measured for the percentage of cells with particles bound using flow cytometry. Data are mean ± SEM, n=3; ****p<0.0001. (B) T cells were stained with CFSE and incubated with functionalized particles for five days before analyzing using flow cytometer. n=4, **p<0.01, ***p<0.001.

The effect of our particle treatments on cytotoxic behavior was determined by measuring the CD107a expression using flow cytometry. CD107a expression was significantly increased as a result of anti-CD3/28 Dynabeads ($p<0.001$) compared to anti-CD3, anti-CD28, and anti-CD3/28 particles, which displayed no difference between these conditions and only elicited a significantly greater percentage of cells expressing CD107a than untreated primary T cells (Figure 13A, $p<0.0001$). The direct effect of including anti-CD28 antibody on cytotoxicity was determined by incubating co-cultures of primary human T cells and cancer cells with anti-CD3, anti-CD28, 1:4 anti-CD3/28 particles or negative controls (Figure 13B). Our particle formulations that included anti-CD3 antibody elicited significant primary T cell cytotoxicity in comparison to the untreated control ($p<0.05$) and further, treatment with the 1:4 anti-CD3/28 particle resulted in significantly more cancer cell death than anti-CD3/28 Dynabeads ($p<0.05$). Additionally, although not significant, anti-CD3 particles showed increased cytotoxicity compared to

anti-CD3/28 Dynabeads (p=0.0819) that could possibly become significant with an increase in sample size. These results suggest an interesting phenomenon in which anti-CD3/28 Dynabeads cause more cells to release granules, but do not result in higher cytotoxicity – possibly, the magnitude of degranulation elicited from these commercial particles is less than that from our particle formulations. Taken together, these data show that while including anti-CD28 antibody on our particles has no impact on T cell binding or CD107a expression – and only slightly improved proliferation – this inclusion is critical for enhanced T cell cytotoxic responses.

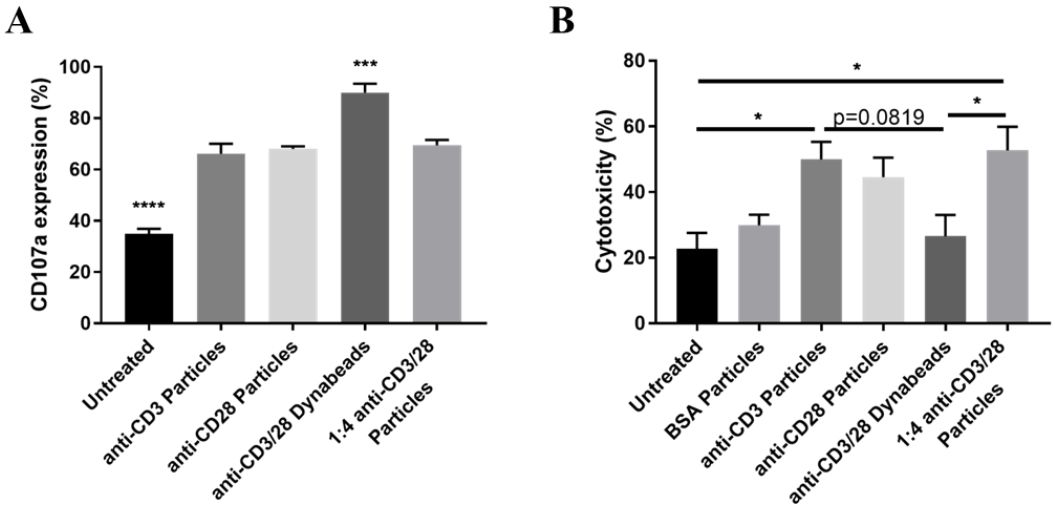

Figure 13: T cell Cytotoxicity from anti-CD3/28 Particles. (A, B) Co-cultures of T cells and cancer cells were treated with various particle conditions. (A) CD107a was stained using alexa fluor 488 anti-human CD107a and measured using flow cytometry. Data are represented at mean ± SEM, n=6; ***p<0.001, ****p<0.0001. (B) Cytotoxicity was measured via live/dead flowmetric assay. n=4; *p<0.05.

3.4 Discussion

Particles are routinely and extensively used by researchers for T cell activation in a wide variety of applications, including selecting and/or expanding antigen-specific T cells(169,

175, 194). Density of cellular signals and particle size critically affect the presentation of molecular signal(167, 195) and thus how T cells initiate activation and cytotoxic responses. Particle size and molecular density can induce tunable cellular behaviors(167) and modulate the immune system(167) *in vitro*; therefore, investigating the effect of particle size and molecular surface saturation on signal presentation offers valuable insight into modulating T cell processes. In this study we examine how presentation of molecular signals affects the biological activity of T cells to maximize activation and downstream cytotoxic effects.

Anti-CD3 antibody is widely used to non-specifically activate T cells, both immobilized and in soluble form, by engaging the TCR/CD3 complex to cause downstream induction of effector cell activation, proliferation, and cytotoxicity(196). Our results show that this activation response can be modified through changes in the particle size and conjugation densities. We successfully conjugated carboxylated particle surfaces using EDC with varying surface densities of anti-CD3 antibodies (Figure 1, Figure 2, Table 1). Antibodies are comprised of a highly conserved Fc region and two F(ab) regions which are responsible for binding specific antigens and thus are highly variable(170, 197). The Fc region is more hydrophobic than the F(ab) regions and will typically orient closest to the particle surface even with site non-specific conjugation schemes – orienting the $F(ab)_2$ region outward(198, 199) to engage the TCR and initiate T cell activation. Increasing the conjugation density of anti-CD3 antibody should result in greater TCR engagement and thus increased activation responses. However, we unexpectedly determined that highest densities of anti-CD3 antibody resulted in less GrB secretion, and ostensibly, less T cell activation, as shown in **Figure 3**A. We postulate that

this reduced activation is related to the reduced accessibility of the anti-CD3 F(ab) regions; we determined that $F(ab)_2$ region availability positively correlated with T cell activation (Table 2). As greater amounts of $F(ab)_2$ region were available, greater concentrations of GrB were measured. The reasons for this decreased accessibility at high functionalization amounts are not clear. Previous studies in immunosorbance observed high immobilization densities of proteins resulted in reduced specific activity of that protein, most likely due to steric hindrance or slight denaturing due to overly dense antibody packing(200), to which the more conserved Fc antibody region is less susceptible. Additionally, the non-specific conjugation scheme may result in instances of misorientation that amplify at higher conjugation densities. This possible denaturation or misorientation may explain why the anti-CD3 Fc region availability continues to increase as the conjugation density also increases (**Figure 3**A). Additionally, our study investigates anti-CD3 antibody accessibility to large, whole-protein antigens, either fluorescent secondary antibodies or T cell receptor complexes, and anti-CD3 antibody accessibility to such antigens is innately low and thus susceptible to binding site obstruction due to steric hindrance and misorientation(195). We speculate that these factors contribute to the corresponding GrB secretion and $F(ab)_2$ region accessibility peaks at 25 μg (0.3 and 1.0 μm) or 50 μg (3.0 μm), and the restricted $F(ab)_2$ region availability at the higher particle surface coverages. From these data, we can conclude that maximal T cell activation will most likely occur when the anti-CD3 antibody $F(ab)_2$ region is most available for interaction with immune cells.

Delivering equivalent anti-CD3 antibody on particles of different sizes reveals a clear size-dependency of T cell activation, in which small (0.3 μm) particles produced

significantly higher GrB concentrations from T cells than larger (3.0 μm and 1.0 μm) particles (**Figure 3**B). Smaller particles have been shown to bind more frequently to cells(201), which would increase activation in our application and produce higher immune responses than larger particles(167, 171). Our data are consistent with prior research that show larger particles can induce higher T cell activation responses(202), but when equivalent amounts of anti-CD3 are controlled, the trend reverses. This could be a result of the higher curvature innate to the geometry of smaller particles or increased number of initiation sites on the cell. This higher curvature of 0.3 μm particles may result in greater accessibility of TCR binding region of anti-CD3 antibodies to TCR/CD3 complexes on T cells, especially given the large antigen size(167, 195), and therefore elicit greater T cell activation. This result demonstrates that dosing T cells with 0.3 μm and 1.0 μm particles did not result in significantly more GrB release than their respective 0 μg controls at lower concentrations (Figure 2A). Therefore we can conclude that smaller particles trigger greater T cell activation at relevant doses.

Based on these data, we selected to use the 0.3 μm particle conjugated with 25 μg of anti-CD3 antibody (corresponding to 41% particle surface saturation, Table 1) for further study. Greater GrB secretion was measured when particles were used to deliver anti-CD3 or anti-CD3/28 antibody to T cells, compared to equivalent soluble antibody, most likely due to the dense presentation of stimulating molecules that are present on particle surfaces. It is possible for these particles to bind strongly to T cells through multivalent interactions(166), thus eliciting a high immune response (2, 15, 18); whereas soluble anti-CD3 antibody will activate T cells only through many mono- or bivalent interactions from numerous antibodies, resulting in less crosslinking and thus less

activation. This multivalent advantage leads not only to greater activation (**Figure 4**), but greater cytotoxicity; cytotoxicity studies determined that anti-CD3 particles induced significantly greater T cell cytotoxicity compared to equivalent dosing with soluble antibody (Figure 5). The correlation between T cell activation and downstream cytotoxicity was calculated (Figure 6) and we found a positive association between the two data sets, indicating that greater T cell activation may lead to similarly higher cytotoxicity. Interestingly, while there was no significant difference in the amount of GrB secreted by T cells or the proliferation of primary human T cells following incubation of anti-CD3/28 Dynabeads and anti-CD3 particles (**Figure 4**), we found Dynabead treatment resulted in significantly less cytotoxicity than anti-CD3 particles (Figure 5A-B). However, primary T cell CD107a expression – a marker of degranulation – was significantly increased on Dynabead-treated cells compared to our anti-CD3 particles (Figure 5C). The mechanism behind these results – similar GrB secretion, decreased cytotoxicity, and higher CD107a expression compared to our anti-CD3 particles – has not been fully elucidated, but particle size, unknown antibody labeling density and patterning, and dosing likely contribute to the observed effect. Anti-CD3/28 Dynabeads are 15x larger than our optimal anti-CD3 particles (**Figure 3**B) and, based on our previous findings regarding particle size, should result in less immunogenicity. Furthermore, T cells were dosed with Dynabeads according to the manufacturer's protocol, whereas anti-CD3 particle doses were optimized based on an optimization experiment (Figure 14). Although not likely, it is possible that including co-stimulation with anti-CD28 antibody on Dynabeads reduces the amount of anti-CD3 antibody presented, and therefore reduces cytotoxicity in comparison to anti-CD3 only particles.

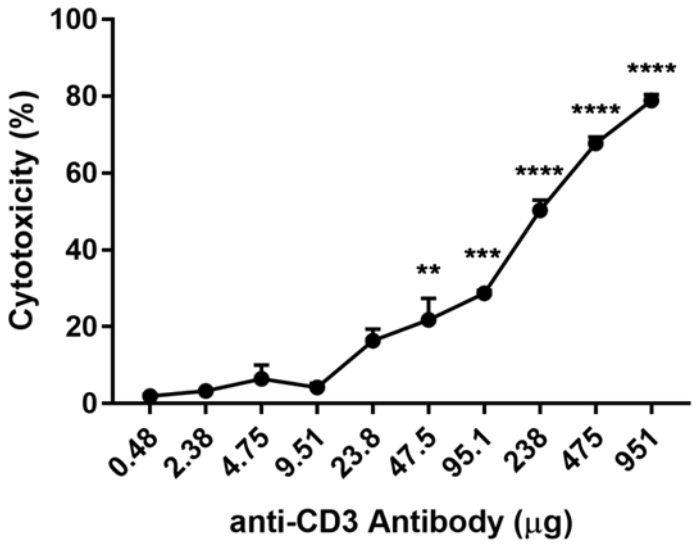

Figure 14: Particle Dosing. Cultures of Jurkat and cancer cells were dosed with increasing amounts of anti-CD3 particles and then assessed for cytotoxicity using a live/dead assay. Data are represented as mean ± SEM, n=4; **p<0.01, ***p<0.001, ****p<0.0001.

To explore the effect of our anti-CD3 particles have on T cell and cancer cell interactions, a necessity for conventionally native T cell cytotoxicity, three different experimental designs were examined: conditioned media, where cancer cells are treated with the supernatant of particle-activated cytotoxic T cells; transwell, in which a porous membrane separates cancer and T cells with anti-CD3 particles; and direct co-culture, in which particles and all cell types are present in the same culture space to freely allow physical contact between cancer and immune cells (Figure 9). The designs allow for different degrees of interaction between cell types, over time and distance. Direct co-culture experiments resulted in significantly more cancer cell death than conditioned media and transwell constructs, indicating that the freedom for T cells to interact with cancer cells is critical for the significant killing of cancer cells. The necessity of cell interactions for effective cytotoxicity is not surprising; cytotoxic T cells become activated

in the native immune milieu when bound to target cells and, once activated, secrete cytolytic granules proximally and with high directionality across nanometers of extracellular space(203). Cancer cells then receive a highly localized and concentrated dose of perforin and granzymes, thereby initiating an apoptotic signaling cascade. Without this concentrated dose, as demonstrated with conditioned media and transwell conditions, significant cytotoxicity is not likely. It is possible that the need for a highly concentrated dose is why Dynabeads elicit less cancer cell death, despite similar T cell activation responses (**Figure 4**) and evidence of high T cell cytotoxicity (Figure 5C); the larger Dynabead may separate the T cell and its cognate cancer cell such that it interferes with cytolytic granule diffusion, resulting in lower cytotoxic cancer cell death. Further studies will be necessary to investigate this hypothesis. We can conclude, however, that the ability of our anti-CD3 particles to promote close T cell interaction with cancer cells is crucial for effective cytotoxicity against cancer cells.

Anti-CD3 antibody has been studied extensively alone and with anti-CD28 antibody as a co-stimulatory molecule due to its ability to activate T cells non-specifically. However, using anti-CD3 antibody to non-specifically activate T cells has been shown to be problematic; without a co-activation signal (e.g. CD28), anti-CD3 only activated T cells will usually become less functional or undergo apoptosis(192). To stimulate T cells *in vitro*, researchers typically use commercially available anti-CD3/28 beads (in which the labeling density is proprietary) or functionalize with anti-CD3 and anti-CD28 antibodies in equivalent amounts(175, 190), resulting in 1:1 anti-CD3/28 particles. This ratio is common practice due to the establishment that following activation through the TCR/CD3 complex, CD28 will associate with this macromolecule to promote

cell survival and upregulate cell metabolism on a one-to-one basis(188, 192). However, our results indicate that a 1:1 ratio of anti-CD3/28 antibodies does not elicit the highest amount of primary T cell proliferation (Figure 11B); cells incubated with particles containing higher ratios of anti-CD28 antibody to anti-CD3 antibody showed significantly increased proliferation compared to 1:1 anti-CD3/28 particles ($p<0.05$ at least). T cell binding studies further revealed that 1:4 anti-CD3/28 particles bound significantly more T cells than 1:2 anti-CD3/28 particles (Figure 11A). From these results, we selected 1:4 anti-CD3/28 particles for continued study. It should be noted that we investigated these particle effects on primary T cells, not only CD8+ T cells, so it is possible that a different ratio is more appropriate for CD8+ T cells only. However, given that the absolute values of our proliferation and T cell targeting assays for all particle conditions were fairly similar, we are confident that the effect of a precise CD8+ T cell anti-CD3/28 ratio should not be so large and distinct that our studies using a particle we optimized for T cells are divergent.

While we had previously observed similar proliferation responses from human primary T cells due to anti-CD3 particle or anti-CD3/28 Dynabead treatment (**Figure 4**B and Figure 12B), anti-CD28 antibody significantly increased proliferation; this was observed for both 1:4 anti-CD3/28 and anti-CD28 particles (Figure 12B). The ability of anti-CD28 only particles to enhance proliferation is not well researched, but previous studies have shown that extensive CD28 crosslinking can induce T cell activation/proliferation(204, 205). However, this crosslinking did not translate into cytotoxicity (Figure 13). The inclusion of anti-CD28 antibody onto our anti-CD3 particles does enhanced cytotoxicity though; 1:4 anti-CD3/28 particles elicited

significantly greater cytotoxic cancer death than anti-CD3/28 Dynabeads or the untreated control whereas anti-CD3 particle treatment resulted in increased cytotoxicity compared to untreated cells only (Figure 13).

Interestingly, anti-CD3, anti-CD28, and 1:4 anti-CD3/28 particles bound to more T cells but resulted in significantly fewer cells expressing CD107a than did anti-CD3/28 Dynabeads, which bound to significantly fewer cells (Figure 12A and Figure 13A). This suggests that anti-CD3/28 Dynabeads activate T cells more efficiently than our particles (anti-CD3, anti-CD28, and 1:4 anti-CD3/28). The reason for this inefficiency is unclear, but may be size- or patterning- related. Further binding studies are necessary.

Understanding how particle size and molecular density of anti-CD3/28 antibodies conjugated to particles are important not only for preclinical T cell activation and expansion studies, but also for all particle-based immunotherapies, such as artificial antigen presenting cells(115). We anticipate our findings can translate to any biomaterial surface used to non-specifically or specifically stimulate T cells. These results are relevant not only for the *in vitro* activation of T cells, but they are also important for understanding the downstream effects following non-specific cytotoxic T cell activation by particles. While selecting and expanding T cells can be important for its own end, the functionality of those T cells against relevant target cells can be improved by optimizing the T cell proximity to target cells for effective cytotoxicity. Future investigations into the specific activation of T cells – replacing anti-CD3 with antigen or antigenic peptide presented in the context of MHC – will help us to better understand how the conclusions reached here effect antigen-specific T cell stimulation. Furthermore, the inclusion of cancer-binding moieties will also be examined. In summary, our optimized anti-CD3/28

particles improve upon existing and commercial methods for T cell activation and may be a powerful addition to the rational biomaterial design library for T cell cytotoxicity.

3.5 Conclusions

We have successfully demonstrated the effect of particle size, molecular density, and activating molecule on T cell activation and cytotoxicity. Decreasing particle size and optimizing surface coverage results in increased GrB release. T cell activation and cytotoxicity is also dependent on the activating molecule(s). Cytotoxicity studies showed that anti-CD3 particles were more effective than soluble antibody alone and demonstrated that immune cell proximity to cancer cells was responsible for cancer cell death. We conclude that 1:4 ratio of anti-CD3/28 displayed on small 300 nm particles represent a highly promising platform for T cell activation, expansion, or cytotoxicity in which specificity may be included with the substitution of anti-CD3 antibody for antigenic molecules.

CHAPTER 4. CHARACTERIZING THE BIOPHYSICAL T CELL ACTIVATION RESPONSE

4.1 Introduction

Immunotherapeutic treatments are increasingly showing great potential as effective cancer treatments(12, 98). Central to these strategies is reestablishing immune cell function within the tumor microenvironment; although immune cells regularly migrate to the tumor site, they cannot always mount a successful immune response due to immunsuppressive signals secreted and expressed by cancer cells(19). Artificial antigen presenting cells (aAPC) – particle- or particle-like platforms that mimic antigen presenting cells (i.e. dendritic cells) – are being investigated as a possible therapeutic to initiate an immune response to cancer(161, 175). The most common iteration of this overall strategy involves activating T cells, usually CD8+ T cells(173, 179). The activation of these cytotoxic T cells causes cytoltyic granule secretion. These granules contain perforin and various granzymes, which then trigger apoptosis in the targeted cancer cell. Thus, by activating CD8+ T cells within the tumor environment, an immune system driven anti-cancer response can eradicate the tumor. aAPCs have shown pre-clinical success in this area(173, 179). Recent publications have emphasized aAPCs that are nanoscale(175) and biomimetic(181, 206); these strategies have resulted in robust T cell responses, including proliferation and expression of different activation markers(162, 181, 206, 207). However, while activation markers such as proliferation, granzyme b secretion, and even immune synapse formation have been examined, researchers have not yet examined the effect of aAPCs on the biophysical activation response of T cells.

T cell activation affects cell motility, migration, and stiffness, among others – all of which are driven by changes in the cytoskeletal structure of the cell(208-210). Cytolytic granule secretion by cytotoxic T cells, especially, is only possible with a dynamic and responsive cytoskeleton(211). When CD8+ T cells are activated, immune synapses form due to extensive actin remodeling; signaling and adhesion molecules, such as CD3, CD8, LFA-1, and ICAM-1, are clustered together, so that activation signals are more strongly transduced and sustained(212). Microtubules rearrange, and the microtubule organizing center (MTOC) translocates to the immune synapse to guide cytolytic granules to release in a highly directional manner toward its bound cognate cell(211, 213). Immune synapse formation by activated T cells introduces asymmetry within the cell, concentrating actin, microtubulin, and various signaling proteins within particular areas of the cell, instead evenly distributed over the whole cell.

The immune synapse has been extensively studied and has been implicated in a variety of processes, including TCR signaling(209), cytokine or cytolytic granule release(211), and T cell polarity(214). However, the broader implications of T cell activation from particle-based immunotherapies and the subsequent formation of the immune synapse on mechanics of the whole cell is not fully understood nor well studied. Whole cell mechanics – stiffness, viscosity, motility – can give insight into cell behavior, such as migration, or be used as phenotypic biomarker. In this study, we evaluated the biomechanical response to our 0.3 μm anti-CD3 and anti-CD3/28 particles. We investigated immune synapse formation and correlated it with T cell polarity resulting from cytoskeletal rearrangement. This cytoskeletal remodeling also seems to be responsible for the measured cell softening and faster relaxation time we observed from

AFM studies. T cell activation reduced cell motility but increased cancer cell binding, indicating this treatment would be most effective within the tumor microenvironment.

4.2 Materials and Methods

4.2.1 Cell Culture

Primary human CD8+ T cells were cultured in RPMI 1640 cell culture media (ATCC, Manassas, VA) supplemented with 10% fetal bovine serum (FBS; Atlanta Biologicals; Norcross, GA) and 1% penicillin-streptomycin (Sigma Aldrich, St. Louis, MO) and maintained between 1 x 10^5 and 1 x 10^6 cells/mL. CD8+ T cells were isolated from peripheral human blood using EasySep CD8+ T cell Isolation Kit (Stem Cell Technologies; Vancouver, Canada). The human ovarian cancer cell lines HeyA8 was gifted from the McDonald laboratory (Georgia Institute of Technology, Atlanta, GA). HeyA8 monolayers were cultured using the same cell growth medium as the T cells were passaged after flask confluency reached at least 70%. All cells were maintained at 37 °C with 5% CO_2. All cells used were below passage 30 with viability assessed using trypan blue.

4.2.2 Particle functionalization

0.3 μm silica particles (Bangs Laboratories, Fishers, IN) were conjugated with anti-CD3, anti-CD3/28 antibodies (Biolegend, San Diego, CA), or BSA (Sigma Aldrich, St Louis, MO) as a control, using APTES silanization, as described previously(215). Briefly, silica particles were washed with acetone, and then incubated for two min at room temperature with a 2% APTES (Sigma Aldrich) solution. Particles were then washed twice with dd

H_2O and heated to complete the silanization process. Particles were then incubated with 1 mg/mL anti-CD3 and anti-CD28 antibodies for 1 hour at room temperature on an end-over-end spinner. Finally, particles were washed twice with PBS and stored at 8 ºC.

4.2.3 Immune synapse formation

CD8+ T cells were treated with anti-CD3 and anti-CD3/28 particles, as well as particles labeled with control protein, and incubated for 1 hour at 37 ºC with 5% CO_2. Following incubation, cells were deposited onto Cell Tak coated coverslips and centrifuged at 300 x G for 3 min to cause cell adhesion. To image the formation of the immune synapse, cells were fixed with 4% PFA (Sigma Aldrich), permeabilized with 0.1% Triton-X (Sigma Aldrich), and labeled with alexa fluor 488 anti-human LFA-1 (ThermoFisher Scientific, Waltham, MA) and alexa fluor 647 anti-human Mac-1 (VWR, Radnor, PA). Cells were imaged using at 63x (Plan Apochromat 1.4 NA oil) using a Leiss LSM 700 scan head mounted on an AxioObserver Z1 inverted microscope stage. Approximately 50 cells were imaged per condition from three independent experiments.

4.2.4 AFM

AFM nanoindentation was performed on an Asylum Research MFP3D AFM (Santa Barbara, CA), mounted on an inverted Nikon Eclipse Ti (NIKON DETAILS) at 20x and run with Asylum 12. Bruker MCLTO-10 AFM tips were manually beaded with a 4.47um diameter polystyrene bead. Before each experiment, the tip's spring constant was calibrated using indention against glass surfaces and Asylum's thermal fluctuation method. Individual T cells were prepared in a FluoroDish (World Precision Instruments, Sarasota, FL) following a three hour incubation with BSA or anti-CD3/28 particles. Cells

were indented at 2um/s up to 2nN and then the tip was programmed to dwell at a fixed indention for 3 seconds before retracting. An image of each cell was collected for image processing as described elsewhere. Young's modulus was calculated using a custom Matlab (TheMathWorks, Waltham, MA) script, which zeroed the force and indention data about the contact point reported by Asylum's software and then used a linearized force curve approach with a Poisson's ratio of 0.5 to estimate the modulus. Viscous relaxation was fit using a two-parameter relaxation model on contact and force data, also in Matlab.

4.2.5 Cytoskeleton arrangement

F-actin and α-tubulin was imaged following T cell activation with particles. Briefly, $1x10^6$ cells/mL CD8+ T cells were incubated with BSA or anti-CD3/28 particles for three hours at room temperature on an end-over-end spinner. Stimulated T cells were spun down onto glass coverslips or glass bottom 35 mm dishes coated with Cell Tak (Corning, Corning, NY). For F-actin staining, cells were fixed with 4% PFA for 10 min. Cells were washed twice with PBS (ThermoFisher Scientific) and permeabilized using a 0.1% Triton-X solution for 10 min at room temperature. Phalloidin Alexa Fluor 647 (ThermoFisher Scientific) was prepared in PBS according to the manufacturer's instructions and administered to T cells for 20 min in the dark. After staining, cells were washed and counter stained with DAPI (ThermoFisher Scientific) for 5 min before mounting onto glass microscope slides. Microtubulin organization was visualized in live cells using Tubulin Tracker Green (ThermoFisher Scientific). Briefly, T cells were incubated with the tubulin stain for 30 min at 37 ºC, prepared according the manufacturer's instructions. All cells were imaged at 63x using confocal microscopy.

Live cell imaging utilized a CO_2 incubation chamber such that a 5% CO_2 environment was maintained. At minimum, 85 cells were imaged per condition from three separate experiments for the live tubulin imaging, and 35 cells from three experiments for actin imaging.

4.2.6 T cell motility

6 well plates were coated with 5 μg/mL fibronectin at 37 °C for 1 hour and then washed with PBS. Purified T cells were resuspended in Live Cell Imaging buffer (ThermoFisher Scientific) and allowed to settle for one hour before imaging. Image acquisition was conducted on an epifluorescent microscope (TE; Nikon Instruments Inc, Melville, NY) using a 10x objective. Brightfield images were acquired every 5 s for 15 min using Nikon NIS-Elements software (Nikon Instruments Inc) and T cell motility was quantified using the cell tracker plugin of Image J. Track length is defined as the total distance traveled by each cell and displacement is defined as the distance between the between the first and last position of the cell.

4.2.7 T cell-cancer cell binding

The effect our particle treatment has on T cell and cancer cell interactions was assessed by time-lapse live cell imaging. We plated 1.0 x 10^4 cells/mL HeyA8 cells into 24 well culture plates, allowed them to adhere for 24 hours, and then seeded an equivalent number of Jurkat cells and dosed with our anti-CD3 and anti-CD3/28 particles, soluble anti-CD3, BSA particles, or left untreated. Co-cultures were allowed to incubate for one hour and then the plate was transferred to the BioTek Cytation 3 Imaging plate reader (BioTek Instruments, Winooski, VT). Bright field images of each well were taken at 10x

magnification every three minutes for four hours using the Gen5 software (BioTek Instruments). The plate was shaken after each cycle of imaging to displace non-bound T cells. During this time, cells were maintained at 37 ^{0}C and 5% CO2. Binding events and duration was quantified by observing differences between frames. A cell was evaluated as bound if the Jurkat cell moved less than 5 μm and the interaction lasted for two or more frames.

4.2.8 Statistical Analysis

Statistical analysis was conducted in Graphpad Prism (La Jolla, CA) using one way or two-way ANOVA to determine significance of variables. Post-hoc Tukey-Kramer HSD testing was performed to determine significance. Data are represented using mean ± SEM.

4.3 Results

4.3.1 Immune synapse formation

T cells accumulate a number of signaling and adhesion molecules in the contact area with its cognate cell, eventually forming an immune synapse. Mature immune synapses contain a cluster of activation molecules, including TCR/CD3 and CD28, surrounded by a dense ring of adhesion molecules, such as LFA-1(216). To study the ability of our particles to trigger immune synapse formation, we incubated T cells with anti-CD3, anti-CD3/28, or control protein particles. Representative images of each condition are shown in Figure 15. A no particle condition was included as a negative control. T cells were stained for LFA-1 and Mac-1 and analysed using confocal microscopy. In the absence of

anti-CD3 antibody on particles, most T cells displayed an equal distribution of LFA-1. In contrast, anti-CD3 and anti-CD3/28 particles elicited clustering of LFA-1 on the T cell surface, with anti-CD3/28 particles displaying an increased clustering response compared to the anti-CD3 only particles. Although Mac-1 is present on all T cells, its expression is upregulated in the immune synapse of newly activated T cells(217); thus the accumulation of Mac-1 into a particular area of the cell is characteristic of immune synapse formation. Like LFA-1 clustering, the inclusion of anti-CD28 antibody onto the particle greatly increased the signal we observed. Unfortunately, we could not characterize the locations of formed immune synapses with bound particles as our 300 nm particles are too small to be clearly identified in bright-field images.

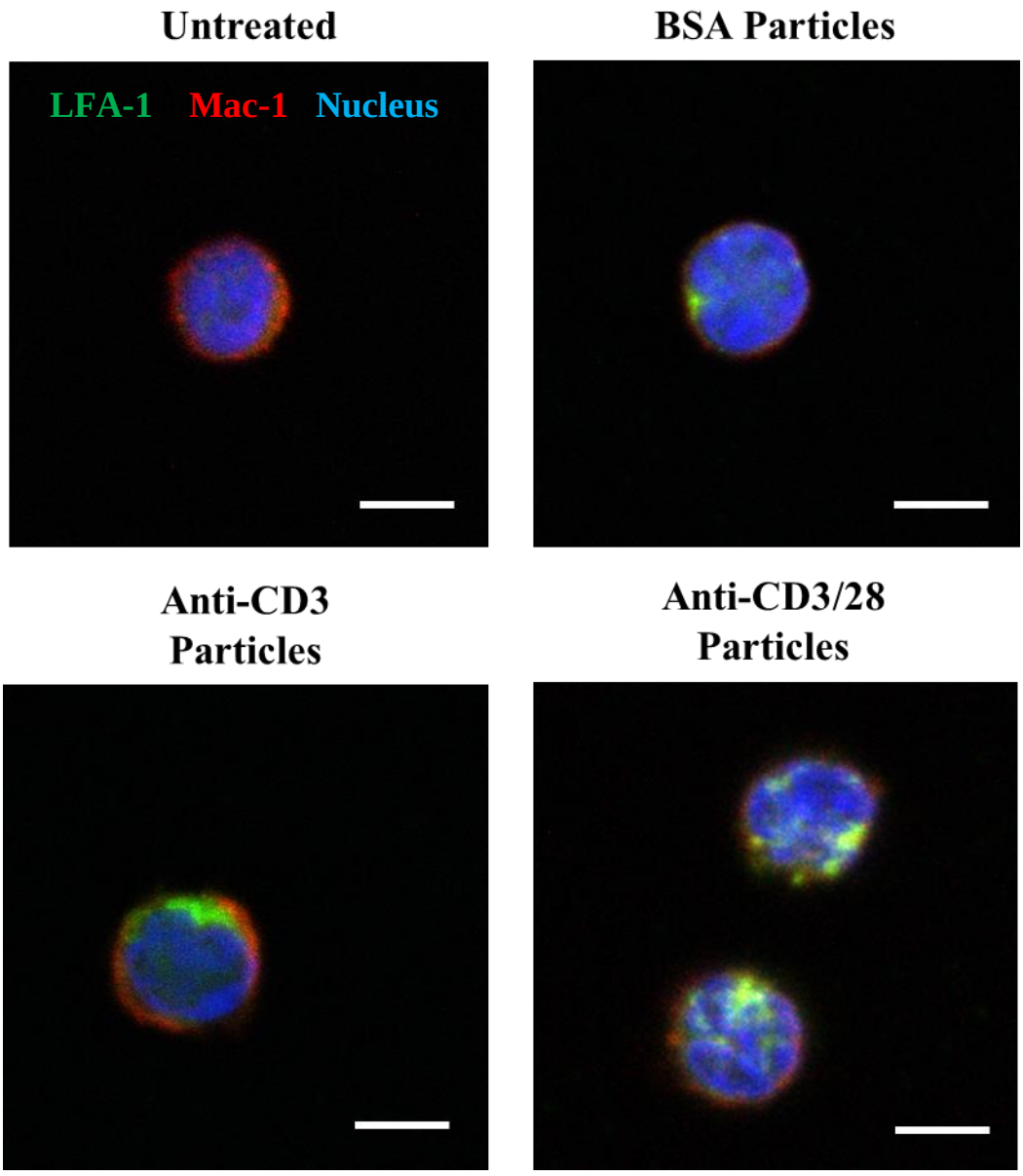

Figure 15: Immune Synapse Formation. CD8+ T cells were incubated alone or with BSA, anti-CD3, or anti-CD3/28 particles for one hour, after which cells were fixed, permeabilized, and stained for LFA-1, Mac-1, and the nucleus. Scale bar = 5 μm.

4.3.2 Cytoskeletal Arrangement

To further elucidate how our particles affect T cell immune synapse formation and the underlying activated T cell mechanics, we investigated the arrangement of two

cytoskeletal molecules, F-actin and α-microtubulin. Actin accumulates at the immune synapse and microtubules will reorganize such that the microtubule organizing center (MTOC) translocates near the immune synapse(213). In the case of CD8+ T cells, microtubules direct cytolytic granules to be secreted in a highly direction manner, from the immune synapse toward the bound, cognate cell(211). To ensure cells were binding to particles and thus initiating immune synapse formation, T cells were incubated with particles for one hour before labelling cells for either α-tubulin or F-actin. In comparison to our no particle and BSA particle conditions, anti-CD3 and anti-CD3/28 particles demonstrated a high degree of cell polarity, in which a high cytoskeletal signal was observed to be concentrated at certain region in the cell (Figure 16). This polarity was enhanced when anti-CD28 antibody was included on each particle. The negative control T cells displayed an even expression of F-actin and α-tubulin within the cell.

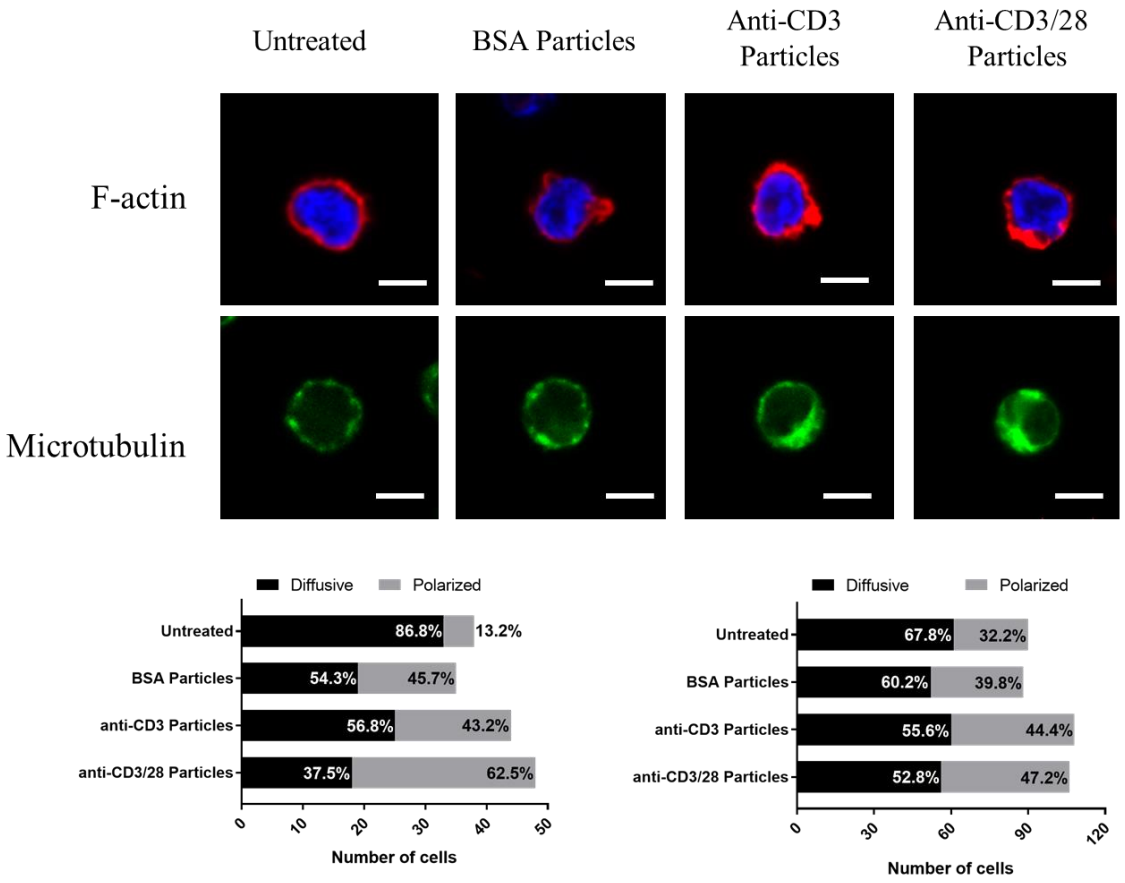

Figure 16: Cytoskeletal Arrangement. T cells were incubated with BSA, anti-CD3, and anti-CD3/28 particles for three hours. F-actin staining was performed following paraformaldehyde fixation and permeabilization. T cells were also stained with DAPI. Live cells were stained for α-tubulin using phalloidin 488. Cells were imaged and analyzed to count cells that contained either polarized or diffusive cytoskeletal arrangements. Scale bar = 5 μm. F-actin is quantified on the left and α-tubulin is quantified on the right.

4.3.3 AFM

Cell stiffness and viscosity changes following T cell activation with anti-CD3 or anti-CD28 particles were measured using AFM. T cells were incubated with activating or protein control particles, as well as no particles, for one hour and then allowed to adhere to a coverslip coated with Cell Tak. Fluor dishes containing live cell imaging solution

were used to perform these measurements. Brightfield images of cells were taken following force measurements to measure T cell size. As shown in Figure 17C, T cells were only significantly different sizes when we compared our fixed PFA control to our BSA control particle condition.

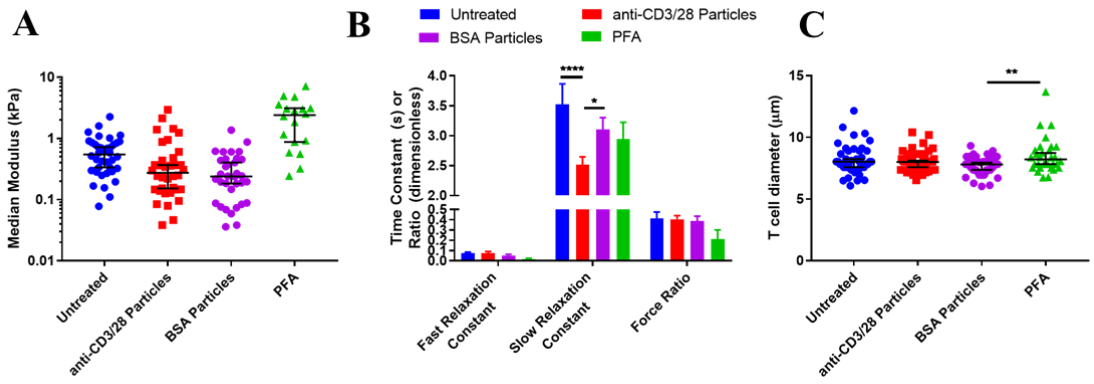

Figure 17: Mechanical Properties of anti-CD3/28 Particle-Activated T cells. Atomic force microscopy was used to measure Young's Modulus (A) and determine the viscoelastic properties of activated or unactivated T cells (B). Images of each measured cell were taken and the T cell diameter calculated (C). Data are represented as mean ± SD. *p<0.05, **p<0.01, ****p<0.0001.

Figure 17A shows that T cells activated using anti-CD3/28 particles exhibit a significantly lower Young's Modulus compared to unactivated T cells (p<0.05). These stiffness results reflect the elastic properties of activated (or non-activated) T cells. However, as cells also contain a viscoelastic component, examining these parameters by altering AFM measurements can give further insight into the cellular mechanics of activated T cells. Figure 17B shows that while there is no difference between our conditions when we measure the fast relaxation constant and the force ratio between the fast and slow relaxation constants, the slow relaxation constant does demonstrate significant differences between activated and naïve T cells. T cells activated with anti-

CD3/28 particles displayed a significantly smaller slow relaxation constant, indicating that over longer time spans, activated T cells relax faster. The exact mechanism behind slow and fast relaxation times – and in fact, the general mechanisms responsible for viscoelastic properties in cells – is the subject of much debate. Cytosol flow within the cell(218), cytoskeleton arrangement and rigidity(219), and the plasma membrane(220) are all thought to contribute to viscoelastic behavior, but research investigating these factors in an isolated manner is still necessary before additional conclusions may be reached.

4.3.4 T cell Motility

When naïve T cells are activated by APCs *in vivo*, a cascade of events is triggered, typically including clonal expansion, differentiation, and migration to the disease location(221). Since activated T cells show a softened and pliable cytoskeleton, we hypothesized that T cell motility would increase as T cells interact more readily with their environment and search for their cognate cells. However, as our data show in Figure 18, activated T cells actually travel a shorter distance in vitro (Figure 18A-B) and move more slowly compared to their non-activated counterparts (Figure 18C). This result may be influenced perhaps by the ligand used to coat dishes; fibronectin is expressed during inflammation, and naturally bind more readily to activated T cells compared to non-activated T cells, which may have increased cell adhesion and thus arrested motility(222). Furthermore, as no chemokine gradient was present to encourage T cell migration in a particular direction, activated T cells had no motivation to continue moving after binding to a relevant adhesion molecule like fibronectin. This observation was further investigated by examining T cell infiltration within cell spheroids in CHAPTER 5.

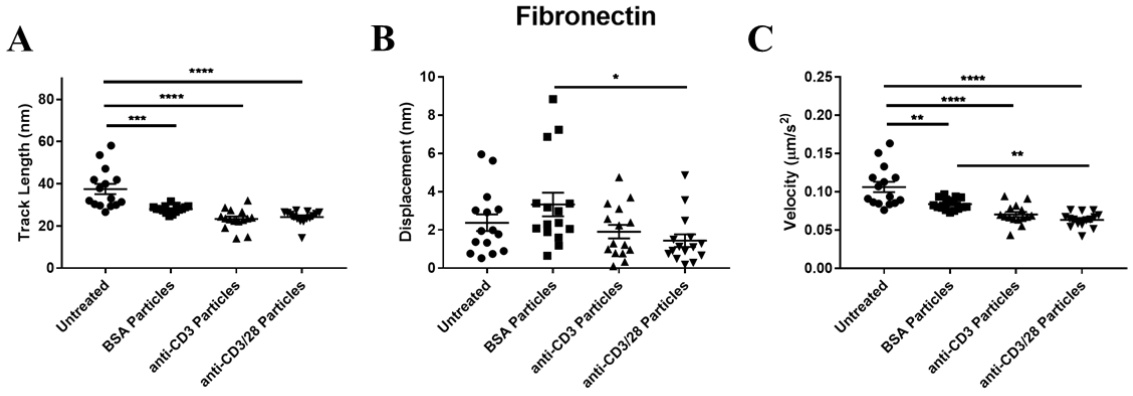

Figure 18: T cell Motility. T cells were incubated in fibronectin-coated dishes for one hour and imaged for motility over 15 minutes, at a frame rate of one image every 5 s. Data are represented as mean ± SEM; n=7, *p<0.05, **p<0.01, ***p<0.001, p<0.0001.

4.3.5 T cell-cancer cell binding

T cell and cancer cellular interactions post-treatment were evaluated using live cell imaging over four hours, as shown in Figure 19. T cells treated with anti-CD3 and anti-CD3/28 particles displayed increased interactions with cancer cells, binding more frequently than untreated co-cultures ($p<0.05$). Anti-CD3 particle-activated T cells also bound to cancer cells for a longer duration than untreated T cells or T cells treated with BSA-labeled particles ($p<0.05$). However, anti-CD3/28 particles caused T cells to bind to cancer cells for a significantly longer time ($p<0.0001$). This is most likely due to the presence of anti-CD28 antibody, which enhances activation and cognate cell binding.

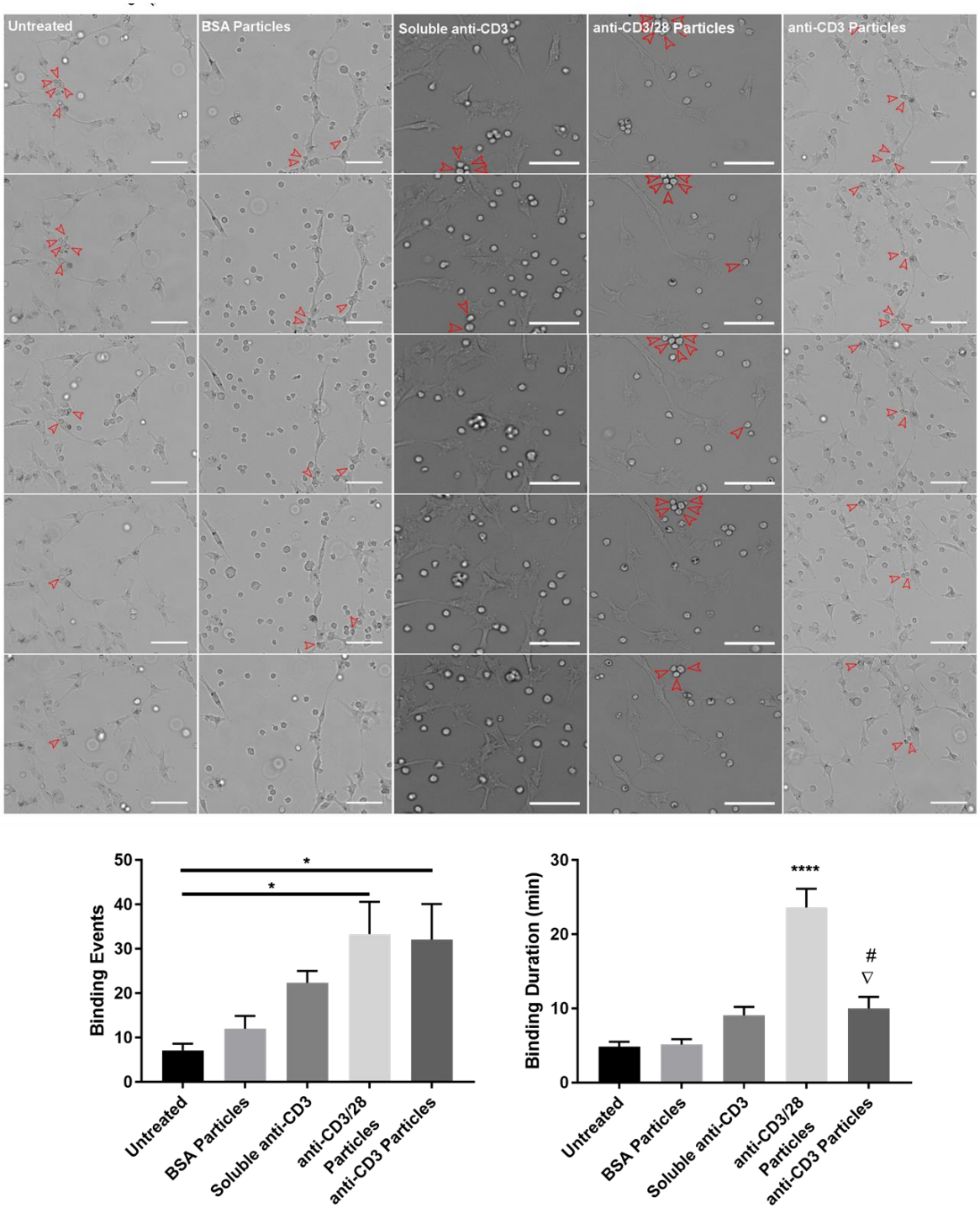

Figure 19: Cell-Cell Binding. Cancer cells were seeded into wells and allowed to adhere for 24 hours. Jurkat cells and particles were added and allowed to incubate for one hour before imaging. Images were taken every three minutes for four hours. Number and duration of T cell binding events were calculated (c). n=8; *p<0.05, ****p<0.0001,

#p<0.05 with student t-test against untreated condition, ∇p<0.05 with student t-test against BSA particles. Scale bar = 200 μm.

4.4 Discussion

The biophysical response of T cells to stimuli gives critical insight into activated T cell behavior, which is significant when designing activation platforms for these cells. For example, there is an understanding that leukocyte stiffness may be modulated by the immune system to mediate trafficking – that softened leukocytes more readily enter and stay in circulation(223). Additionally, it is known that TNF-α and IL-1β cause leukocytes to stiffen(210, 224), demonstrating that the inflammatory cytokines secreted by cancer cells promote a mechanical phenotype in T cells that make them less likely to respond in an anti-cancer fashion. Understanding these processes can inform the mode and location of delivery for immunomodulatory biomaterials as well as the size, multivalency, and stiffness of these materials – factors that heavily influence the degree of activation even possible(225, 226). For example, activating a CD8+ T cell away from the tumor microenvironment can negatively affect its ability to migrate. Thus, elucidating the biophysical implications of T cell activation in response to immunomodulatory particles is an important consideration when designing these platforms.

In this study, we investigated the effect of aAPC stimulation on T cell activation and examination of the biophysical response. T cells stimulated with anti-CD3 and anti-CD3/28 particles formed immune synapses (Figure 15) and also underwent substantial cytoskeletal remodeling that drives immune synapse development (Figure 16). Cytoskeletal accumulation at the immune synapse(s) of activated T cells, as demonstrated by us and others, has significant consequences on a variety of T cell properties. First,

activated T cells were less stiff than their unactivated counterparts and showed faster relaxation after compression, despite the increased volume of F-actin measured in activated T cells (Figure 16, Figure 17). Cell softening is traditionally associated with non-aligned, discontinuous F-actin(223, 227). So while more F-actin is present in activated T cells, its polarization is consistent with cells become softer, not stiffer.

It has been recently suggested that the cytoskeleton in activated T cells is more pliable and thus able to respond more dynamically over a short time – a critical feature for immune synapse formation and associated downstream cellular activity(209). A less rigid cytoskeleton enhances the ability of actin to remodel, which affects the size and signaling intensity of the immune synapse. The increased pliability of the actin network in activated T cells may further correlate with membrane flexibility which is especially important in CD8+ T cells, as these effector cells will spread over their target cells, exhibiting large deformations so that large contact areas between T cells and their cognates are possible(209). The ability of T cells to deform is also important for extravasation and the increased pliability of activated T cell cytoskeletons is likely a contributing factor to the fast relaxation time we observed from the AFM measurements (Figure 17). Additionally, the accumulation of F-actin and α-tubulin at the immune synapse, instead of distributed evenly throughout the cell, could further allow for faster relaxation.

It should be noted that costimulatory signaling through CD28 mediates cell softening, which is why our anti-CD3/28 particles elicit greater T cell activation, immune synapse formation with associated cytoskeletal remodelling, and softening compared to anti-CD3 only particles. These results suggest that anti-CD3/28 particle engagement

induces signaling through CD28 on the T cell, and amplifies the overall activation signal. However, previous studies have shown that CD28 engagement alone is not enough to fully activate T cells, so signaling through CD28 cannot be directly responsible for increased T cell activation(224). Instead, CD28 must work primarily as an amplifier for signaling through TCR/CD3 engagement.

When we performed live cell imaging studies to examine the binding behavior of T cells activated with anti-CD3 and anti-CD3/28 particles, we observed that in comparison to the untreated or control protein particle conditions, the activated T cells bound to cancer cells more frequently and for greater duration (Figure 19). Since reduced cell motility was observed from activated T cells (Figure 18), we originally hypothesized that activated T cells would exhibit a more motile phenotype, with enhanced rates migration, searching for a cognate cell. We observed that activated T cells traveled less distance and were slower than non-activated T cells, possibly due to activated T cells binding more frequently and for a longer duration to fibronectin, a protein T cells would typically bind *in vivo*. This coupled with evidence that upon adhesion, cells typically stop migratory behavior(228, 229), gives reason to why activated T cells exhibit less motility than unactivated T cells. Additionally, studies have demonstrated that sustained T cell activation inhibits crawling by blocking shape change and new edge formation and causes membrane spreading over its cognate cell(209, 214, 230, 231). Since cell motility depends on large changes within the actin and microtubule structure(208, 232) – T cell activation would inhibit additional cytoskeletal remodeling beyond immune synapse formation. Thus, once T cells are activated, they are primed to bind to other cells.

4.5 Conclusions

In conclusion, this work suggests that aAPCs are suitable for activating T cells within the tumor microenvironment. Our anti-CD3/28 particles – and to a lesser extent, our anti-CD3 particles – cause immune synapses to form and reduce cell stiffness – events driven by considerable cytoskeleton remodeling due to T cell activation. Changes in biomechanical properties influence T cell behavior, reducing T cell motility and increasing T cell binding to cancer cells. Our work presented here suggests that aAPCs would optimally be administered primarily to resident CD8+ T cells within the tumor microenvironment to take advantage of resident immune cells. Future studies involving signaling and adhesion antibody patterning on aAPCs, to mimic the immune synapse – similar to studies performed previously by the Yu Laboratory(181), may amplify the T cell activation response as reported using flat, 2D surfaces. Because the TCR is small and has a low affinity toward antigen, presenting activating proteins in a particular way may increase the biophysical activated T cell response presented in this study(233).

CHAPTER 5. EVALUATE THE EFFECTS OF SPATIALLY SEGREGATING BIOLOGICAL SIGNALS ON T CELL – CANCER CELL CROSSLINKING AND DOWNSTREAM CYTOTOXICITY USING JANUS PARTICLES

5.1 Introduction

CD8+ T cells are effector immune cells which recognize antigens on cancer cells (and other pathogenic cells), bind strongly to these cells, and secrete cytolytic granules containing perforin and various granzymes to the bound cancer cell in a highly directional manner(4). The secretion cause the target cell to undergo apoptosis and die. The ability to activate these cells *in vivo* within the immunosuppressive tumor microenvironment is critically important for cancer treatment, as the presence and activity of these cells within patient tumors has shown to be associated with better clinical outcomes(20). Activating CD8+ T cells *in vitro* is thus a key step for many immunotherapies. Priming an effector T cell response in patients against a specific cancer antigen using antigen presenting cells (APCs) is costly, time consuming, varies widely between patients. To address these issues, researchers have developed artificial APCs (aAPCs) to activate T cells in a more standardized manner. aAPCs display either anti-CD3 antibody or antigenic peptide-MHC complex for unspecific or specific activation, respectively, typically combined with co-stimulatory molecule anti-CD28 antibody. Antigen-specific priming of naïve T cells can be difficult, with the need for repeated stimulation and prolonged culturing, as relatively few antigen specific T cells are available(234). Researchers have solved this problem by either enhancing activation

responses through optimizing particle size, shape, and multivalency or by nonspecifically activating T cells(161). But non-antigen specific activation can result in unregulated T cell activation, leading to healthy tissue damage or even autoimmune disease. We hypothesize the inclusion of a cancer-targeting ligand coupled physically to the T cell activation, we can effectively extend tumor cell specificity to each aAPC.

Janus particles, bifunctional particles with biologically or chemically distinct hemispheres, have a wide range of possible applications, particularly as therapeutic agents(173, 181, 215). Janus particles are innately multifunctional and maintain a highly dense and localized presentation of each signal that is impossible on traditional heterofunctional particles, thereby allowing for strong and simultaneous targeting and therapeutic behavior. Concentrated signal is important to enhance cellular responses(166); this is true especially with T cell activation, in which increased calcium signaling was observed when anti-CD3 antibody was clustered, as opposed to uniformly distributed across particle surfaces(173). While biological Janus particles have been used activate T cells(173, 181, 182), study phagocytosis(183-185), and kill cancer cells(235, 236), there has been no research thus far in which both hemispheres are used to elicit biologically unique behaviors from different cells. In this study, we have functionalized Janus particles to activate CD8+ T cells and bind specific cancer cells concurrently. Using a technique previously published by the Sulchek lab(215), we conjugated anti-CD3 and anti-CD28 antibodies onto the silica base hemisphere and anti-folate receptor (FR) antibody onto the gold-coated hemisphere of each Janus particle. We found that Janus particles are capable of activating T cells, targeting cancer cells, and thus enhancing T cell- cancer cell crosslinking and downstream cytotoxicity. Although silica particles

uniformly functionalized with all three molecules do produce an anti-tumor effect and contribute towards T cell infiltration, Janus particles significantly increased cytotoxicity of the targeted cells.

5.2 Materials and Methods

5.2.1 Cell Culture

The human ovarian cancer cell lines HeyA8 and Ovcar-3 were gifted from the McDonald laboratory (Georgia Institute of Technology, Atlanta, GA). HeyA8 and Ovcar-3 monolayers were cultured using RPMI-1640 cell culture media (ATCC, Manassas, VA) supplemented with 1% penicillin-streptomycin (Sigma Aldrich, St. Louis, MO) and 10% and 20% FBS (Atlanta Biologicals; Norcross, GA), respectively. Human dermal fibroblasts, hDF, were gifted from the Nerem laboratory (Georgia Institute of Technology, Atlanta, GA) and cultured using DMEM (Cellgro; Corning, Corning, NY) supplemented with 1% penicillin-streptomycin, 10% FBS, and 1% L-glutamine (Invitrogen, Carlsbad, CA). CD8+ T cells were isolated from peripheral blood collected from human donors in the Waller laboratory (Emory University, Atlanta, GA) using a negative selection isolation kit (Stemcell Technologies, Vancouver, Canada). All cells were maintained at 37 ºC with 5% CO_2. All cells used were below passage 30 with viability assessed using trypan blue.

5.2.2 Particle functionalization

Janus particles were fabricated as previously described in Tang et al. (2012). Briefly, 0.296 μm silica particles were deposited onto clean glass slides in monolayers and then

coated with a 20 nm gold layer following a 5 nm titanium adhesion layer at 2 Å/s using a metal evaporation process (CHA E-Beam Evaporator). Janus particles were removed from glass slides using sonication in deionized water and then filtered to remove gold debris. Gold coated silica particles were washed twice with PBS and then the silica hemisphere was silanized by washing the Janus particles in acetone and incubating with a 2% APTES-acetone solution for 2 min, washing twice with DI water, and drying in the oven. The activated particles were then incubated with anti-CD3 and anti-CD28 antibodies for one hour, crosslinking the antibodies with the silica surface only. Next, our Janus particles were incubated for 4 hours with 1mM biotin-PEG4-thiol (Nanocs, Boston, MA) to biotinylate the gold hemisphere. Complete functionalization was achieved by incubating the particles with anti-folate receptor (FR) antibody – streptavidin conjugates, thereby forming biotin-streptavidin complexes. Anti-FR antibody - streptavidin conjugates were produced using the Lightning Link streptavidin conjugation kit (Novus Biologicals, Littleton, CO). Later, functionalization using with anti-FR/E-cadherin antibody-streptavidin conjugates was assessed.

Uniform silica particles were functionalized using the same silanization process to activate the silica particle surface as previously described. Surface-activated silica particles were incubated with a mixture of anti-CD3, anti-CD28 (Biolegend; San Diego, CA), and anti-FR antibodies (Santa Cruz Biotechnologies, Dallas, TX) to conjugate in a random arrangement. Protein control particles were functionalized with streptavidin (ThermoFisher Scientific) on both the silica hemisphere and following biotin-PEG-thiol activation of the gold hemisphere. Single-hemisphere control particles were also produced such that anti-CD3/28 antibodies were conjugated as usual using APTES

silanization. Following biotin-PEG-thiol functionalization on the gold hemisphere, particles were incubated with streptavidin for one hour. Anti-FR control particles were produced by conjugating streptavidin to the silica surface and functionalizing the gold hemisphere with streptavidin-anti-FR antibody conjugates. For ease of discussing, these control particles will be referred to as anti-CD3/28 J. and anti-FR J. particles, respectively.

For characterization purposes, anti-CD3/28 antibodies were replaced with FITC BSA (Sigma Aldrich, St Louis, MO) and alexa fluor 647 streptavidin (Invitrogen) was used to complete gold hemisphere functionalization following biotin-PEG-thiol conjugation.

5.2.3 Particle characterization

Particle surface functionalization and protein conjugation was characterized following each step of the complete functionalization process for both Janus and uniform particles using the tunable resistive pulse sensing (TRPS) principle (qNANO Gold; IZON, Cambridge, MA). Particles were suspended in a solution of filtered 0.02% tween 20 (Signma Aldrich) in PSB (ThermoFisher Scientific) before measuring particle size distribution, surface change, and concentration.

Janus particle multi-functionality and protein spatial segregation was confirmed using flow cytometry and confocal microscopy. Confocal microscopy (Zeiss; Obekochen, Germany) was used to visually demonstrate the discrete spatial segregation between different protein functionalization processes on the two hemispheres. This segregation is quantified by measuring mean fluorescence intensity (MFI) over each hemisphere on

each image. 20 images per condition were taken, at 63X magnification. Particle multi-functionality was determined using a BD Acuri C6 flow cytometer (Franklin Lakes, NJ). At least 25,000 events were recorded per sample measured.

5.2.4 Cell targeting

The ability of Janus particles to target specific cancer cells was assessed by incubating particles – first at various anti-FR densities and then different particle formulations (uniform or Janus) – against different target cell types at 37 ºC for eight hours, on an end-over-end spinner. To prevent cell adhesion, complete cell medium were supplemented with 0.5M EDTA (ThermoFisher Scientific). Following incubation, particles were stained with PE anti-mouse secondary fluorescent antibody (Biolegend) and analyzed for binding using flow cytometry. The ability of anti-FR particles to selective target Ovcar-3 cells was also visualized using confocal microscopy. Ovcar-3, HeyA8, and hDF cells were grown on coverslips to 80% confluency before staining with a red fluorescent probe (Cell Tracker Deep Red, Thermo Fisher Scientific). Green fluorescent particles were labeled with anti-FR antibody or streptavidin using the conjugation scheme just described, and incubated with the cells for eight hours before washing and staining with Hoechst. Coverslips were mounted onto glass coverslips and imaged using a Zeiss 700 confocal microscope. Particle binding image quantification was performed using Volocity 6.3 Image Analysis software (Perkin Elmer, Waltham, MA).

5.2.5 T cell activation

CD8+ T cell activation was measured by fluorescently staining for the presence of CD107a, a marker of degranulation. Briefly, primary human CD8+ T cells were dosed

with the relevant treatment groups, incubated for 3 hours, and then assessed for FITC mouse anti-human CD107a (Biolegend) using flow cytometry.

5.2.6 Cell binding and particle crosslinking

The target cell – cancer cell crosslinking capability of Janus particles was assessed using confocal microscopy. Cancer and T cells were labeled with cell tracker red and green, respectively, and then incubated with anti-CD3/28/FR Janus particles at 37 ºC in the dark. After two hours, each sample was spun down onto Cel1 Tak (Corning; Corning, NY) coated coverslips at 300 x G for 3 minutes. Adhered cells were fluorescently labeled with CellMask orange plasma membrane stain (ThermoFisher Scientific) and then fixed with 4% paraformaldehyde (Sigma Aldrich). Cells were counterstained with DAPI (ThermoFisher Scientific) and then mounted onto glass coverslips for confocal imaging. Janus control particles and uniformly coated particles, in addition to no particles, were also assessed.

5.2.7 Co-culture cytotoxicity

The ability of the Janus and control particles to elicit cancer cell death, due to activated T cell – cancer cell crosslinking, was evaluated with a live/dead fluorescent staining kit (Invitrogen; Eugene, OR). Forward and side-scatter was used to differentiate T cells from cancer cells. Ovarian cancer cells were plated, allowed to adhere for 8 hours to reach homeostasis, and treated with primary human CD8+ T cells and particles for 24 hours. Cells were then harvested, stained for viability, and analyzed using flow cytometry. At least 25,000 events were recorded for each sample. When investigating E:T ratios on cancer cell cytotoxicity, an increasing number of T cells were used with equivalent

particle doses. The targeted ovarian cancer cell type was varied so that cell-specific cytotoxicity due to Janus and non-Janus particle targeting could be evaluated.

5.2.8 Spheroid Formation and Characterization

Solid tumor spheroids were formed by seeding 5 x 10^3 cells/well in 100 μL/well of 20% methylcellulose thickened RPMI-1640 media, supplemented with 15% BSA and 1% penicillin-streptomycin. All spheroids were grown in round bottom, ultralow attachment 96 well plates (Corning; Corning, NY), and maintained at 37 °C with 5% CO_2 and rotated on an orbital shaker at 60 rpm. Tumor spheroids were used for functional assays following four days of culturing. Growth was monitored using phase contrast microscopy. To characterize spheroids, Ovcar-3 cells were stained red with Cell Tracker Deep Red (Thermo Fisher Scientific, Waltham, MA), and after four days of culture, imaged using a Zeiss 700 confocal microscope (Oberkkochen, Germany). Diameters of the spheroids were measured using ZEN imaging software from Zeiss, shown in Figure 29, along with a representative image of the Ovcar-3 spheroid.

5.2.9 Spheroid Cytotoxicity

Spheroid cytotoxicity was determined using confocal microscopy, instead of flow cytometry, so we could examine where within the 3D architecture of the spheroid cancer cell death occurred. To examine complete cell death, unstained Ovcar-3 cells were grown into spheroids, treated with Janus and control particles, along with 5 x 10^3 CD8+ T cells. After 24 hours, spheroids were stained using a live/dead staining kit with calcein AM and ethidium homodimer-1 for one hour. After which and nuclei were labelled with hoechst, and mounted onto glass coverslips for imaging. To examine T cell infiltration as a result

of particle treatment, Ovcar-3 cells were labeled withCell Tracker Deep Red (ThermoFisher Scientific) and CD8+ T cells were labeled with Cell Tracker Green (ThermoFisher Scientific) before treating with yellow dead cell stain (Thermofisher Scientific). Again, spheroids were mounted onto glass coverslips and imaged using confocal microscopy.

5.2.10 In vivo biodistribution and toxicity

BALB\c mice were used to evaluate particle biodistribution and toxicity due to particle treatment after 1 hour, 4 hours, and 24 hours. Briefly, mice were injected intravenously with 2.5 μg anti-mouse Janus or isotype control particles. PBS vehicle was also examined for some experiments. At the appropriate time point, mice were euthanized and the heart, lung, liver, kidney and spleen harvested and imaged for particle distribution. Biodistribution was also assessed after 72 hours; 1.25 μg Janus or control particle dose was used at this time point only. Systemic toxicity following particle treatment was evaluated by measuring the concentration of IL1-β, IL-2, IL-4, IL-6, INF-γ, and TNF-α present in serum using luminex (Life Technologies, Carlsbad, CA). To examine T cell activation, splenocytes were stained using PE/Cy7 anti-mouse CD3, APC anti-mouse CD4, FITC anti-mouse CD8, and PE anti-mouse CD69 (Biolegend) and fluorescent intensity was measured using flow cytometry.

5.2.11 Statistical analysis

Statistical analysis was conducted in Graphpad Prism (La Jolla, CA) using one way or two-way ANOVA to determine variable significance. Post-hoc Tukey-Kramer HSD or

Student T testing was performed to determine significant differences between conditions. Data are represented using mean ± SEM.

5.3 Results

5.3.1 Anti-Folate Receptor Functionalized Particles Preferentially Target Ovcar-3 Cells

To determine investigate the ability of anti-FR particles to specifically target Ovcar-3 cells (a human ovarian cancer cell line over-expressing FR), anti-FR antibody was conjugated onto cells at densities previously explored in CHAPTER 3. As shown in Figure 20A, we found that the 25 μg particle condition elicited significantly higher Ovcar-3 cell targeting capability, than 0 and 12.5 μg conditions ($p<0.01$ and $p<0.05$, respectively). This antibody density was then selected to further study the ability to specifically target cells over-expressing folate receptor. HeyA8 and hDF (a human ovarian cancer cell line and an immortalized human dermal fibroblast cell line with constitutive FR expression) were used to investigate particle selective targeting. Ovcar-3 cells were targeted by particles to a significantly greater extent than HeyA8 and hDF cells (Figure 20B, $p<0.0001$), as assessed by flow cytometry. Anti-FR particle binding was also assessed using confocal microscopy, which revealed that our particles preferentially target Ovcar-3 cells over HeyA8 cells ($p<0.0001$) (Figure 20C-D). While there was no difference in anti-FR particle interactions between Ovcar-3 cells and hDF cells according to our image analysis, it is impossible to differentiate between particle endocytosis and binding. Given that our flow cytometry data presented in Figure 20B exclusively measures particle binding, it is reasonable to attribute the lack of difference shown in

Figure 20D between Ovcar-3 and hDF cells to hDF cells endocytosing the anti-FR particles.

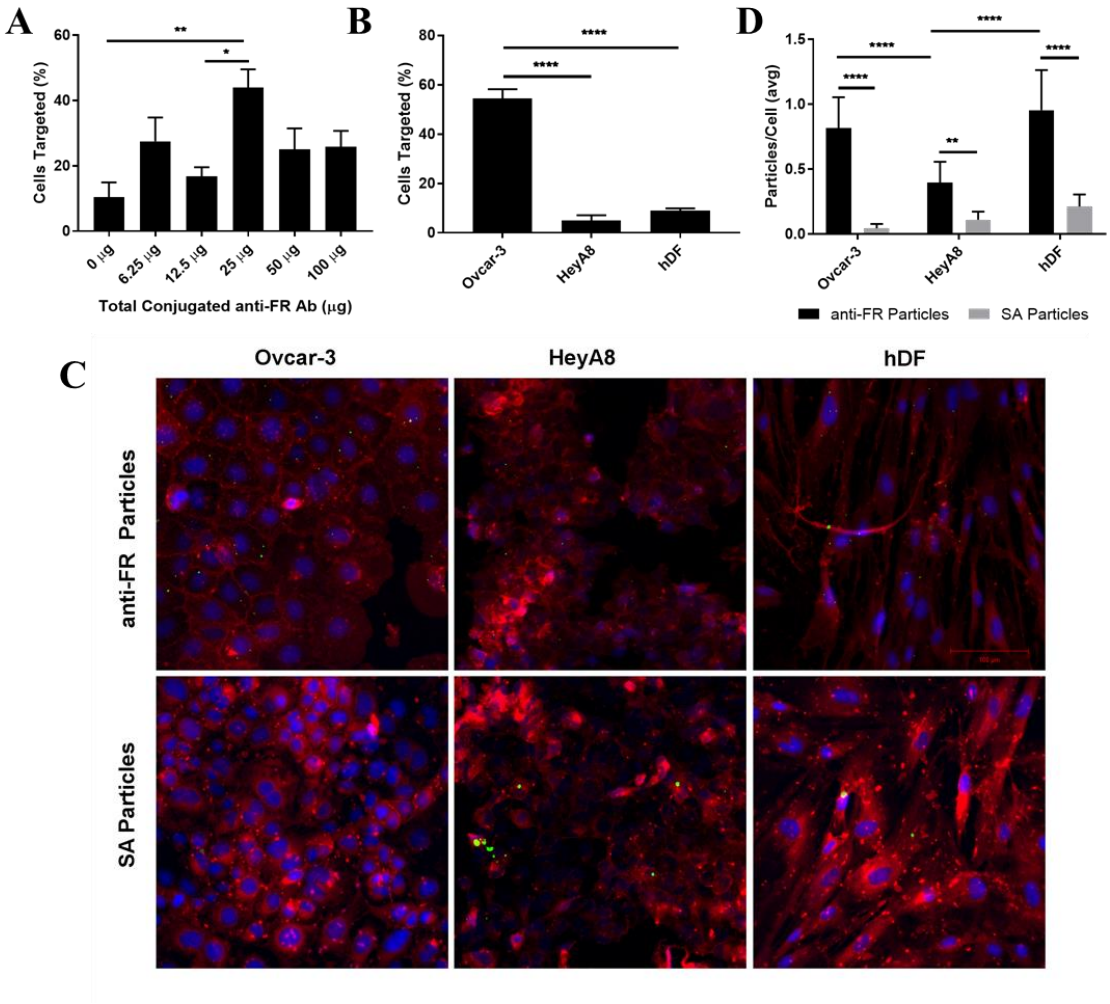

Figure 20: anti-FR Particle Characterization. (A) Particles functionalized with various densities of anti-FR antibody were incubated with Ovcar-3 cells to optimize cell targeting capability. Data are represented as mean ± SEM, n=4; **p<0.01, *p<0.05. (B) Specific cell targeting was verified by incubating anti-FR particles with FR-expressing cells (Ovcar-3) and non-FR expressing cells (HeyA8, hDF). n=4; ****p<0.0001. (C, D) Target cells were seeded onto coverslips and treated with fluorescent anti-FR or BSA particles for 8 hours. Representative images of each condition are shown. Scale bar = 100 μm (C). Particle targeting was quantified by counting the number of particles per frame and normalizing by the number of cells per frame (D). n=4.

5.3.2 Janus Particle Functionalization and Characterization

The Janus particle functionalization process, due to the many steps involved, required some optimization. We evaluated five different schemes, of which two yielded dually functionalized Janus particles. For the purposes of characterization, BSA was functionalized to the silica hemisphere and streptavidin was functionalized to the gold coated hemisphere. The schemes are as follows: 1) Silica: Plain silica particle, APTES silanization and BSA incubation; 2) Janus-1: Gold-coated Janus particle, APTES silanization and BSA incubation; 3) Janus-2: Gold-coated Janus particle, APTES silanization, BSA incubation, biotin-PEG-thiol functionalization, and streptavidin incubation; 4) Janus-3: Gold-coated Janus particle, biotin-PEG-thiol functionalization and streptavidin incubation; 5). Janus-4: Gold-coated Janus particle, biotin-PEG-thiol functionalization, APTES silanization, BSA incubation, and streptavidin incubation. When evaluating the success of these functionalization processes, we measured both particle size and particle concentration. We expected particle size to increase as we altered the particle surface, and indeed, we did observe that trend. Figure 21A shows that over the course of the entire conjugation process, particle size did increase from its original diameter (approximately 300 nm). However, the two different schemes resulting in a fully functionalized Janus particle did not produce particles of equivalent sizes; Janus-2 particles were greater than Janus-4 particles. This is perhaps due to biotin-PEG-thiol and being exposed to the acetone involved in APTES silanization. Acetone disrupts tertiary bonds in proteins and therefore may have denatured the biotin-PEG thiol, making it unable to bind effectively to streptavidin. We also evaluated particle concentration to verify that neither a particular conjugation step nor a specific scheme resulted in a

decrease in concentration compared to other steps or schemes. As shown in Figure 21B, particle concentration during all functionalization schemes remained steady.

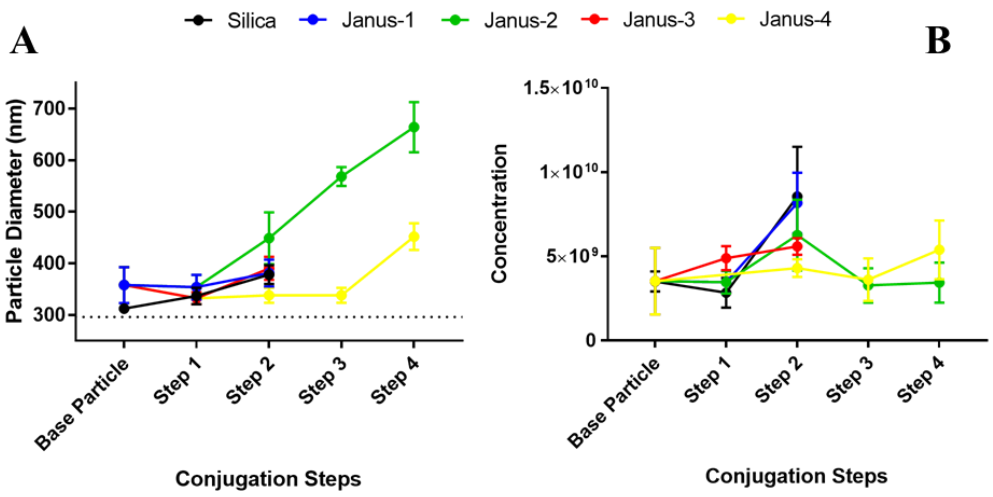

Figure 21: Janus Particle Conjugation Characterization. After each step in the conjugation process of functionalizing Janus particles, particle size (A) and concentration (B) were measured using the TRPS principal with an IZON qNano. Data are represented as mean ± SEM; n=3.

As shown in Figure 22, Janus particles exhibited spatial segregation of proteins. When analyze using flow, single hemisphere-functionalized particles exhibited over 98% particle functionalization following APTES silanization and nearly 67% functionalization of the gold hemisphere. The reason for this lower functionalization is due to the number of steps required – incubation of biotin-PEG-thiol, formation of antibody-streptavidin constructs, and then final conjugation of the constructs with the biotinylated particle. Any inefficiency at any of these three steps would be propagated and increased, overall reducing the efficiency of the gold functionalization. Dual functionalization of Janus particles resulted in a 58% yield. Confocal microscopy was used to visually validate this functionalization and to assess if the two signals were spatially segregated onto their

respective hemispheres. Representative images in Figure 22 depict single and dually functional particles and show that spatial segregation was achieved using the described protocol to functionalize Janus particles.

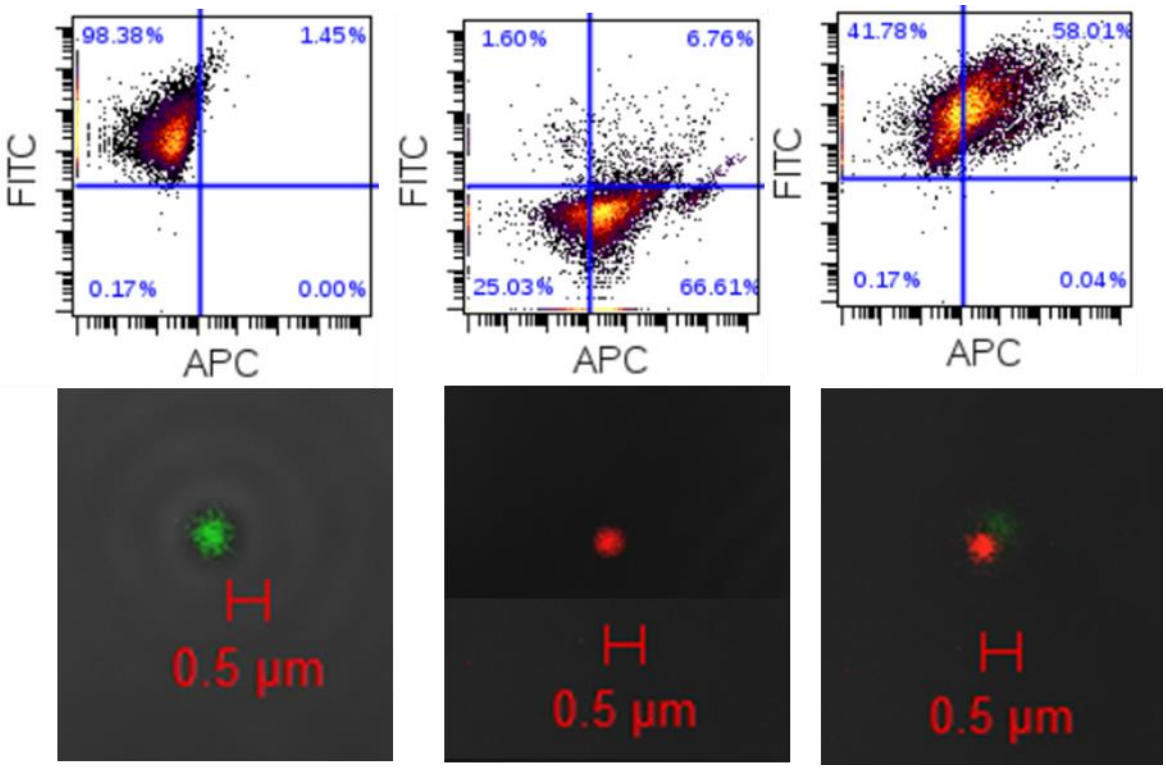

Figure 22: Janus Particle Functionalization Characterization. Flow cytometry and confocal microscopy was used to verify particle multifunctionality and spatial segregation of signal. For characterization purposes, FITC-BSA was used to functionalize the silica hemisphere and alexa fluor 647 streptavidin was used to functionalize the gold hemisphere following biotin-PEG-thiol conjugation.

5.3.3 Cell Targeting

The ability of our particles to target T cells was investigated with all particle formulations against primary human T cells. Unsurprisingly, all particles that displayed anti-CD3/28 antibodies targeted significantly more T cells than all other particles, as represented in Figure 23A. We found that simply including anti-FR antibody onto particles significantly

increased the number of Ovcar-3 cells with bound particles (Figure 23B). Interestingly, anti-FR J. particles elicited the greatest Ovcar-3 binding activity, significantly more than Janus particles containing both anti-FR antibody and anti-CD3/28 antibodies. It is possible that the SA control protein contributes slightly to the increased binding measured, as the SA particles did bind to some Ovcar-3 cells (Figure 23B). It is more likely that the inclusion of anti-CD3/28 antibodies on the Janus and control uniform particles somehow interfered with the binding capability of these particles, either through steric hindrance or by discouraging continued Ovcar-3 interaction with the particle. Also, since Janus particles have a clear orientation, it is possible that higher doses of Janus particles are necessary to reach an identical amount of binding compared to anti-FR J. particles. However, despite any reduction in targeting ability due to anti-CD3/28 antibodies, Figure 23C shows that our particles target significantly more Ovcar-3 cells than our control HeyA8 or hDF cells.

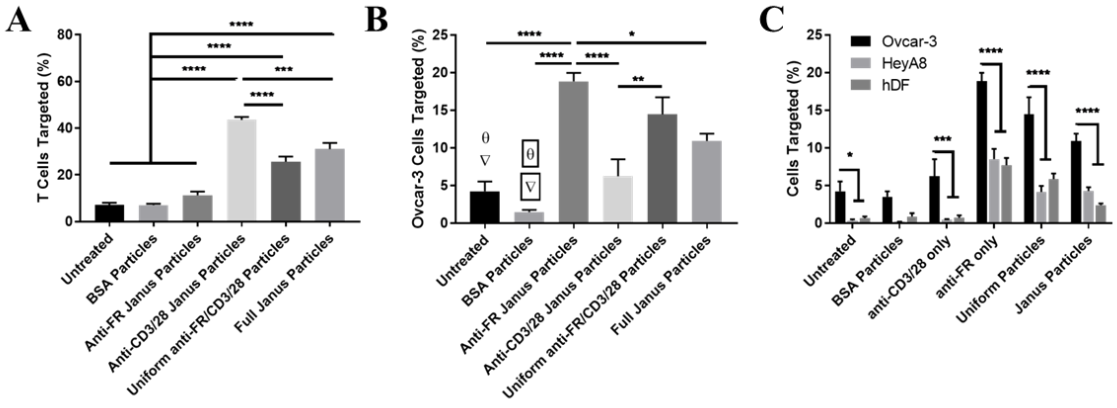

Figure 23: Janus Particle Targeting. CD8+ T cells (A), Ovcar-3 (B, C), HeyA8, and hDF cells (C) were incubated for 2 hours with all particle formulations. Secondary fluorescent staining against the conjugated antibodies was measured using flow cytometry to determine the percentage of cells with bound particles. Data are represented mean ± SEM; n=6, *p<0.05, **p<0.01, ***p<0.001, ****p<0.0001.

5.3.4 T cell Activation

Janus particles were found to activate T cells, despite only half the particle displaying T cell stimulating molecules, anti-CD3 and anti-CD28 antibodies. CD8+ T cells were purified from peripheral blood using EasySep immunomagnetic negative selection (STEMCELL Technologies). Cells were activated using all five particle formulations for 3 hours on an end-over-end spinner and maintained at 37 ºC and 5% CO_2. CD107a expression – a marker for degranulation – was measured using flow cytometry. As shown in Figure 24, particles displaying anti-CD3/28 antibodies activated significantly more cells than particles without the T cell-stimulating molecules ($p<0.05$ at least). Additionally, while Janus particles did not elicit greater activation than anti-CD3/28 J. particles, they did provoke more cells to become activated than uniformly coated uniform particles, together these results suggest that segregating the relevant molecules onto a single hemisphere promotes T cell activation.

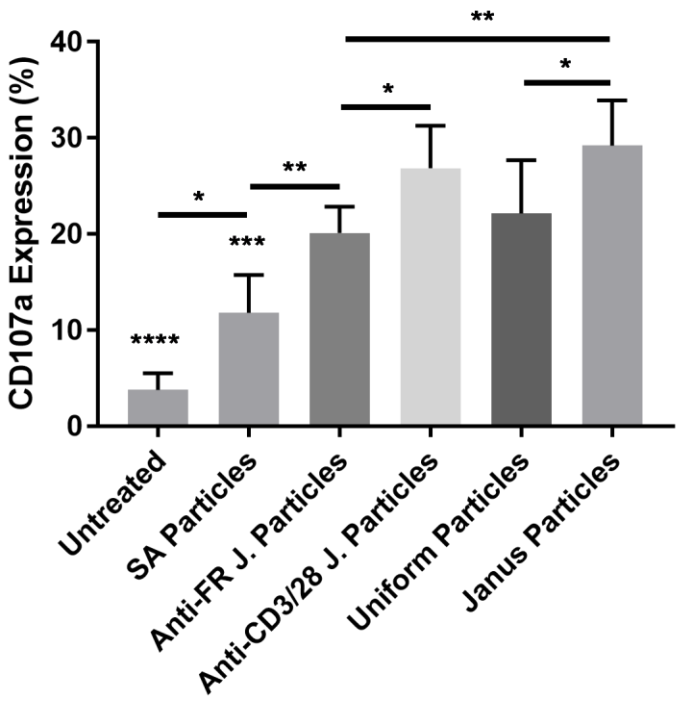

Figure 24: T cell Activation from Janus Particles. T cell activation was measured by the expression of CD107a. Cells were analyzed for the surface expression of CD107a by staining with FITC anti-human CD107a and then measuring the resultant signal using flow cytometry. Data are represented as mean ± SEM, n=6; *p<0.05, **p<0.01, ***p<0.001, ****p<0.0001.

5.3.5 Interactions between Cancer and T cells

For this work, non-antigen-specific T cell and cancer cell pairs were used to reduce spontaneous binding and thus drive cancer cell-T cell interactions using our particle treatments. To determine whether T cells and Ovcar-3 cells would form conjugates in the presence of our particles, we used confocal microscopy. T cells were labelled with Cell Tracker green and Ovcar-3 cells were labelled with Cell Tracker Deep Red. Cells were mixed at a 1:1 ratio, treated with particles, and incubated for three hours. All cells were allowed to adhere to coverslips coated with Cell Tak and then stained using Cell Mask orange to visualize their plasma membranes. Following paraformaldehyde fixation,

nuclei were stained with DAPI and mounted onto glass microscope slides. Figure 26 shows that while some spontaneous binding occurred between T cells and cancer cells, the number of T cells per cancer cell and the frequency of conjugation increased when cells were treated with particles that targeted both cells types – i.e. uniform and Janus particles. However, we observed that Janus particles elicited far more binding events than did uniformly functionalized particles, most likely due to the segregation and therefore concentration of targeting molecules on each particle hemisphere. These results show that our Janus particle treatment prompts T cell-cancer cell interactions and hence is likely to increase cancer cell death. Given the short time frame examined, this crosslinking assay does not provide information on cytotoxicity, which was examined in the following set of experiments.

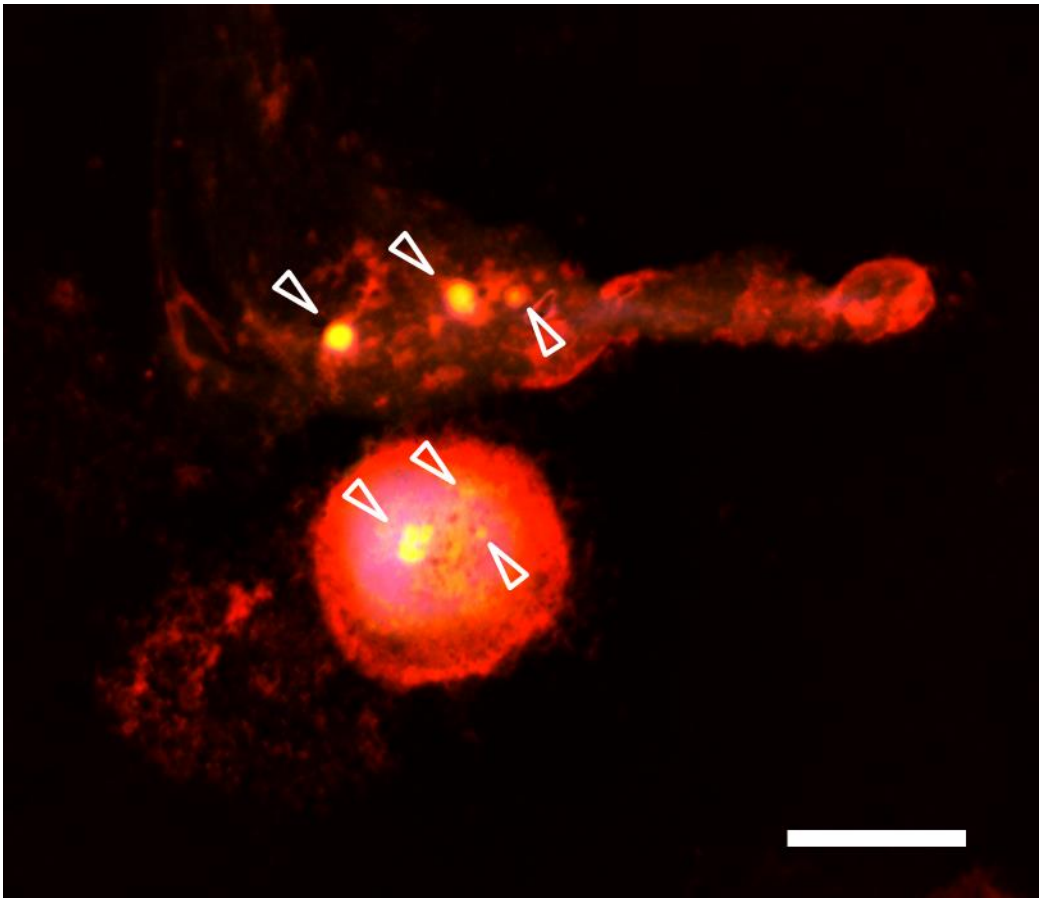

Figure 25: Janus Particles cause significant T cell - cancer cell binding. Janus particles facilitated T cell binding to cancer cells, as shown in this representative image. T cells or clusters of T cells are indicated with white arrows. Scale bar = 30 μm.

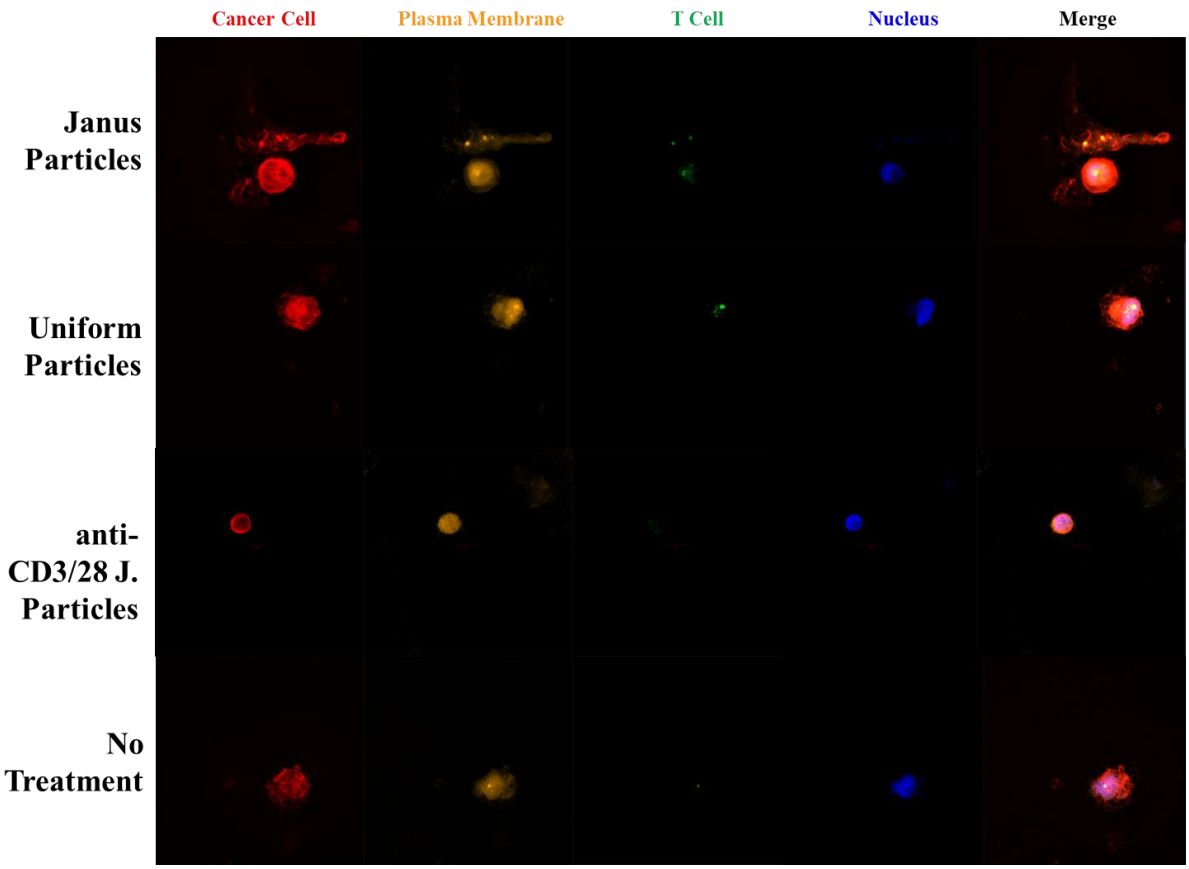

Figure 26: Janus Particles exhibit high cellular crosslinking. To determine T cell – cancer cell binding, cancer cells, CD8+ T cells, and particles were incubated together for 8 hours. Pre-incubation, cancer cells were labeled with red fluorescent stain and T cells with green fluorescent stain. Post-incubation, cell conjugates were labeled with Hoechst and orange cell mask plasma membrane stain. Representative images of Janus, uniform, and anti-CD3/28 J. particles, and a no particle control condition, are shown.

5.3.6 Cytotoxicity

To better understand how T cell – cancer cell crosslinking (Figure 26) due to our particle treatments may lead to cancer cell death, cytotoxicity was assessed using a live/dead staining procedure with calcein AM and ethidium homodimer-1. Briefly, cancer cells were plated in either 24-well or 48-well plates and allowed to reach homeostasis overnight. An equivalent number of CD8+ T cells were treated with each particle condition added to the cancer cell culture. As shown in Figure 27A, Janus particles

elicited the greatest amount of cytotoxicity, significantly more than both uniform ($p<0.001$) and anti-CD3/28 J. particles ($p<0.05$). Unexpectedly, anti-CD3/28 J. particles also caused significantly greater cytotoxicity than uniform particles ($p<0.001$). This is perhaps caused by higher T cell activation using the anti-CD3/28 J. particles, compared to uniform particles (Figure 24). These comparisons were evaluated at a 1:1 E:T ratio. Differences between groups formulated to elicit T cell activation – Janus, anti-CD3/28 J., and uniform particles – increased as the E:T ratio increased (Figure 27B). As the particle dose was equivalent at all conditions (i.e. not increasing to reflect increasing T cell number), increased cytotoxicity demonstrates that T cell number, or T cell activity to our particle treatment, rather than particle dosing, is the limiting factor in the effectiveness of using Janus particles as an immunotherapeutic strategy.

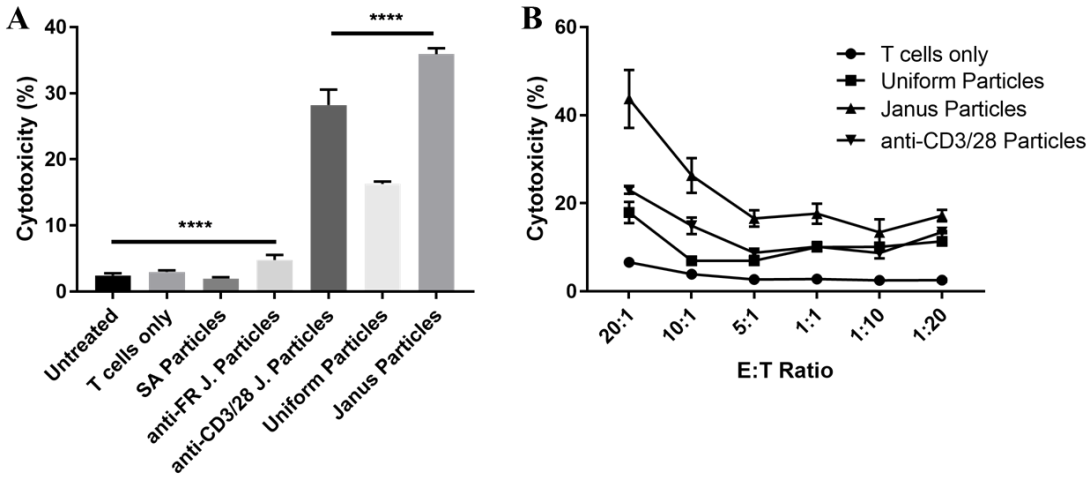

Figure 27: Particle-induced Cytotoxicity. (A, B) Cell viability was measured using flow cytometry following fluorescent staining with live/dead probes. Data are represented as mean ± SEM, n=6; ****$p<0.0001$.

To examine whether cell-specific cytotoxicity could be achieved from Janus particles and not from activating T cells in an antigen-specific manner, we evaluated the

percentage of untargeted HeyA8 cell death compared to targeted Ovcar-3 cell death. As shown in Figure 28, significantly less cytotoxicity was observed using HeyA8 cells. Janus particles elicited the greatest difference between the two cell types ($p<0.001$), compared to anti-CD3/28 J. ($p<0.01$) and uniform particles ($p<0.001$). This is most likely due to the enhanced targeting present on Janus particles in comparison to the other particle formulations (Figure 23). As uniform particles contain both T cell activating and cancer cell targeting molecules dispersed over the entire particle surface, thereby reducing the concentration of each signal, the difference between Ovcar-3 and HeyA8 cells is reduced. This reduction of signal is also why we observed less cytotoxic death of HeyA8 than when treating with Janus particles. Although, theoretically, cancer cell specificity is higher on Janus particles than uniform particles, and should thus result in higher HeyA8 cytotoxicity measured, anti-CD3/28 antibodies are also dispersed over the particle surface which reduces the intensity of this T cell activating signal. As we have previously demonstrated that anti-CD3 particles will elicit significant cytotoxicity – compared to negative controls – regardless of the targeted cell type (Figure 7), and anti-CD3/28 J. particles maintain a concentrated T cell activating signal, we hypothesized that anti-CD3/28 J. particles would elicit higher cytotoxicity than uniform particles. Indeed, compared to uniform particles, anti-CD3/28 particles demonstrated less selectivity.

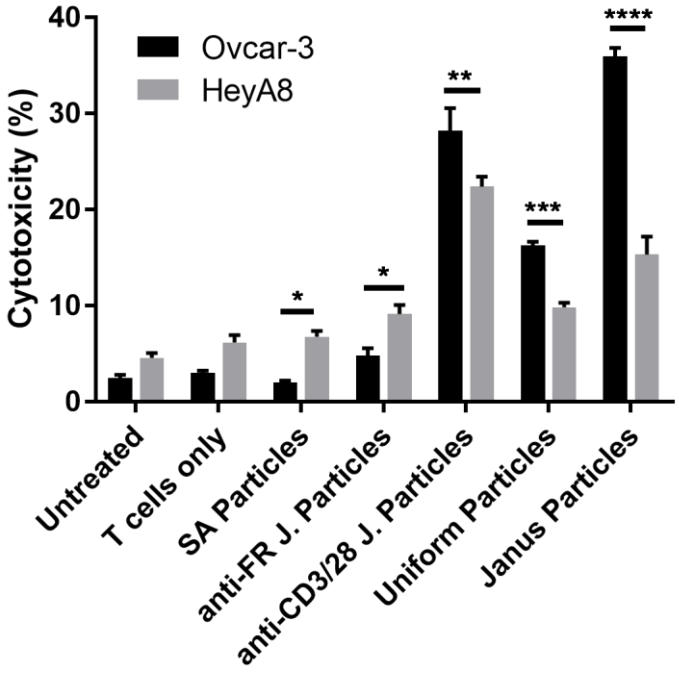

Figure 28: Selectivity of Janus Particles on Cytotoxicity. Ovcar-3 and Hey-A8 cells were incubated with an equivalent number of CD8+ T cells and dosed with particles for 24 hours. Cytotoxicity was measured using a live/dead flow cytometric assay. Data are represented as mean ± SEM; n=6, *p<0.05, **p<0.01, ***p<0.001, ****p<0.0001.

5.3.7 Spheroid Characterization

Next we examined the effect of our Janus particles using an *in vitro* tumor model, Ovcar-3 spheroids. Ovcar-3 cells were stained using Cell Tracker Deep Red fluorescent stain and then 5 x 10^3 cells/well were plated in a round bottom, ultra low attachment 96 well plate. After 4 days of culturing, spheroids were harvested and mounted onto glass microscope slides. Confocal imaging was used to image each spheroid, as shown by the representative image in Figure 29. The diameter of each spheroid was measured using Zen imaging software (Zeiss). After four days, the average spheroid diameter was approximately 1.25 mm.

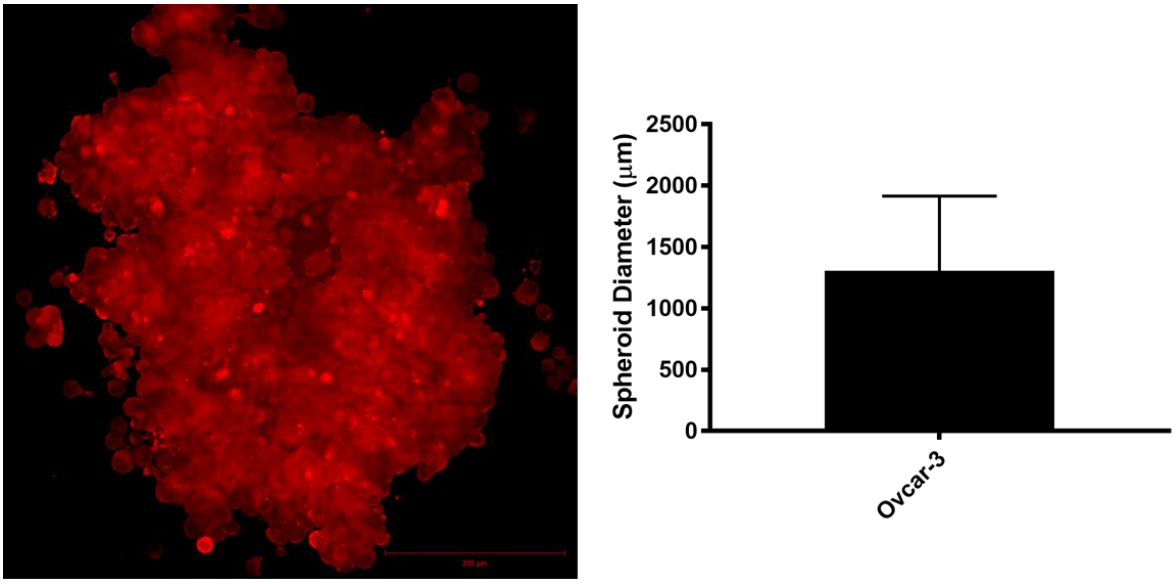

Figure 29: Spheroid Characterization. Ovcar-3 cells were stained with a red fluorescent dye and cultured in an ultra low attachment plate for four days before imaging with confocal microscopy. Each spheroid was measured using Zen imaging software. Scale bar = 200 µm.

5.3.8 Spheroid Cytotoxicity

Cytotoxicity of the spheroids was assessed with the same live/dead cytotoxicity kit used in our 2D culture flow cytometry experiments. Briefly, spheroids were grown for 4 days before getting transferred into a flat bottom 96 well plate and treated simultaneously with CD8+ T cells and particles. After 24 hours, spheroids were stained with calcein AM and ethidium homodimer-1 and Hoechst before mounting onto glass microscope slides. As shown by the representative images in Figure 30, the untreated Ovcar-3 spheroid and T cell only-, SA particle- and anti-FR J. particle-treated spheroids exhibited minimal cytotoxicity. Anti-CD3/28 J. particles exhibited increased cytotoxicity compared to our negative controls and the uniform particle condition. However, the cancer spheroids following uniform particle treatment appear to be semi-disassociated, as the spheroid is no longer cancer cells strongly adhered to each other, as demonstrated in the previous

conditions. Janus particles elicited both the strongest cytotoxicity and the most disassociated morphology, suggesting that Janus particles elicit enough cytotoxicity such that cell-cell adhesions are disrupted. This altered morphology suggests that the inclusion of a targeting molecule allows for deeper penetration of cytotoxicity responses. Supporting this hypothesis is that although anti-CD3/28 J. particle elicit greater cytotoxicity than uniform particles, the cell death is restricted to the surface of the spheroid, according to observations about the images in Figure 29, whereas uniform particle-treated spheroids display cytotoxic cell death within the spheroid as well as on its surface.

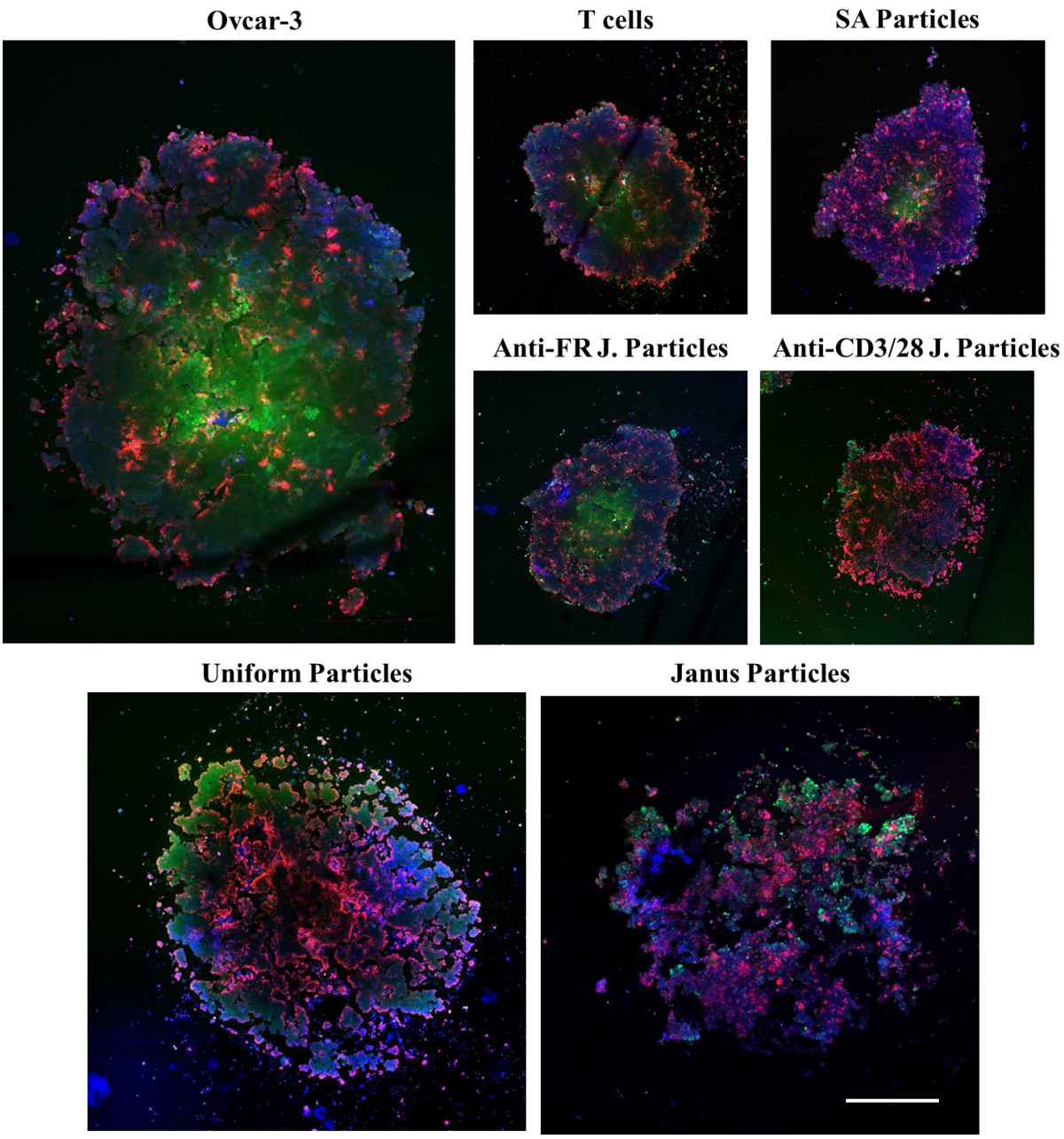

Figure 30: Spheroid Cytotoxicity. Spheroids were evaluated for cytotoxic death using fluorescent live/dead stain. Following 24 hour incubation with CD8+ T cells and particles, spheroids were stained with calcein AM and ethidium homodimer-1 and Hoechst. Representative images are shown of each condition; n=8. Scale bar = 200 μm.

5.3.9 Dual Cancer Cell Targeting

To determine if greater cancer cell death could be elicited by adding an additional cancer cell marker, Janus particles functionalized with anti-FR and anti-e-cadherin, two protein overexpressed on Ovcar-3 cells, were used to treat cancer cells using a 2D and 3D platform. As shown in Figure 31A, the addition of anti-e-cadherin antibody onto the particle did not result in greater cancer cell death compared to Janus particles functionalized with only anti-folate receptor in the 2D cytotoxicity assay. However, when we observe the results of ovarian cancer spheroids treated with Janus particles containing one cancer targeting antibody compared to two cancer targeting antibodies, the differences are noticeable. While the images shown in Figure 31B are largely representative, both conditions provoked highly heterogeneous outcomes. Qualitatively, more spheroids were dissociated, semi-dissociated (as in Figure 31B, top) or in large pieces (as in Figure 31B, bottom) following treatment with either Janus particle formulation. It is not clear whether this spheroid disruption is purely a result of Janus particle dosing or if handling during transferring and staining contributed to the observed dissociated; however, it is unlikely that harsh handling was restricted to the uniform and Janus particle-treated spheroids for all 8 trials. Quantitatively, we observed that Janus particles functionalized with two cancer targeting molecules resulted in a concentration of dead cells on the outside of the spheroid, whereas the single targeting molecule Janus particle elicited cell death that appeared to penetrate into the spheroid. One possible explanation of this observation is that folate receptor is upregulated ubiquitously within the spheroid because it is involved in metabolism, whereas e-cadherin is an adhesion molecule and expressed non-uniformly across tumor spheroids(237). As the flow cytometric assay did not reveal any cytotoxicity differences between the two Janus

particle formulations, it is possible that any differences we observe in the spheroid are exclusive to 3D culture due to the spheroid architecture or that while these two particles direct CD8+ T cell cytotoxic responses in different ways, both result in the same amount of cancer cell death.

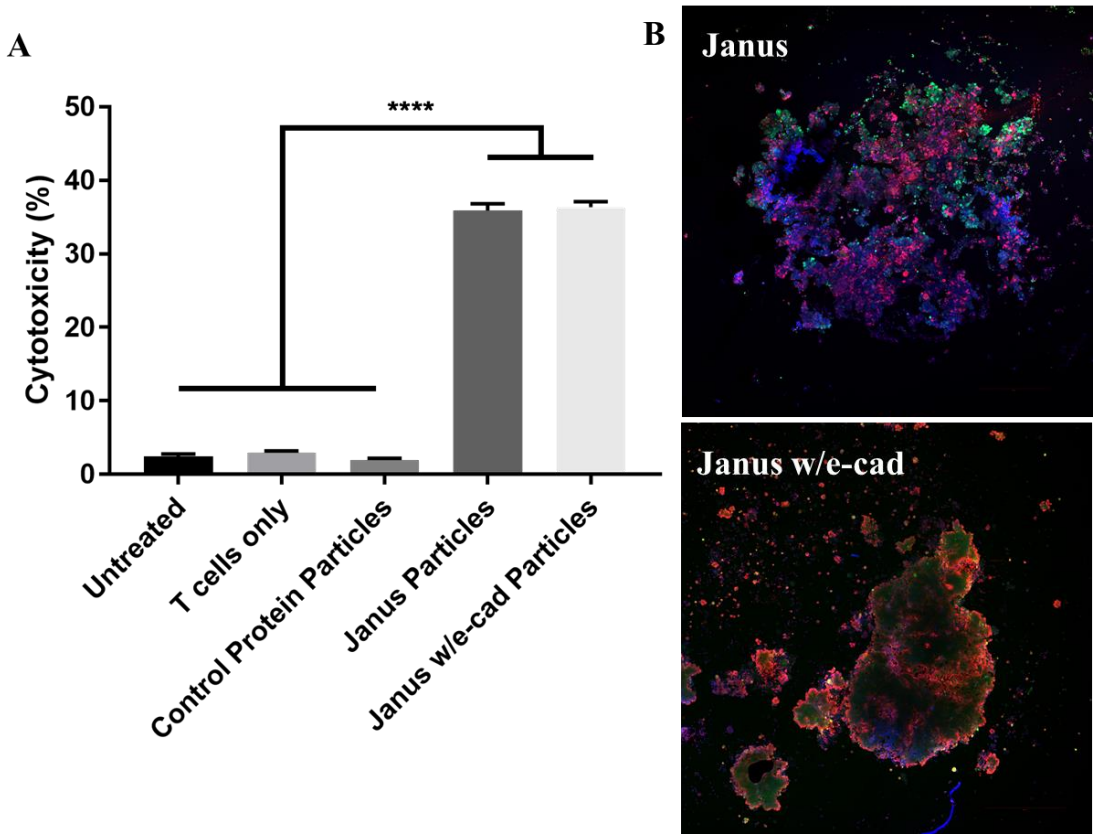

Figure 31: Additional Targeting on Janus Particle does not increase Cytotoxicity. Janus particles displaying both anti-FR and anti-e-cadherin antibodies to target Ovcar-3 cells were incubuated with Ovcar-3 cells using 2D (A) and 3D (B) culture systems. In both cases, cells were dosed with particles and CD8+ T cells for 24 hours and then stained with live/dead labels. (A) Cells were then measured for cytotoxicity using flow cytometry. Data is represented as mean ± SEM; n=6, ****$p<0.0001$. (B) Spheroids were additionally stained with Hoechst and mounted onto glass slides for microscopy. Representative images are shown; n=8.

Although the inclusion of a second cancer-targeting molecule onto our particle platform did not increase cytotoxicity of the targeted cancer cells, we were interested in

the effect on non-targeted cells. As shown in Figure 32, both Janus particle formulations elicited significantly lower cytotoxicity in the non-targeted HeyA8 cells, in comparison to the targeted Ovcar-3 cells. Interestingly, Janus particles that were functionalized with anti-e-cadherin antibody in addition to anti-FR antibody decreased the percentage of HeyA8 cytotoxicity produced as a response to Janus particle treatment ($p<0.05$).). This result suggests the second targeting antibody increases the cancer specificity of treatment, either as a result of decreased non-specific binding or due to less particle binding to cells with low expression of the targeted marker. Theoretically, the inclusion of a second antibody shouldn't have a significant effect on the amount of non-specific binding so it's more likely that fewer particles bind to non-target cells. In the broader context, this effect indicates that the specificity of current cancer cell targeting may be improved by targeting additional antigens or that non-TAA may even be used to target cancer cells specifically; however, additional studies are necessary to test this hypothesis.

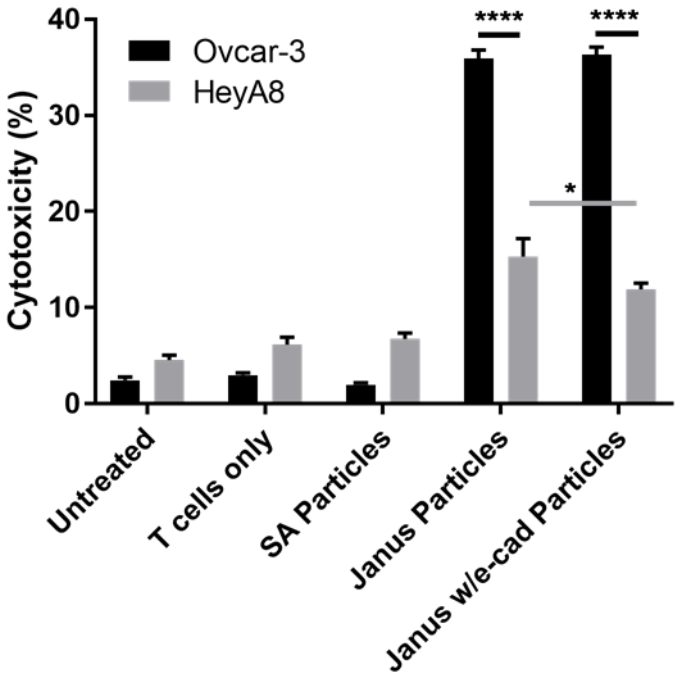

Figure 32: Dual-Cancer targeting Decreases Non-Target Cell Cytotoxicity. Janus particles displaying both anti-FR and anti-e-cadherin antibodies to target Ovcar-3 cells were incubated with Ovcar-e and HeyA8 cells to measure specificity of cell cytotoxicity. Cytotoxicity was determined using a live/dead flow cytometric assay. Data are represented as mean ± SEM; n=6, *p<0.05, ****p<0.0001.

5.3.10 T cell Infiltration

In order to study immune cell infiltration as a result of Janus particle treatment, green fluorescent CD8+ T cells and Janus particles were added simultaneously to cancer spheroids and cultured for 24 hours. As shown in Figure 33, T cells (green) remained mostly on the surface of the spheroid, although some infiltration into the spheroid was observed. Following quantification, we found that Janus particle-activated T cells infiltrated spheroids significantly more, and that the presence of cancer targeting molecule(s) further increased this infiltration. This indicates that both T cell activation and cancer cell targeting improve T cell infiltration into tumor spheroids.

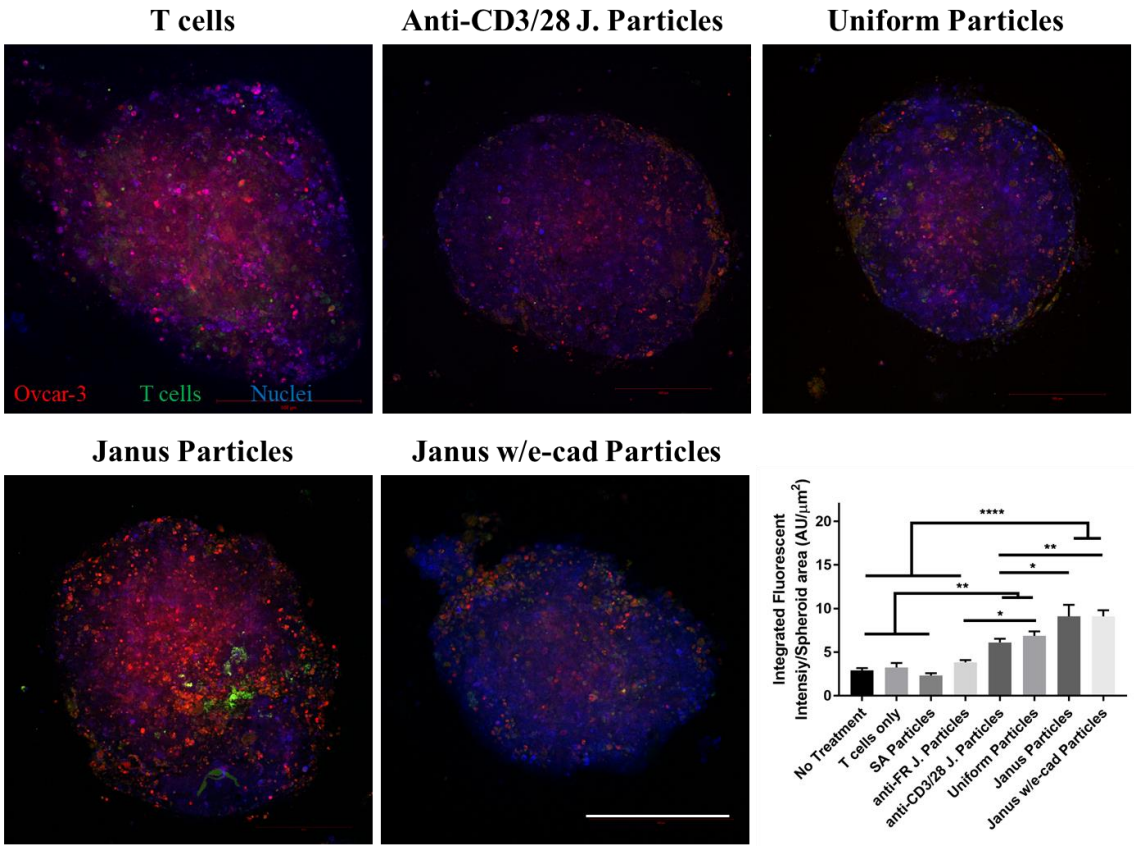

Figure 33: T cell Infiltration following Janus Particle Treatment. Representative image of cancer spheroid treated with Janus particles and CD8+ T cells. Prior to spheroid formation, ovcar-3 cells were labelled with red fluorescent stain. T cells were fluorescently labeled green before dosing spheroids. Following 24 hour incubation, dead cells and nuclei were stained yellow and blue, respectively. Scale bar = 200 μm.

5.3.11 In vivo toxicity following treatment with Janus particles

To determine the *in vivo* response following Janus particle treatment, Janus particles were designed to target carcinoembryonic antigen (CEA), an antigen present usually during embryonic development or by cancerous cells, and injected i.v. into healthy BALB\c mice. Thus, we could examine baseline effects of our particle treatment, i.e. untargeted biodistribution and the potential for systemic toxicity. As Janus particles present a dense concentration of activating molecules, as discussed in CHAPTER 3, toxicity is a

possibility that must be explored. As shown in Figure 34, following Janus or isotype control particles, mice were evaluated after 1 hour, 4 hours, or 24 hours. T cell activity was also evaluated at 72 hours following a half-dose of particles.

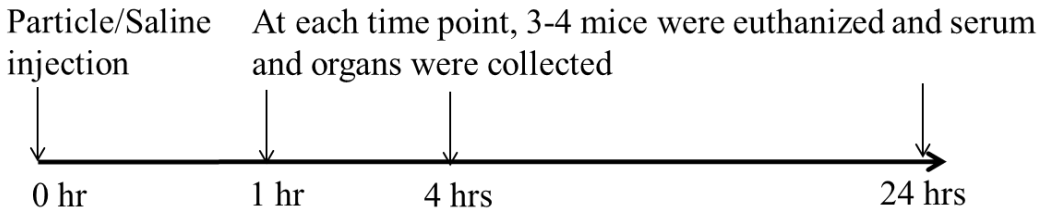

Figure 34: In vivo dosing reginmen. Mice were injected with either Janus or isotype control particles (2.5 μg anti-CD3/28 per mouse). At each time point, mice were euthanized, and relevant organs were harvested and serum was collected.

We evaluated toxicity by measuring the serum concentrations of inflammatory cytokines at each time point following treatment. Both Janus and controls particles showed elevated serum levels of TNF-α and IL-6, one hour post-injection (Figure 35). IL-1β, IL-2, IL-4 and INF-γ were neither detectable at this time point nor at any time point assessed. Additionally, TNF-α and IL-6 were no longer detectable after 4 hours. Broadly, this indicates that systemic toxicity is not occurring and further that Janus particles elicit no more toxicity than control particles. The elevation in TNF-α and IL-6 at one hour could be due to macrophage activation. Both cytokines are secreted by macrophages, professional phagocytes, and might have been elevated as macrophages engulfed the injected particles.

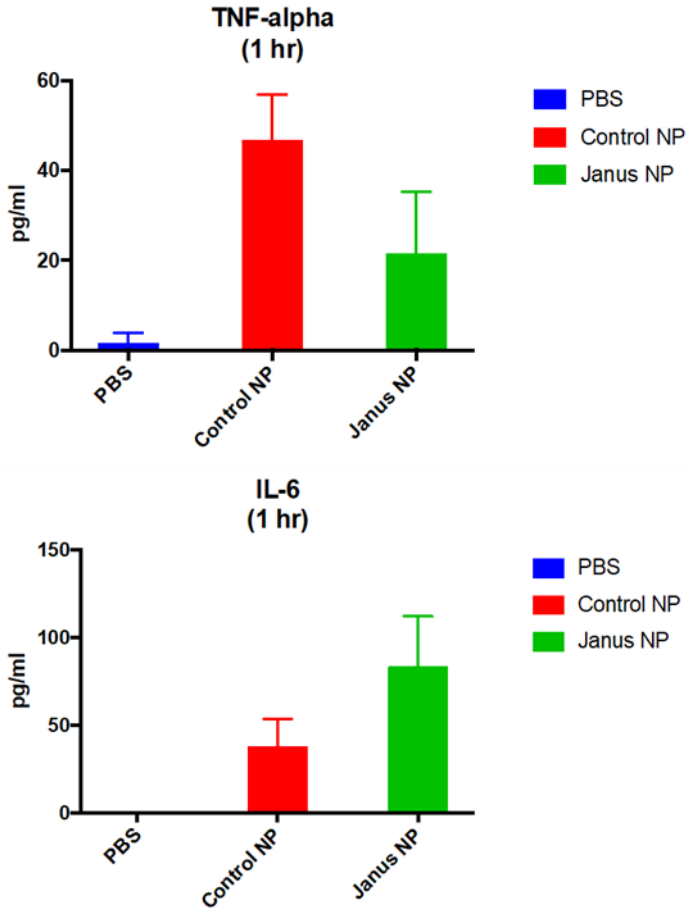

Figure 35: Serum cytokine profile. BALB\c mice were dosed as described above and their serum collected. Luminex was used to determine systemic toxicity by measuring various inflammatory cytokine concentrations. Data are mean ± SD; n=1 (PBS), n=4 (Janus and control particles).

5.3.12 In vivo biodistribution

To visualize the kinetics of particle trafficking in mice, infrared fluorescent imaging was performed using alexa fluor 667 anti-mouse CEA conjugated to Janus particles. Images taken after 4 hours are shown in **Error! Reference source not found.**, and show a lightly higher particle uptake by the liver and kidney in the Janus particle group, compared to the control particles or the PBS group. No differences between groups were observed after 1 hour or 24 hours (as shown in Appendix A). Notably, very little particle

uptake is measured in the spleen while the highest particle signals were measured in the lung, liver, and kidney. This is perhaps an indication that particles are not reaching the spleen and are instead being readily filtered from the blood by the lungs, liver and kidney.

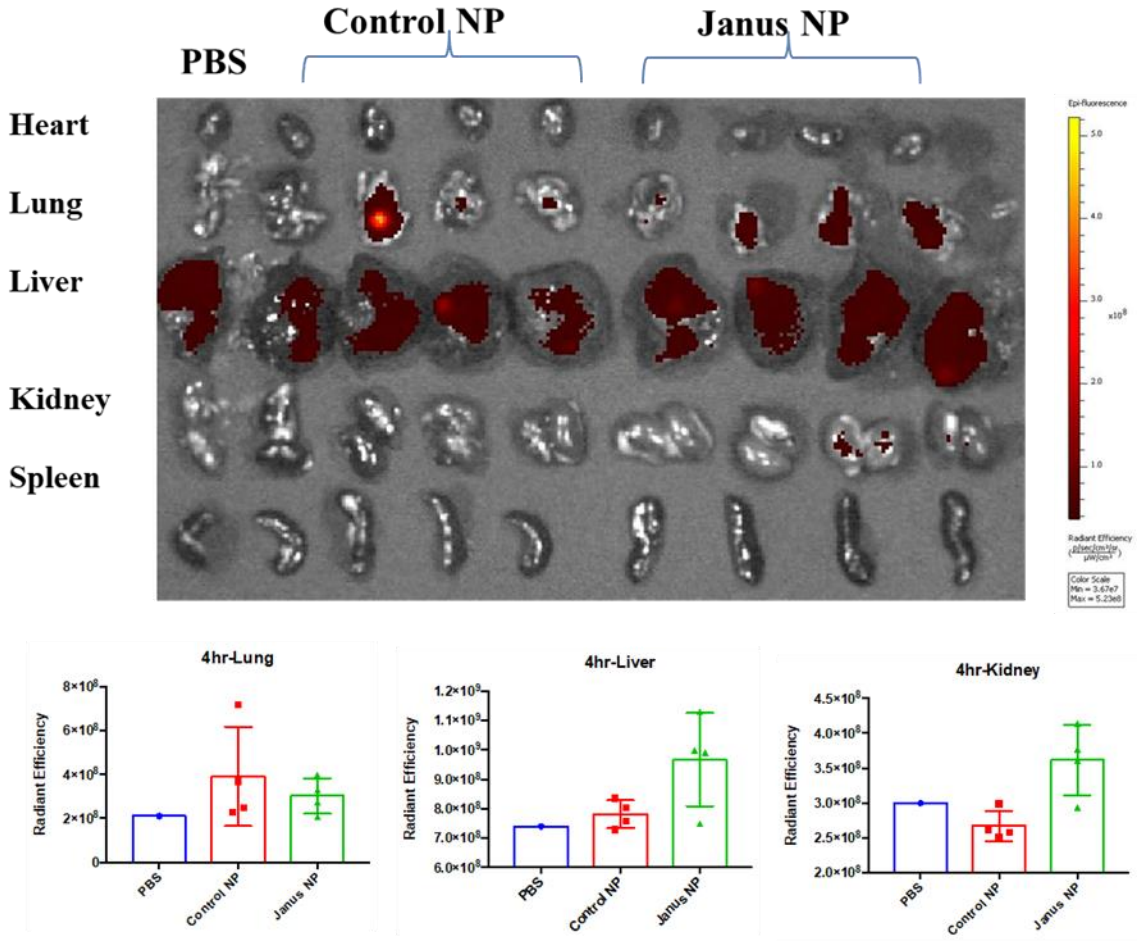

Figure 36: Biodistribution of particles after four hours. BALB\c mice were injected i.v. with Janus or control particles, or PBS. Infrared images of harvested organs were taken to measure particle trafficking. Data = mean ± SD; n = 1 (PBS), n = 4 (Janus and control particles).

5.3.13 Splenic T cell activation following Janus particle treatment

As systemic toxicity was not observed (Figure 35) and particles did not locate to the spleen (Figure 36), it was necessary to determine the impact Janus particles had on T cell functionality and activation. Splenocytes were stained to identify CD4+ and CD8+ T cell subsets and then to measure the percentage of these cells that expressed CD69, a marker of activation. This assay was performed at 24 hours (as shown in) and 72 hours (XYZ). At both time points, no significant differences between conditions were observed. This suggests that although Janus particles present anti-CD3 and anti-CD28 antibodies, splenic T cells exhibit the same amount of activation as isotype control particles. The mechanism behind this result is likely multi-fold: the dose may be too low to elicit an activation response *in vivo*, the particles may not have reached the spleen to activate T cells, or some combination of both explanations. Additional studies investigating particle dose, markers of activated T cells in peripheral blood, or peritoneal delivery of particles should give additional insight about how Janus particles may be used as an immunotherapeutic strategy for cancer treatment.

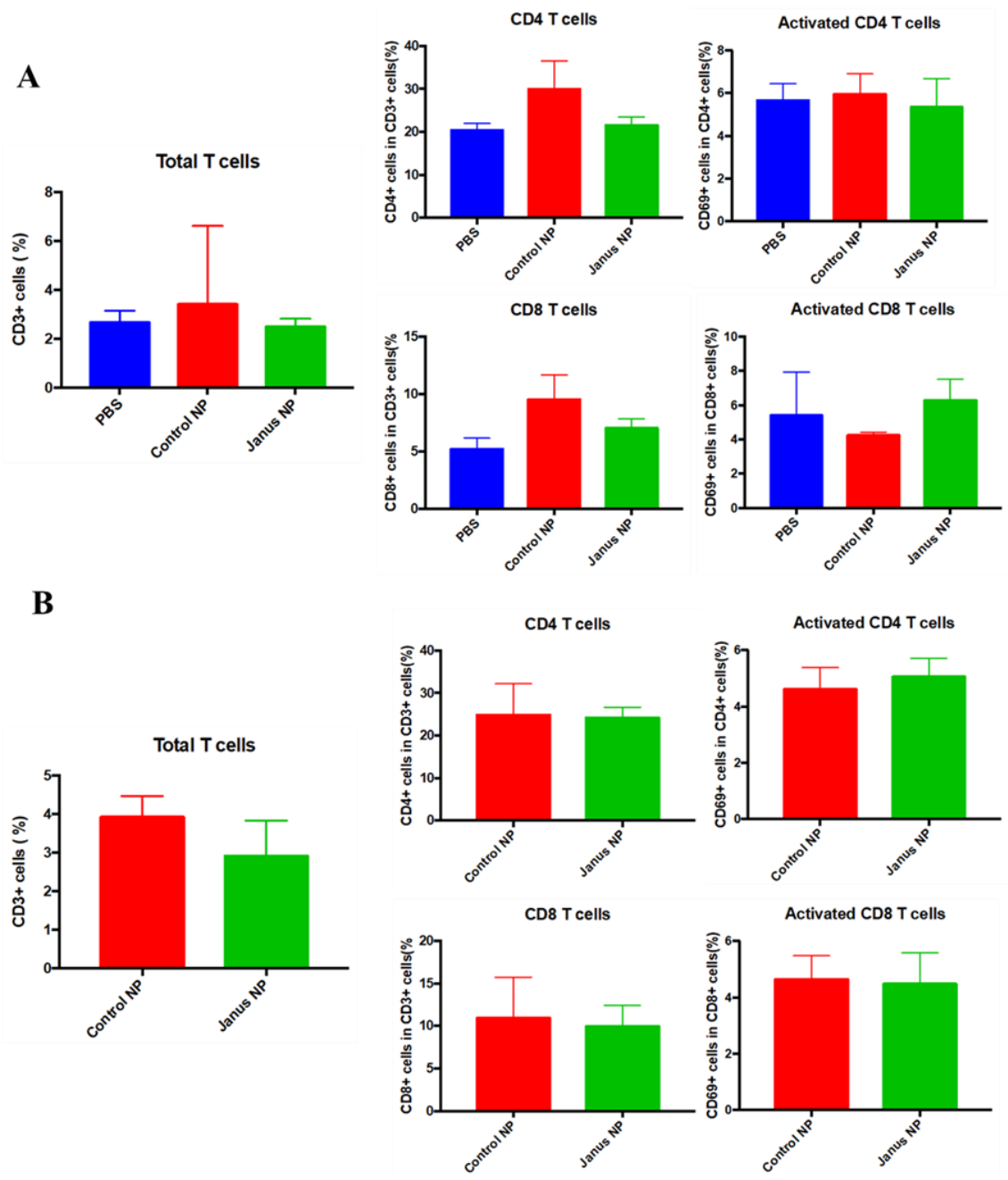

Figure 37: Splenic T cell profile. (A, B) Mice were dosed as previously described and splenic T cell activation was assessed in CD4+ and CD8+ T cell subsets. Data = mean ± SD; n = 4.

5.4 Discussion

The tumor spheroid model presented here provides an in vitro model of an ovarian cancer tumor. 2D cell culture formats lack the significant cell-cell and cell-matrix interactions present in *in vivo* geometries and further force cells into unnatural morphologies(238-241). 3D cell spheroids provide a more accurate representation of cell microenvironment, which allows the modeling of multicellular 3D architecture and function of tissues, including extracellular matrix deposition, physiological barriers, and representative *in vivo* protein expression(239, 242). Cancer spheroids are especially relevant in ovarian cancer contexts, as spheroids best model nonvascularized tumors present in epithelial ovarian cancer. Cell spheroids, thus, may act as *in vitro* tumor analogs. Obviously, the spheroids used in the work presented are limited – they contain only one cell type and we used an immortalized ovarian cancer cell line. Nonetheless, through the use of this spheroid model, we were able to examine not only the extent but also location of cytotoxicity elicited from our particle-activated T cells. This is meaningful as it gives context to our 2D cytotoxicity results (Figure 27). For example anti-CD3/28 J. particles elicited greater cytotoxicity in 2D and 3D culture compared to uniform particles. However, the 3D spheroid culture system revealed that this cytotoxicity is only on the outside of the spheroid (Figure 30). This is most likely because, as there was little to no T cell – cancer cell binding observed following anti-CD3/28 J. particle treatment (Figure 26), activated CD8+ T cells released cytolytic granules simply within the tissue culture well, creating a lytic bath that caused cell death on the outermost layer of the spheroid. Additionally, the spheroid results in Figure 30 show the effectiveness of uniform particles as a cancer immunotherapy; despite the decreased cytotoxicity in 2D culture (Figure 27), the treated spheroid was semi-

disassociated, most likely due to the T cell-cancer cell interactions that occurred (Figure 26). This line of reasoning also explains why Janus particles were superior at eliciting the highest cytotoxicity levels using 2D and 3D *in vitro* culture systems. Because Janus particles displayed an entire hemisphere of densely packed anti-CD3/28 antibodies, T cells were strongly activated, as they were following anti-CD3/28 J. particles (Figure 24). Therefore, regardless of targeting, there would inevitably be some cancer cell cytotoxicity, as described previously about anti-CD3/28 J. particles. The other hemisphere of the Janus particle was densely packed with anti-FR antibody (and also anti-e-cadherin antibody for the second Janus particle), resulting in a high degree of binding, specifically to Ovcar-3 cells (Figure 23). This dual targeting resulted in far greater T cell – cancer cell crosslinking than any other particle formulation; showing both greater numbers of T cells bound, and more cancer cells with bound T cells (Figure 25 and Figure 26). Therefore, treating cancer cells with Janus particles and T cells resulted in activated CD8+ T cells that were crosslinked to targeted cancer cells, causing high cytotoxicity in both 2D and 3D cell cuture, and further spheroid disassociated in cancer spheroid models.

5.5 Conclusions

In conclusion, the work presented here demonstrates the first use of Janus particles to physically crosslink effector and target cell, while simultaneously activating T cells in a nonspecific manner. The resultant crosslinking and activation produces significantly greater cytotoxicity in both 2D and 3D cancer cell culture systems than uniformly coated particles. Janus particles, therefore, should be considered as a potential therapeutic platform for cancer immunotherapy. Whereas bispecific antibodies involve complicated

and expensive manufacturing processes, Janus particles allow for target cell specificity with the ease of non-specific immune cell activation using a platform that may be easily modified. While Janus particle treatment did not translate smoothly into splenic T cell activation *in vivo*, the lack of system wide toxicity is promising. Additional studies will help clarify an appropriate dose and delivery method.

CHAPTER 6. CONCLUSIONS

6.1 Overall Summary

In this presented work, we expand our knowledge of how particles can serve to both bind cancer cells and coordinate activated T cells responses. The mechanics behind non-antigen specific T cell activation by investigating how particle size, antibody functionalization density, and activating signal elicit the greatest degree of T cell response all informed the particle design. We utilized this information to design Janus particles that selectively kill cancer cells while activating resident cytotoxic T cells in a non-specific manner.

In Specific Aim 1, we demonstrated the effect of particle size, molecular density, and activating molecule on T cell activation and cytotoxicity. 300 nm particles, compared to 1 μm and 3 μm, and approximately 50% anti-CD3 antibody surface coverage results in increased GrB release. T cell activation and cytotoxicity depends on the activating molecule(s) as well: cytotoxicity studies showed that anti-CD3 particles were more effective than soluble antibody alone and demonstrated that immune cell proximity to cancer cells was responsible for cancer cell death. Including anti-CD28 antibody for co-stimultation resulted in increased T cell activation that was characterized by more robust immune synapse formation, cytoskeletal remodeling, and cell softening. The *significance of this work* lies in the establishment that anti-CD3/28 particles can non-specifically activate T cells to the extent that cancer cell are killed, although in an untargeted manner.

In Specific Aim 2, we engineered Janus particles to display T cell-activating molecules on one hemisphere and cancer targeting antibodies on the other hemisphere and explored the effect of this particle to elicit cancer cell death using a 2D and 3D ovarian cancer model. We demonstrate that this particle is capable of activating T cells and targeting both CD8+ T cells and Ovcar-3 cells over other cell lines, including ovarian cancer cell lines. We hypothesized that this specific targeting would physically crosslink immune cells and Ovcar-3 cells, and indeed, we observed that Janus particles over other particles tested increased T cell binding to cancer cells and thus, also enhanced cytotoxicity over other tested particles. We show for the first time that Janus particles are superior to uniformly coated particles when directing a non-specific T cell activation response to a specific cancer cell. Additionally, we demonstrate that while adding a second cancer targeting molecule does not increase cytotoxicity of the targeted cells, it does reduce cytotoxicity of non-targeted cells. An exploratory *in vivo* study substantiated the safety of our Janus particle approach. Taken together, these results suggest that Janus particles are an effective cancer immunotherapy platform. The *significance of this work* lies in demonstrating the importance of segregating T cell-activating and cancer cell-targeting signals and the improved specific anti-cancer outcomes.

These results also highlight the need for additional selectivity studies in which cancer cells do not display well established markers that may be used for targeting purposes. Antigen specific T cell activation should also be studied in comparison to non-specific activation, to ensure that off target effects are minimal; it's possible that the immune-activating hemisphere of the Janus particle contains molecules for both specific and non-specific T cell activation. Further activation studies using NK cells are also

possible and could be an interesting approach to leverage the innate immune system against specific cancer cells. The Janus particle platform should also be tested against tumors in an animal model, so that we can evaluate the effectiveness of this novel approach against cancer. Additional *in vivo* studies would aid in our understanding of how immunosuppressive cues within the tumor microenvironment affect Janus particle performance.

The work presented herein contains the first studies in which Janus particles are used to physically bind and bring together effector immune cells and target cancerous cells. While bispecific antibodies accomplish similar actions, our Janus particle treatment combines this strategy with multivalency, which can be leveraged to present not only strong immune activating signals but also multiple cancer targeting molecules, leading to strong cytotoxic T cell responses against specific cancer cells. Janus particles offer a unique strategy in which we can tune immune activation to limit overstimulation, elicit cancer-specific death in a non-antigen specific manner, and easily alter cancer targeting molecules to accommodate cancer and disease heterogeneity; the multifunctionality and modularity inherent to particles are not found with single molecule treatments. This novel and promising approach to cancer immunotherapy should be developed and studied further. The results from this work can also be applied to the greater biomaterial and immunoengineering fields to not only better understand biophysical design parameters for the appropriate outcome but also to positively contribute towards better disease treatment and patient outcomes.

APPENDIX

A. Supplemental for *in vivo* biodistribution study

6.1.1 Biodistribution after 1 hour

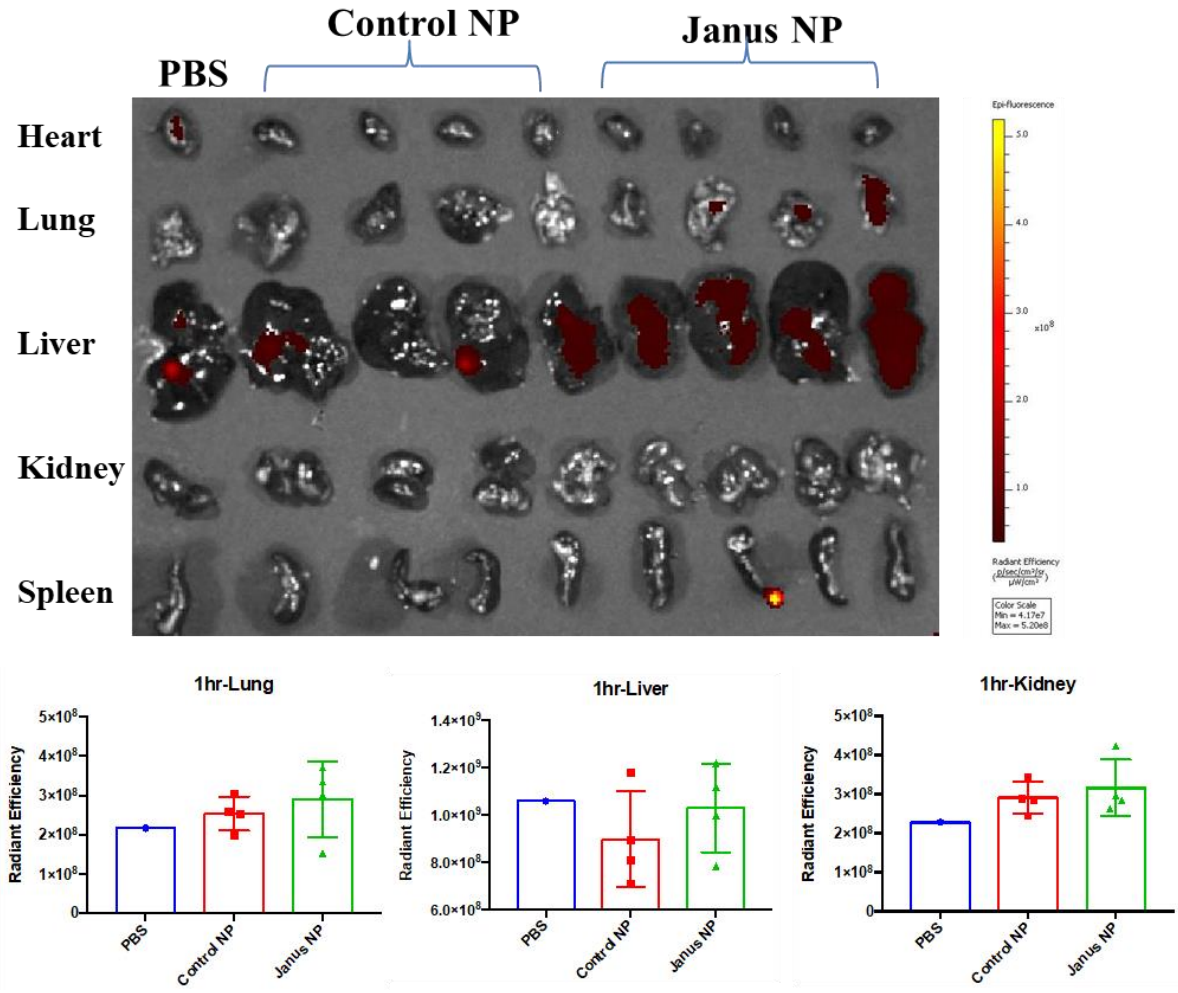

Figure 38: Particle or vehicle biodistribution after 1 hour.

6.1.2 Biodistribution after 24 hours

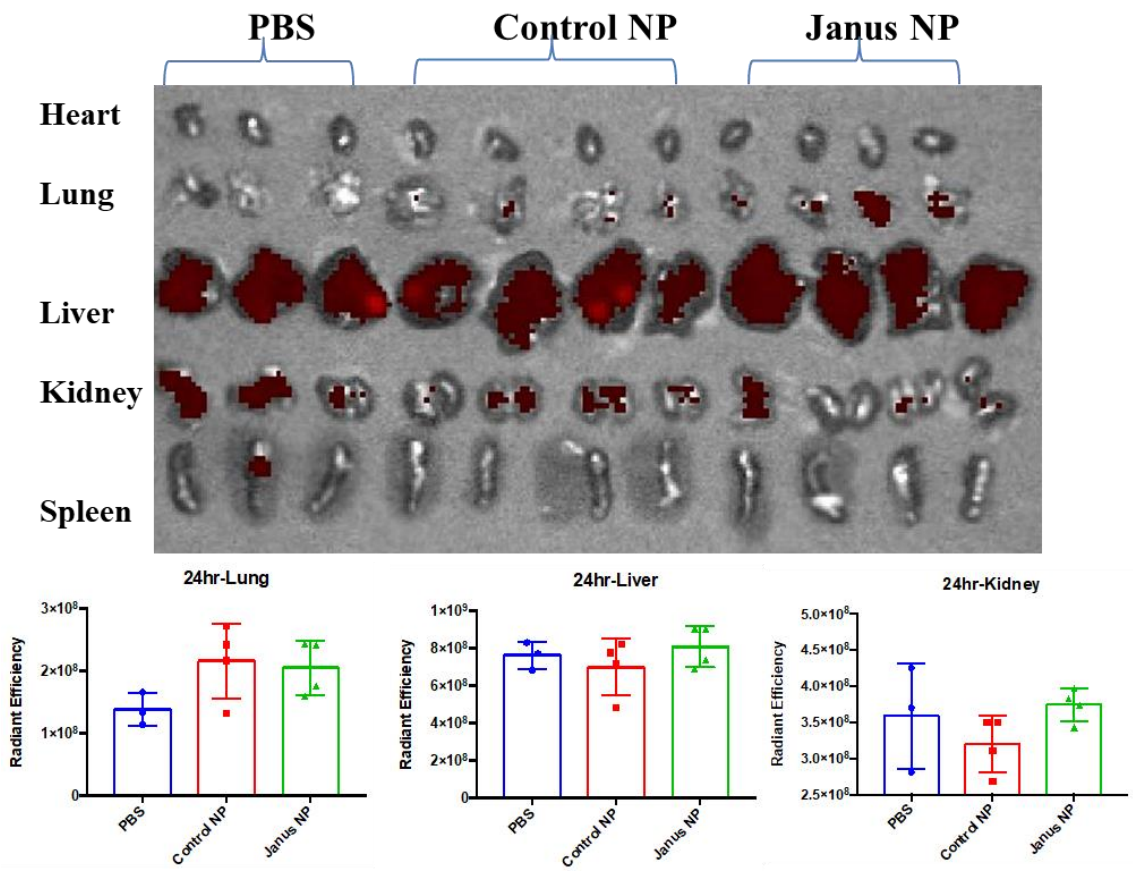

Figure 39: Particle or vehicle biodistribution after 24 hours.

REFERENCES

1. Preston CC, Goode EL, Hartmann LC, Kalli KR, Knutson KL. Immunity and immune suppression in human ovarian cancer. Immunotherapy. 2011;3(4):539-56. doi: 10.2217/imt.11.20. PubMed PMID: 21463194; PubMed Central PMCID: PMC3147144.

2. Vesely MD, Kershaw MH, Schreiber RD, Smyth MJ. Natural innate and adaptive immunity to cancer. Annual review of immunology. 2011;29:235-71. doi: 10.1146/annurev-immunol-031210-101324. PubMed PMID: 21219185.

3. Colotta F, Allavena P, Sica A, Garlanda C, Mantovani A. Cancer-related inflammation, the seventh hallmark of cancer: links to genetic instability. Carcinogenesis. 2009;30(7):1073-81. doi: 10.1093/carcin/bgp127. PubMed PMID: 19468060.

4. Andersen MH, Schrama D, Thor Straten P, Becker JC. Cytotoxic T cells. The Journal of investigative dermatology. 2006;126(1):32-41. doi: 10.1038/sj.jid.5700001. PubMed PMID: 16417215.

5. Yoshimura A, Muto G. TGF-beta function in immune suppression. Current topics in microbiology and immunology. 2011;350:127-47. doi: 10.1007/82_2010_87. PubMed PMID: 20680806.

6. Dunn GP, Bruce AT, Ikeda H, Old LJ, Schreiber RD. Cancer immunoediting: from immunosurveillance to tumor escape. Nature immunology. 2002;3(11):991-8. doi: 10.1038/ni1102-991. PubMed PMID: 12407406.

7. Schreiber RD, Old LJ, Smyth MJ. Cancer immunoediting: integrating immunity's roles in cancer suppression and promotion. Science. 2011;331(6024):1565-70. doi: 10.1126/science.1203486. PubMed PMID: 21436444.

8. Wick DA, Webb JR, Nielsen JS, Martin SD, Kroeger DR, Milne K, et al. Surveillance of the tumor mutanome by T cells during progression from primary to recurrent ovarian cancer. Clinical cancer research : an official journal of the American Association for Cancer Research. 2014;20(5):1125-34. doi: 10.1158/1078-0432.CCR-13-2147. PubMed PMID: 24323902.

9. Sulchek TA, Friddle RW, Langry K, Lau EY, Albrecht H, Ratto TV, et al. Dynamic force spectroscopy of parallel individual Mucin1-antibody bonds. PNAS. 2005;102(46):16638-43.

10. Pacheco P, White D, Sulchek T. Effects of Microparticle Size and Fc Density on Macrophage Phagocytosis. PLoS One. 2013;8(4). doi: e60989

10.1371/journal.pone.0060989. PubMed PMID: WOS:000317911500012.

11. Pacheco P, Le B, White D, Sulchek T. Tunable Complement Activation by Particles with Variable Size and Fc Density. Nano LIFE. 2013;3.

12. Odunsi K. Immunotherapy in ovarian cancer. Annals of oncology : official journal of the European Society for Medical Oncology. 2017;28(suppl_8):viii1-viii7. doi: 10.1093/annonc/mdx444. PubMed PMID: 29232467; PubMed Central PMCID: PMC5834124.

13. Siegel RL, Miller KD, Jemal A. Cancer Statistics, 2017. CA: a cancer journal for clinicians. 2017;67(1):7-30. doi: 10.3322/caac.21387. PubMed PMID: 28055103.

14. Kulbe H, Chakravarty P, Leinster DA, Charles KA, Kwong J, Thompson RG, et al. A dynamic inflammatory cytokine network in the human ovarian cancer microenvironment. Cancer research. 2012;72(1):66-75. doi: 10.1158/0008-5472.CAN-11-2178. PubMed PMID: 22065722; PubMed Central PMCID: PMC3252703.

15. Lengyel E. Ovarian cancer development and metastasis. The American journal of pathology. 2010;177(3):1053-64. doi: 10.2353/ajpath.2010.100105. PubMed PMID: 20651229; PubMed Central PMCID: PMC2928939.

16. Pradeep S, Kim SW, Wu SY, Nishimura M, Chaluvally-Raghavan P, Miyake T, et al. Hematogenous metastasis of ovarian cancer: rethinking mode of spread. Cancer cell. 2014;26(1):77-91. doi: 10.1016/j.ccr.2014.05.002. PubMed PMID: 25026212; PubMed Central PMCID: PMC4100212.

17. Gerber SA, Rybalko VY, Bigelow CE, Lugade AA, Foster TH, Frelinger JG, et al. Preferential attachment of peritoneal tumor metastases to omental immune aggregates and possible role of a unique vascular microenvironment in metastatic survival and growth. The American journal of pathology. 2006;169(5):1739-52. doi: 10.2353/ajpath.2006.051222. PubMed PMID: 17071597; PubMed Central PMCID: PMC1780209.

18. Mills K, Fuh K. Recent Advances in Understanding, Diagnosing, and Treating Ovarian Cancer. F1000Research. 2017;6:84. doi: 10.12688/f1000research.9977.1. PubMed PMID: 28184293; PubMed Central PMCID: PMC5288682.

19. Worzfeld T, Pogge von Strandmann E, Huber M, Adhikary T, Wagner U, Reinartz S, et al. The Unique Molecular and Cellular Microenvironment of Ovarian Cancer. Frontiers in oncology. 2017;7:24. doi: 10.3389/fonc.2017.00024. PubMed PMID: 28275576; PubMed Central PMCID: PMC5319992.

20. Bremnes RM, Al-Shibli K, Donnem T, Sirera R, Al-Saad S, Andersen S, et al. The role of tumor-infiltrating immune cells and chronic inflammation at the tumor site on cancer development, progression, and prognosis: emphasis on non-small cell lung cancer. Journal of thoracic oncology : official publication of the International Association for the

Study of Lung Cancer. 2011;6(4):824-33. doi: 10.1097/JTO.0b013e3182037b76. PubMed PMID: 21173711.

21. de Visser KE, Eichten A, Coussens LM. Paradoxical roles of the immune system during cancer development. Nature reviews Cancer. 2006;6(1):24-37. doi: 10.1038/nrc1782. PubMed PMID: 16397525.

22. Joyce JA, Pollard JW. Microenvironmental regulation of metastasis. Nature reviews Cancer. 2009;9(4):239-52. doi: 10.1038/nrc2618. PubMed PMID: 19279573; PubMed Central PMCID: PMC3251309.

23. Zhang Y, Tang H, Cai J, Zhang T, Guo J, Feng D, et al. Ovarian cancer-associated fibroblasts contribute to epithelial ovarian carcinoma metastasis by promoting angiogenesis, lymphangiogenesis and tumor cell invasion. Cancer letters. 2011;303(1):47-55. doi: 10.1016/j.canlet.2011.01.011. PubMed PMID: 21310528.

24. Elkabets M, Gifford AM, Scheel C, Nilsson B, Reinhardt F, Bray MA, et al. Human tumors instigate granulin-expressing hematopoietic cells that promote malignancy by activating stromal fibroblasts in mice. The Journal of clinical investigation. 2011;121(2):784-99. doi: 10.1172/JCI43757. PubMed PMID: 21266779; PubMed Central PMCID: PMC3026724.

25. Cai J, Tang H, Xu L, Wang X, Yang C, Ruan S, et al. Fibroblasts in omentum activated by tumor cells promote ovarian cancer growth, adhesion and invasiveness. Carcinogenesis. 2012;33(1):20-9. doi: 10.1093/carcin/bgr230. PubMed PMID: 22021907.

26. Direkze NC, Hodivala-Dilke K, Jeffery R, Hunt T, Poulsom R, Oukrif D, et al. Bone marrow contribution to tumor-associated myofibroblasts and fibroblasts. Cancer research. 2004;64(23):8492-5. doi: 10.1158/0008-5472.CAN-04-1708. PubMed PMID: 15574751.

27. Ishii G, Sangai T, Oda T, Aoyagi Y, Hasebe T, Kanomata N, et al. Bone-marrow-derived myofibroblasts contribute to the cancer-induced stromal reaction. Biochemical and biophysical research communications. 2003;309(1):232-40. PubMed PMID: 12943687.

28. Sugimoto H, Mundel TM, Kieran MW, Kalluri R. Identification of fibroblast heterogeneity in the tumor microenvironment. Cancer biology & therapy. 2006;5(12):1640-6. PubMed PMID: 17106243.

29. Morgan RJ, Jr., Alvarez RD, Armstrong DK, Burger RA, Chen LM, Copeland L, et al. Ovarian cancer, version 2.2013. Journal of the National Comprehensive Cancer Network : JNCCN. 2013;11(10):1199-209. PubMed PMID: 24142821.

30. Mammen M, Choi SK, Whitesides GM. Polyvalent interactions in biological systems: Implications for design and use of multivalent ligands and inhibitors. Angew Chem Int Edit. 1998;37(20):2755-94. PubMed PMID: ISI:000076892300001.

31. Rubio V, Stuge TB, Singh N, Betts MR, Weber JS, Roederer M, et al. Ex vivo identification, isolation and analysis of tumor-cytolytic T cells. Nat Med. 2003;9(11):1377-82. doi: 10.1038/nm942. PubMed PMID: WOS:000186319700027.

32. Zhang L, Conejo-Garcia JR, Katsaros D, Gimotty PA, Massobrio M, Regnani G, et al. Intratumoral T cells, recurrence, and survival in epithelial ovarian cancer. The New England journal of medicine. 2003;348(3):203-13. doi: 10.1056/NEJMoa020177. PubMed PMID: 12529460.

33. Sato E, Olson SH, Ahn J, Bundy B, Nishikawa H, Qian F, et al. Intraepithelial CD8+ tumor-infiltrating lymphocytes and a high CD8+/regulatory T cell ratio are associated with favorable prognosis in ovarian cancer. Proceedings of the National Academy of Sciences of the United States of America. 2005;102(51):18538-43. doi: 10.1073/pnas.0509182102. PubMed PMID: 16344461; PubMed Central PMCID: PMC1311741.

34. Hwang WT, Adams SF, Tahirovic E, Hagemann IS, Coukos G. Prognostic significance of tumor-infiltrating T cells in ovarian cancer: a meta-analysis. Gynecologic oncology. 2012;124(2):192-8. doi: 10.1016/j.ygyno.2011.09.039. PubMed PMID: 22040834; PubMed Central PMCID: PMC3298445.

35. Hamanishi J, Mandai M, Iwasaki M, Okazaki T, Tanaka Y, Yamaguchi K, et al. Programmed cell death 1 ligand 1 and tumor-infiltrating CD8+ T lymphocytes are prognostic factors of human ovarian cancer. Proceedings of the National Academy of Sciences of the United States of America. 2007;104(9):3360-5. doi: 10.1073/pnas.0611533104. PubMed PMID: 17360651; PubMed Central PMCID: PMC1805580.

36. Callahan MJ, Nagymanyoki Z, Bonome T, Johnson ME, Litkouhi B, Sullivan EH, et al. Increased HLA-DMB expression in the tumor epithelium is associated with increased CTL infiltration and improved prognosis in advanced-stage serous ovarian cancer. Clinical cancer research : an official journal of the American Association for Cancer Research. 2008;14(23):7667-73. doi: 10.1158/1078-0432.CCR-08-0479. PubMed PMID: 19047092; PubMed Central PMCID: PMC3000165.

37. Kooi S, Zhang HZ, Patenia R, Edwards CL, Platsoucas CD, Freedman RS. HLA class I expression on human ovarian carcinoma cells correlates with T-cell infiltration in vivo and T-cell expansion in vitro in low concentrations of recombinant interleukin-2. Cellular immunology. 1996;174(2):116-28. doi: 10.1006/cimm.1996.0301. PubMed PMID: 8954611.

38. Milne K, Kobel M, Kalloger SE, Barnes RO, Gao D, Gilks CB, et al. Systematic analysis of immune infiltrates in high-grade serous ovarian cancer reveals CD20, FoxP3 and TIA-1 as positive prognostic factors. PloS one. 2009;4(7):e6412. doi: 10.1371/journal.pone.0006412. PubMed PMID: 19641607; PubMed Central PMCID: PMC2712762.

39. Nielsen JS, Sahota RA, Milne K, Kost SE, Nesslinger NJ, Watson PH, et al. CD20+ tumor-infiltrating lymphocytes have an atypical CD27- memory phenotype and together with CD8+ T cells promote favorable prognosis in ovarian cancer. Clinical cancer research : an official journal of the American Association for Cancer Research. 2012;18(12):3281-92. doi: 10.1158/1078-0432.CCR-12-0234. PubMed PMID: 22553348.

40. Nielsen JS, Nelson BH. Tumor-infiltrating B cells and T cells: Working together to promote patient survival. Oncoimmunology. 2012;1(9):1623-5. doi: 10.4161/onci.21650. PubMed PMID: 23264915; PubMed Central PMCID: PMC3525624.

41. Wang X, Deavers M, Patenia R, Bassett RL, Jr., Mueller P, Ma Q, et al. Monocyte/macrophage and T-cell infiltrates in peritoneum of patients with ovarian cancer or benign pelvic disease. Journal of translational medicine. 2006;4:30. doi: 10.1186/1479-5876-4-30. PubMed PMID: 16824216; PubMed Central PMCID: PMC1550428.

42. Zhang S, Yu M, Deng H, Shen G, Wei Y. Polyclonal rabbit anti-human ovarian cancer globulins inhibit tumor growth through apoptosis involving the caspase signaling. Scientific reports. 2014;4:4984. doi: 10.1038/srep04984. PubMed PMID: 24828460; PubMed Central PMCID: PMC4021334.

43. Cappuccini F, Lucci JA, 3rd, Dett CA, Gatanaga M, Ininns EK, Gatanaga T, et al. Trafficking of syngeneic murine lymphokine activated killer T cells following intraperitoneal administration in normal and tumor bearing mice. Gynecologic oncology. 1992;46(2):163-9. PubMed PMID: 1500017.

44. Lynch L, O'Shea D, Winter DC, Geoghegan J, Doherty DG, O'Farrelly C. Invariant NKT cells and CD1d(+) cells amass in human omentum and are depleted in patients with cancer and obesity. European journal of immunology. 2009;39(7):1893-901. doi: 10.1002/eji.200939349. PubMed PMID: 19585513.

45. Ansel KM, Harris RB, Cyster JG. CXCL13 is required for B1 cell homing, natural antibody production, and body cavity immunity. Immunity. 2002;16(1):67-76. PubMed PMID: 11825566.

46. Beelen RH, Fluitsma DM, Hoefsmit EC. The cellular composition of omentum milky spots and the ultrastructure of milky spot macrophages and reticulum cells. Journal of the Reticuloendothelial Society. 1980;28(6):585-99. PubMed PMID: 6450834.

47. Carlow DA, Gold MR, Ziltener HJ. Lymphocytes in the peritoneum home to the omentum and are activated by resident dendritic cells. Journal of immunology. 2009;183(2):1155-65. doi: 10.4049/jimmunol.0900409. PubMed PMID: 19553538.

48. Chatterjee M, Wojciechowski J, Tainsky MA. Discovery of antibody biomarkers using protein microarrays of tumor antigens cloned in high throughput. Methods in

molecular biology. 2009;520:21-38. doi: 10.1007/978-1-60327-811-9_3. PubMed PMID: 19381945.

49. Old LJ, Boyse EA. Immunology of Experimental Tumors. Annual review of medicine. 1964;15:167-86. doi: 10.1146/annurev.me.15.020164.001123. PubMed PMID: 14139934.

50. Cheever MA, Allison JP, Ferris AS, Finn OJ, Hastings BM, Hecht TT, et al. The prioritization of cancer antigens: a national cancer institute pilot project for the acceleration of translational research. Clinical cancer research : an official journal of the American Association for Cancer Research. 2009;15(17):5323-37. doi: 10.1158/1078-0432.CCR-09-0737. PubMed PMID: 19723653; PubMed Central PMCID: PMC5779623.

51. van der Bruggen P, Traversari C, Chomez P, Lurquin C, De Plaen E, Van den Eynde B, et al. A gene encoding an antigen recognized by cytolytic T lymphocytes on a human melanoma. Science. 1991;254(5038):1643-7. PubMed PMID: 1840703.

52. Vesely MD, Kershaw MH, Schreiber RD, Smyth MJ. Natural Innate and Adaptive Immunity to Cancer. In: Paul WE, Littman DR, Yokoyama WM, editors. Annual Review of Immunology, Vol 29. Annual Review of Immunology. 29. Palo Alto: Annual Reviews; 2011. p. 235-71.

53. Kataoka T, Schroter M, Hahne M, Schneider P, Irmler M, Thome M, et al. FLIP prevents apoptosis induced by death receptors but not by perforin/granzyme B, chemotherapeutic drugs, and gamma irradiation. Journal of immunology. 1998;161(8):3936-42. PubMed PMID: 9780161.

54. Hinz S, Trauzold A, Boenicke L, Sandberg C, Beckmann S, Bayer E, et al. Bcl-XL protects pancreatic adenocarcinoma cells against CD95- and TRAIL-receptor-mediated apoptosis. Oncogene. 2000;19(48):5477-86. doi: 10.1038/sj.onc.1203936. PubMed PMID: 11114725.

55. Khong HT, Restifo NP. Natural selection of tumor variants in the generation of "tumor escape" phenotypes. Nature immunology. 2002;3(11):999-1005. doi: 10.1038/ni1102-999. PubMed PMID: 12407407; PubMed Central PMCID: PMC1508168.

56. Shin MS, Kim HS, Lee SH, Park WS, Kim SY, Park JY, et al. Mutations of tumor necrosis factor-related apoptosis-inducing ligand receptor 1 (TRAIL-R1) and receptor 2 (TRAIL-R2) genes in metastatic breast cancers. Cancer research. 2001;61(13):4942-6. PubMed PMID: 11431320.

57. Takahashi H, Feuerhake F, Kutok JL, Monti S, Dal Cin P, Neuberg D, et al. FAS death domain deletions and cellular FADD-like interleukin 1beta converting enzyme inhibitory protein (long) overexpression: alternative mechanisms for deregulating the extrinsic apoptotic pathway in diffuse large B-cell lymphoma subtypes. Clinical cancer research : an official journal of the American Association for Cancer Research.

2006;12(11 Pt 1):3265-71. doi: 10.1158/1078-0432.CCR-06-0076. PubMed PMID: 16740746.

58. Jin HT, Ahmed R, Okazaki T. Role of PD-1 in regulating T-cell immunity. Current topics in microbiology and immunology. 2011;350:17-37. doi: 10.1007/82_2010_116. PubMed PMID: 21061197.

59. Francisco LM, Sage PT, Sharpe AH. The PD-1 pathway in tolerance and autoimmunity. Immunological reviews. 2010;236:219-42. doi: 10.1111/j.1600-065X.2010.00923.x. PubMed PMID: 20636820; PubMed Central PMCID: PMC2919275.

60. Maine CJ, Aziz NH, Chatterjee J, Hayford C, Brewig N, Whilding L, et al. Programmed death ligand-1 over-expression correlates with malignancy and contributes to immune regulation in ovarian cancer. Cancer immunology, immunotherapy : CII. 2014;63(3):215-24. doi: 10.1007/s00262-013-1503-x. PubMed PMID: 24297569.

61. Ino K. Indoleamine 2,3-dioxygenase and immune tolerance in ovarian cancer. Current opinion in obstetrics & gynecology. 2011;23(1):13-8. doi: 10.1097/GCO.0b013e3283409c79. PubMed PMID: 20930628.

62. Qian F, Villella J, Wallace PK, Mhawech-Fauceglia P, Tario JD, Jr., Andrews C, et al. Efficacy of levo-1-methyl tryptophan and dextro-1-methyl tryptophan in reversing indoleamine-2,3-dioxygenase-mediated arrest of T-cell proliferation in human epithelial ovarian cancer. Cancer research. 2009;69(13):5498-504. doi: 10.1158/0008-5472.CAN-08-2106. PubMed PMID: 19491279.

63. Merogi AJ, Marrogi AJ, Ramesh R, Robinson WR, Fermin CD, Freeman SM. Tumor-host interaction: analysis of cytokines, growth factors, and tumor-infiltrating lymphocytes in ovarian carcinomas. Human pathology. 1997;28(3):321-31. PubMed PMID: 9042797.

64. Wrzesinski SH, Wan YY, Flavell RA. Transforming growth factor-beta and the immune response: implications for anticancer therapy. Clinical cancer research : an official journal of the American Association for Cancer Research. 2007;13(18 Pt 1):5262-70. doi: 10.1158/1078-0432.CCR-07-1157. PubMed PMID: 17875754.

65. Rodriguez GC, Haisley C, Hurteau J, Moser TL, Whitaker R, Bast RC, Jr., et al. Regulation of invasion of epithelial ovarian cancer by transforming growth factor-beta. Gynecologic oncology. 2001;80(2):245-53. doi: 10.1006/gyno.2000.6042. PubMed PMID: 11161867.

66. Kulbe H, Thompson R, Wilson JL, Robinson S, Hagemann T, Fatah R, et al. The inflammatory cytokine tumor necrosis factor-alpha generates an autocrine tumor-promoting network in epithelial ovarian cancer cells. Cancer research. 2007;67(2):585-92. doi: 10.1158/0008-5472.CAN-06-2941. PubMed PMID: 17234767; PubMed Central PMCID: PMC2679985.

67. Kwong J, Chan FL, Wong KK, Birrer MJ, Archibald KM, Balkwill FR, et al. Inflammatory cytokine tumor necrosis factor alpha confers precancerous phenotype in an organoid model of normal human ovarian surface epithelial cells. Neoplasia. 2009;11(6):529-41. PubMed PMID: 19484142; PubMed Central PMCID: PMC2685442.

68. Milliken D, Scotton C, Raju S, Balkwill F, Wilson J. Analysis of chemokines and chemokine receptor expression in ovarian cancer ascites. Clinical cancer research : an official journal of the American Association for Cancer Research. 2002;8(4):1108-14. PubMed PMID: 11948121.

69. Scotton CJ, Wilson JL, Scott K, Stamp G, Wilbanks GD, Fricker S, et al. Multiple actions of the chemokine CXCL12 on epithelial tumor cells in human ovarian cancer. Cancer research. 2002;62(20):5930-8. PubMed PMID: 12384559.

70. Righi E, Kashiwagi S, Yuan J, Santosuosso M, Leblanc P, Ingraham R, et al. CXCL12/CXCR4 blockade induces multimodal antitumor effects that prolong survival in an immunocompetent mouse model of ovarian cancer. Cancer research. 2011;71(16):5522-34. doi: 10.1158/0008-5472.CAN-10-3143. PubMed PMID: 21742774; PubMed Central PMCID: PMC3959864.

71. Plante M, Rubin SC, Wong GY, Federici MG, Finstad CL, Gastl GA. Interleukin-6 level in serum and ascites as a prognostic factor in patients with epithelial ovarian cancer. Cancer. 1994;73(7):1882-8. PubMed PMID: 8137215.

72. Coward J, Kulbe H, Chakravarty P, Leader D, Vassileva V, Leinster DA, et al. Interleukin-6 as a therapeutic target in human ovarian cancer. Clinical cancer research : an official journal of the American Association for Cancer Research. 2011;17(18):6083-96. doi: 10.1158/1078-0432.CCR-11-0945. PubMed PMID: 21795409; PubMed Central PMCID: PMC3182554.

73. Guo Y, Xu F, Lu T, Duan Z, Zhang Z. Interleukin-6 signaling pathway in targeted therapy for cancer. Cancer treatment reviews. 2012;38(7):904-10. doi: 10.1016/j.ctrv.2012.04.007. PubMed PMID: 22651903.

74. Gabrilovich DI, Ishida T, Nadaf S, Ohm JE, Carbone DP. Antibodies to vascular endothelial growth factor enhance the efficacy of cancer immunotherapy by improving endogenous dendritic cell function. Clinical cancer research : an official journal of the American Association for Cancer Research. 1999;5(10):2963-70. PubMed PMID: 10537366.

75. Tiper IV, Temkin SM, Spiegel S, Goldblum SE, Giuntoli RL, 2nd, Oelke M, et al. VEGF Potentiates GD3-Mediated Immunosuppression by Human Ovarian Cancer Cells. Clinical cancer research : an official journal of the American Association for Cancer Research. 2016;22(16):4249-58. doi: 10.1158/1078-0432.CCR-15-2518. PubMed PMID: 27076627; PubMed Central PMCID: PMC4987212.

76. Gavalas NG, Tsiatas M, Tsitsilonis O, Politi E, Ioannou K, Ziogas AC, et al. VEGF directly suppresses activation of T cells from ascites secondary to ovarian cancer

via VEGF receptor type 2. British journal of cancer. 2012;107(11):1869-75. doi: 10.1038/bjc.2012.468. PubMed PMID: 23169339; PubMed Central PMCID: PMC3504940.

77. Terabe M, Berzofsky JA. Immunoregulatory T cells in tumor immunity. Current opinion in immunology. 2004;16(2):157-62. doi: 10.1016/j.coi.2004.01.010. PubMed PMID: 15023407.

78. Erfani N, Hamedi-Shahraki M, Rezaeifard S, Haghshenas M, Rasouli M, Samsami Dehaghani A. FoxP3+ regulatory T cells in peripheral blood of patients with epithelial ovarian cancer. Iranian journal of immunology : IJI. 2014;11(2):105-12. doi: IJIv11i2A5. PubMed PMID: 24975967.

79. Nishikawa H, Jager E, Ritter G, Old LJ, Gnjatic S. CD4+ CD25+ regulatory T cells control the induction of antigen-specific CD4+ helper T cell responses in cancer patients. Blood. 2005;106(3):1008-11. doi: 10.1182/blood-2005-02-0607. PubMed PMID: 15840697.

80. Govindaraj C, Scalzo-Inguanti K, Madondo M, Hallo J, Flanagan K, Quinn M, et al. Impaired Th1 immunity in ovarian cancer patients is mediated by TNFR2+ Tregs within the tumor microenvironment. Clinical immunology. 2013;149(1):97-110. doi: 10.1016/j.clim.2013.07.003. PubMed PMID: 23948613.

81. Genta S, Ghisoni E, Giannone G, Mittica G, Valabrega G. Reprogramming T-cells for adoptive immunotherapy of ovarian cancer. Expert opinion on biological therapy. 2018:1-9. doi: 10.1080/14712598.2018.1425679. PubMed PMID: 29307234.

82. Teng MW, Swann JB, von Scheidt B, Sharkey J, Zerafa N, McLaughlin N, et al. Multiple antitumor mechanisms downstream of prophylactic regulatory T-cell depletion. Cancer research. 2010;70(7):2665-74. doi: 10.1158/0008-5472.CAN-09-1574. PubMed PMID: 20332236.

83. Redjimi N, Raffin C, Raimbaud I, Pignon P, Matsuzaki J, Odunsi K, et al. CXCR3+ T regulatory cells selectively accumulate in human ovarian carcinomas to limit type I immunity. Cancer research. 2012;72(17):4351-60. doi: 10.1158/0008-5472.CAN-12-0579. PubMed PMID: 22798340.

84. Cui TX, Kryczek I, Zhao L, Zhao E, Kuick R, Roh MH, et al. Myeloid-derived suppressor cells enhance stemness of cancer cells by inducing microRNA101 and suppressing the corepressor CtBP2. Immunity. 2013;39(3):611-21. doi: 10.1016/j.immuni.2013.08.025. PubMed PMID: 24012420; PubMed Central PMCID: PMC3831370.

85. Curiel TJ, Coukos G, Zou L, Alvarez X, Cheng P, Mottram P, et al. Specific recruitment of regulatory T cells in ovarian carcinoma fosters immune privilege and predicts reduced survival. Nature medicine. 2004;10(9):942-9. doi: 10.1038/nm1093. PubMed PMID: 15322536.

86. Isobe A, Sawada K, Kinose Y, Ohyagi-Hara C, Nakatsuka E, Makino H, et al. Interleukin 6 receptor is an independent prognostic factor and a potential therapeutic target of ovarian cancer. PloS one. 2015;10(2):e0118080. doi: 10.1371/journal.pone.0118080. PubMed PMID: 25658637; PubMed Central PMCID: PMC4319819.

87. Wang Y, Li L, Guo X, Jin X, Sun W, Zhang X, et al. Interleukin-6 signaling regulates anchorage-independent growth, proliferation, adhesion and invasion in human ovarian cancer cells. Cytokine. 2012;59(2):228-36. doi: 10.1016/j.cyto.2012.04.020. PubMed PMID: 22595649.

88. Malik ST, Griffin DB, Fiers W, Balkwill FR. Paradoxical effects of tumour necrosis factor in experimental ovarian cancer. International journal of cancer. 1989;44(5):918-25. PubMed PMID: 2583871.

89. Terabe M, Swann J, Ambrosino E, Sinha P, Takaku S, Hayakawa Y, et al. A nonclassical non-Valpha14Jalpha18 CD1d-restricted (type II) NKT cell is sufficient for down-regulation of tumor immunosurveillance. The Journal of experimental medicine. 2005;202(12):1627-33. doi: 10.1084/jem.20051381. PubMed PMID: 16365146; PubMed Central PMCID: PMC2212961.

90. DiLillo DJ, Matsushita T, Tedder TF. B10 cells and regulatory B cells balance immune responses during inflammation, autoimmunity, and cancer. Annals of the New York Academy of Sciences. 2010;1183:38-57. doi: 10.1111/j.1749-6632.2009.05137.x. PubMed PMID: 20146707.

91. Salgame P, Convit J, Bloom BR. Immunological suppression by human CD8+ T cells is receptor dependent and HLA-DQ restricted. Proceedings of the National Academy of Sciences of the United States of America. 1991;88(6):2598-602. PubMed PMID: 1826057; PubMed Central PMCID: PMC51280.

92. Subramaniam KS, Tham ST, Mohamed Z, Woo YL, Mat Adenan NA, Chung I. Cancer-associated fibroblasts promote proliferation of endometrial cancer cells. PloS one. 2013;8(7):e68923. doi: 10.1371/journal.pone.0068923. PubMed PMID: 23922669; PubMed Central PMCID: PMC3724864.

93. Fiaschi T, Giannoni E, Taddei ML, Cirri P, Marini A, Pintus G, et al. Carbonic anhydrase IX from cancer-associated fibroblasts drives epithelial-mesenchymal transition in prostate carcinoma cells. Cell cycle. 2013;12(11):1791-801. doi: 10.4161/cc.24902. PubMed PMID: 23656776; PubMed Central PMCID: PMC3713137.

94. Liao D, Luo Y, Markowitz D, Xiang R, Reisfeld RA. Cancer associated fibroblasts promote tumor growth and metastasis by modulating the tumor immune microenvironment in a 4T1 murine breast cancer model. PloS one. 2009;4(11):e7965. doi: 10.1371/journal.pone.0007965. PubMed PMID: 19956757; PubMed Central PMCID: PMC2775953.

95. Comito G, Giannoni E, Segura CP, Barcellos-de-Souza P, Raspollini MR, Baroni G, et al. Cancer-associated fibroblasts and M2-polarized macrophages synergize during prostate carcinoma progression. Oncogene. 2014;33(19):2423-31. doi: 10.1038/onc.2013.191. PubMed PMID: 23728338.

96. Motzer RJ, Hutson TE, Ren M, Dutcus C, Larkin J. Independent assessment of lenvatinib plus everolimus in patients with metastatic renal cell carcinoma. The Lancet Oncology. 2016;17(1):e4-5. doi: 10.1016/S1470-2045(15)00543-4. PubMed PMID: 26758760.

97. Kandalaft LE, Powell DJ, Jr., Singh N, Coukos G. Immunotherapy for ovarian cancer: what's next? Journal of clinical oncology : official journal of the American Society of Clinical Oncology. 2011;29(7):925-33. doi: 10.1200/JCO.2009.27.2369. PubMed PMID: 21079136; PubMed Central PMCID: PMC3068064.

98. Krishnan V, Berek JS, Dorigo O. Immunotherapy in ovarian cancer. Current problems in cancer. 2017;41(1):48-63. doi: 10.1016/j.currproblcancer.2016.11.003. PubMed PMID: 28169004.

99. Burges A, Wimberger P, Kumper C, Gorbounova V, Sommer H, Schmalfeldt B, et al. Effective relief of malignant ascites in patients with advanced ovarian cancer by a trifunctional anti-EpCAM x anti-CD3 antibody: a phase I/II study. Clinical cancer research : an official journal of the American Association for Cancer Research. 2007;13(13):3899-905. doi: 10.1158/1078-0432.CCR-06-2769. PubMed PMID: 17606723.

100. Heiss MM, Murawa P, Koralewski P, Kutarska E, Kolesnik OO, Ivanchenko VV, et al. The trifunctional antibody catumaxomab for the treatment of malignant ascites due to epithelial cancer: Results of a prospective randomized phase II/III trial. International journal of cancer. 2010;127(9):2209-21. doi: 10.1002/ijc.25423. PubMed PMID: 20473913; PubMed Central PMCID: PMC2958458.

101. Hardwick N, Frankel PH, Cristea M. New Approaches for Immune Directed Treatment for Ovarian Cancer. Current treatment options in oncology. 2016;17(3):14. doi: 10.1007/s11864-016-0389-1. PubMed PMID: 26942589.

102. Baert T, Vergote I, Coosemans A. Ovarian cancer and the immune system. Gynecologic oncology reports. 2017;19:57-8. doi: 10.1016/j.gore.2017.01.002. PubMed PMID: 28127584; PubMed Central PMCID: PMC5247278.

103. Pakish JB, Jazaeri AA. Immunotherapy in Gynecologic Cancers: Are We There Yet? Current treatment options in oncology. 2017;18(10):59. doi: 10.1007/s11864-017-0504-y. PubMed PMID: 28840453.

104. Martin Lluesma S, Wolfer A, Harari A, Kandalaft LE. Cancer Vaccines in Ovarian Cancer: How Can We Improve? Biomedicines. 2016;4(2). doi: 10.3390/biomedicines4020010. PubMed PMID: 28536377; PubMed Central PMCID: PMC5344251.

105. Waki K, Kawano K, Tsuda N, Ushijima K, Itoh K, Yamada A. Plasma Levels of High-Mobility Group Box 1 during Peptide Vaccination in Patients with Recurrent Ovarian Cancer. Journal of immunology research. 2017;2017:1423683. doi: 10.1155/2017/1423683. PubMed PMID: 28536706; PubMed Central PMCID: PMC5426075.

106. Suzuki S, Sakata J, Utsumi F, Sekiya R, Kajiyama H, Shibata K, et al. Efficacy of glypican-3-derived peptide vaccine therapy on the survival of patients with refractory ovarian clear cell carcinoma. Oncoimmunology. 2016;5(11):e1238542. doi: 10.1080/2162402X.2016.1238542. PubMed PMID: 27999758; PubMed Central PMCID: PMC5139642.

107. O'Hara MH, Stashwick C, Plesa G, Tanyi JL. Overcoming barriers of car T-cell therapy in patients with mesothelin-expressing cancers. Immunotherapy. 2017. doi: 10.2217/imt-2017-0026. PubMed PMID: 28771103.

108. Zuo S, Wen Y, Panha H, Dai G, Wang L, Ren X, et al. Modification of cytokine-induced killer cells with folate receptor alpha (FRalpha)-specific chimeric antigen receptors enhances their antitumor immunity toward FRalpha-positive ovarian cancers. Molecular immunology. 2017;85:293-304. doi: 10.1016/j.molimm.2017.03.017. PubMed PMID: 28360017.

109. Ang WX, Li Z, Chi Z, Du SH, Chen C, Tay JC, et al. Intraperitoneal immunotherapy with T cells stably and transiently expressing anti-EpCAM CAR in xenograft models of peritoneal carcinomatosis. Oncotarget. 2017. doi: 10.18632/oncotarget.14592. PubMed PMID: 28088790.

110. Smith JB, Lanitis E, Dangaj D, Buza E, Poussin M, Stashwick C, et al. Tumor Regression and Delayed Onset Toxicity Following B7-H4 CAR T Cell Therapy. Molecular therapy : the journal of the American Society of Gene Therapy. 2016;24(11):1987-99. doi: 10.1038/mt.2016.149. PubMed PMID: 27439899; PubMed Central PMCID: PMC5154474.

111. Jiang J, Dong L, Wang L, Wang L, Zhang J, Chen F, et al. HER2-targeted antibody drug conjugates for ovarian cancer therapy. European journal of pharmaceutical sciences : official journal of the European Federation for Pharmaceutical Sciences. 2016;93:274-86. doi: 10.1016/j.ejps.2016.08.015. PubMed PMID: 27509865.

112. Imai A, Ichigo S, Matsunami K, Takagi H, Kawabata I. Ovarian function following targeted anti-angiogenic therapy with bevacizumab. Molecular and clinical oncology. 2017;6(6):807-10. doi: 10.3892/mco.2017.1237. PubMed PMID: 28588768; PubMed Central PMCID: PMC5451849.

113. Menderes G, Bonazzoli E, Bellone S, Black J, Altwerger G, Masserdotti A, et al. SYD985, a novel duocarmycin-based HER2-targeting antibody-drug conjugate, shows promising antitumor activity in epithelial ovarian carcinoma with HER2/Neu expression. Gynecologic oncology. 2017;146(1):179-86. doi: 10.1016/j.ygyno.2017.04.023. PubMed PMID: 28473206; PubMed Central PMCID: PMC5533304.

114. Pacheco PM, Le B, White D, Sulchek T. TUNABLE COMPLEMENT ACTIVATION BY PARTICLES WITH VARIABLE SIZE AND Fc DENSITY. Nano LIFE. 2013;3(2):1341001. doi: 10.1142/S1793984413410018. PubMed PMID: 24009645; PubMed Central PMCID: PMC3759286.

115. Perica K, Kosmides AK, Schneck JP. Linking form to function: Biophysical aspects of artificial antigen presenting cell design. Biochimica et biophysica acta. 2015;1853(4):781-90. doi: 10.1016/j.bbamcr.2014.09.001. PubMed PMID: 25200637; PubMed Central PMCID: PMC4344884.

116. Tse BW, Collins A, Oehler MK, Zippelius A, Heinzelmann-Schwarz VA. Antibody-based immunotherapy for ovarian cancer: where are we at? Annals of oncology : official journal of the European Society for Medical Oncology. 2014;25(2):322-31. doi: 10.1093/annonc/mdt405. PubMed PMID: 24285017.

117. Callahan MK, Wolchok JD. At the bedside: CTLA-4- and PD-1-blocking antibodies in cancer immunotherapy. Journal of leukocyte biology. 2013;94(1):41-53. doi: 10.1189/jlb.1212631. PubMed PMID: 23667165.

118. Huang RY, Francois A, McGray AR, Miliotto A, Odunsi K. Compensatory upregulation of PD-1, LAG-3, and CTLA-4 limits the efficacy of single-agent checkpoint blockade in metastatic ovarian cancer. Oncoimmunology. 2017;6(1):e1249561. doi: 10.1080/2162402X.2016.1249561. PubMed PMID: 28197366.

119. Kim JY, Cho CH, Song HS. Targeted therapy of ovarian cancer including immune check point inhibitor. The Korean journal of internal medicine. 2017. doi: 10.3904/kjim.2017.008. PubMed PMID: 28823141.

120. Hodi FS, Butler M, Oble DA, Seiden MV, Haluska FG, Kruse A, et al. Immunologic and clinical effects of antibody blockade of cytotoxic T lymphocyte-associated antigen 4 in previously vaccinated cancer patients. Proceedings of the National Academy of Sciences of the United States of America. 2008;105(8):3005-10. doi: 10.1073/pnas.0712237105. PubMed PMID: 18287062; PubMed Central PMCID: PMC2268575.

121. Postow MA, Callahan MK, Wolchok JD. Immune Checkpoint Blockade in Cancer Therapy. Journal of clinical oncology : official journal of the American Society of Clinical Oncology. 2015;33(17):1974-82. doi: 10.1200/JCO.2014.59.4358. PubMed PMID: 25605845; PubMed Central PMCID: PMC4980573.

122. Hamanishi J, Mandai M, Ikeda T, Minami M, Kawaguchi A, Murayama T, et al. Safety and Antitumor Activity of Anti-PD-1 Antibody, Nivolumab, in Patients With Platinum-Resistant Ovarian Cancer. Journal of clinical oncology : official journal of the American Society of Clinical Oncology. 2015;33(34):4015-22. doi: 10.1200/JCO.2015.62.3397. PubMed PMID: 26351349.

123. Varga A, Piha-Paul SA, Ott PA, Mehnert JM, Berton-Rigaud D, Johnson EA, et al. Antitumor activity and safety of pembrolizumab in patients (pts) with PD-L1 positive

advanced ovarian cancer: Interim results from a phase Ib study. Journal of Clinical Oncology. 2015;33(15). PubMed PMID: WOS:000358036901169.

124. Disis ML, Patel MR, Pant S, Hamilton EP, Lockhart AC, Kelly K, et al. Avelumab (MSB0010718C; anti-PD-L1) in patients with recurrent/refractory ovarian cancer from the JAVELIN Solid Tumor phase Ib trial: Safety and clinical activity. Journal of Clinical Oncology. 2016;34(15). PubMed PMID: WOS:000404711501207.

125. Hamanishi J, Mandai M, Ikeda T, Minami M, Kawaguchi A, Matsumura N, et al. Efficacy and safety of anti-PD-1 antibody (Nivolumab: BMS-936558, ONO-4538) in patients with platinum-resistant ovarian cancer. Journal of Clinical Oncology. 2014;32(15). PubMed PMID: WOS:000358613203496.

126. Brahmer JR, Tykodi SS, Chow LQ, Hwu WJ, Topalian SL, Hwu P, et al. Safety and activity of anti-PD-L1 antibody in patients with advanced cancer. The New England journal of medicine. 2012;366(26):2455-65. doi: 10.1056/NEJMoa1200694. PubMed PMID: 22658128; PubMed Central PMCID: PMC3563263.

127. Reck M, Rodriguez-Abreu D, Robinson AG, Hui R, Csoszi T, Fulop A, et al. Pembrolizumab versus Chemotherapy for PD-L1-Positive Non-Small-Cell Lung Cancer. The New England journal of medicine. 2016;375(19):1823-33. doi: 10.1056/NEJMoa1606774. PubMed PMID: 27718847.

128. Brahmer J, Reckamp KL, Baas P, Crino L, Eberhardt WE, Poddubskaya E, et al. Nivolumab versus Docetaxel in Advanced Squamous-Cell Non-Small-Cell Lung Cancer. The New England journal of medicine. 2015;373(2):123-35. doi: 10.1056/NEJMoa1504627. PubMed PMID: 26028407; PubMed Central PMCID: PMC4681400.

129. Folkman J. Anti-angiogenesis: new concept for therapy of solid tumors. Annals of surgery. 1972;175(3):409-16. PubMed PMID: 5077799; PubMed Central PMCID: PMC1355186.

130. Burger RA. Overview of anti-angiogenic agents in development for ovarian cancer. Gynecologic oncology. 2011;121(1):230-8. doi: 10.1016/j.ygyno.2010.11.035. PubMed PMID: 21215996.

131. Alvarez AA, Krigman HR, Whitaker RS, Dodge RK, Rodriguez GC. The prognostic significance of angiogenesis in epithelial ovarian carcinoma. Clinical cancer research : an official journal of the American Association for Cancer Research. 1999;5(3):587-91. PubMed PMID: 10100710.

132. Zhang L, Yang N, Park JW, Katsaros D, Fracchioli S, Cao G, et al. Tumor-derived vascular endothelial growth factor up-regulates angiopoietin-2 in host endothelium and destabilizes host vasculature, supporting angiogenesis in ovarian cancer. Cancer research. 2003;63(12):3403-12. PubMed PMID: 12810677.

133. Oza AM, Cook AD, Pfisterer J, Embleton A, Ledermann JA, Pujade-Lauraine E, et al. Standard chemotherapy with or without bevacizumab for women with newly diagnosed ovarian cancer (ICON7): overall survival results of a phase 3 randomised trial. The Lancet Oncology. 2015;16(8):928-36. doi: 10.1016/S1470-2045(15)00086-8. PubMed PMID: 26115797; PubMed Central PMCID: PMC4648090.

134. Burger RA, Brady MF, Bookman MA, Fleming GF, Monk BJ, Huang H, et al. Incorporation of bevacizumab in the primary treatment of ovarian cancer. The New England journal of medicine. 2011;365(26):2473-83. doi: 10.1056/NEJMoa1104390. PubMed PMID: 22204724.

135. Perren TJ, Swart AM, Pfisterer J, Ledermann JA, Pujade-Lauraine E, Kristensen G, et al. A phase 3 trial of bevacizumab in ovarian cancer. The New England journal of medicine. 2011;365(26):2484-96. doi: 10.1056/NEJMoa1103799. PubMed PMID: 22204725.

136. Gotlieb WH, Amant F, Advani S, Goswami C, Hirte H, Provencher D, et al. Intravenous aflibercept for treatment of recurrent symptomatic malignant ascites in patients with advanced ovarian cancer: a phase 2, randomised, double-blind, placebo-controlled study. The Lancet Oncology. 2012;13(2):154-62. doi: 10.1016/S1470-2045(11)70338-2. PubMed PMID: 22192729.

137. Monk BJ, Poveda A, Vergote I, Raspagliesi F, Fujiwara K, Bae DS, et al. Anti-angiopoietin therapy with trebananib for recurrent ovarian cancer (TRINOVA-1): a randomised, multicentre, double-blind, placebo-controlled phase 3 trial. The Lancet Oncology. 2014;15(8):799-808. doi: 10.1016/S1470-2045(14)70244-X. PubMed PMID: 24950985.

138. Schmid BC, Oehler MK. Improvements in progression-free and overall survival due to the use of anti-angiogenic agents in gynecologic cancers. Current treatment options in oncology. 2015;16(1):318. doi: 10.1007/s11864-014-0318-0. PubMed PMID: 25750175.

139. Hilberg F, Roth GJ, Krssak M, Kautschitsch S, Sommergruber W, Tontsch-Grunt U, et al. BIBF 1120: triple angiokinase inhibitor with sustained receptor blockade and good antitumor efficacy. Cancer research. 2008;68(12):4774-82. doi: 10.1158/0008-5472.CAN-07-6307. PubMed PMID: 18559524.

140. Kalli KR, Oberg AL, Keeney GL, Christianson TJ, Low PS, Knutson KL, et al. Folate receptor alpha as a tumor target in epithelial ovarian cancer. Gynecologic oncology. 2008;108(3):619-26. doi: 10.1016/j.ygyno.2007.11.020. PubMed PMID: 18222534; PubMed Central PMCID: PMC2707764.

141. Ashworth A. A synthetic lethal therapeutic approach: poly(ADP) ribose polymerase inhibitors for the treatment of cancers deficient in DNA double-strand break repair. Journal of clinical oncology : official journal of the American Society of Clinical Oncology. 2008;26(22):3785-90. doi: 10.1200/JCO.2008.16.0812. PubMed PMID: 18591545.

142. Cancer Genome Atlas Research N. Integrated genomic analyses of ovarian carcinoma. Nature. 2011;474(7353):609-15. doi: 10.1038/nature10166. PubMed PMID: 21720365; PubMed Central PMCID: PMC3163504.

143. Armstrong DK, White AJ, Weil SC, Phillips M, Coleman RL. Farletuzumab (a monoclonal antibody against folate receptor alpha) in relapsed platinum-sensitive ovarian cancer. Gynecologic oncology. 2013;129(3):452-8. doi: 10.1016/j.ygyno.2013.03.002. PubMed PMID: 23474348.

144. Walters CL, Arend RC, Armstrong DK, Naumann RW, Alvarez RD. Folate and folate receptor alpha antagonists mechanism of action in ovarian cancer. Gynecologic oncology. 2013;131(2):493-8. doi: 10.1016/j.ygyno.2013.07.080. PubMed PMID: 23863359.

145. Naumann RW, Coleman RL, Burger RA, Sausville EA, Kutarska E, Ghamande SA, et al. PRECEDENT: a randomized phase II trial comparing vintafolide (EC145) and pegylated liposomal doxorubicin (PLD) in combination versus PLD alone in patients with platinum-resistant ovarian cancer. Journal of clinical oncology : official journal of the American Society of Clinical Oncology. 2013;31(35):4400-6. doi: 10.1200/JCO.2013.49.7685. PubMed PMID: 24127448.

146. Matsuzaki J, Gnjatic S, Mhawech-Fauceglia P, Beck A, Miller A, Tsuji T, et al. Tumor-infiltrating NY-ESO-1-specific CD8+ T cells are negatively regulated by LAG-3 and PD-1 in human ovarian cancer. Proceedings of the National Academy of Sciences of the United States of America. 2010;107(17):7875-80. doi: 10.1073/pnas.1003345107. PubMed PMID: 20385810; PubMed Central PMCID: PMC2867907.

147. Chames P, Baty D. Bispecific antibodies for cancer therapy. Curr Opin Drug Discov Dev. 2009;12(2):276-83. PubMed PMID: WOS:000264500500011.

148. Linke R, Klein A, Seimetz D. Catumaxomab: clinical development and future directions. mAbs. 2010;2(2):129-36. PubMed PMID: 20190561; PubMed Central PMCID: PMC2840231.

149. Lopez-Albaitero A, Xu H, Guo H, Wang L, Wu Z, Tran H, et al. Overcoming resistance to HER2-targeted therapy with a novel HER2/CD3 bispecific antibody. Oncoimmunology. 2017;6(3):e1267891. doi: 10.1080/2162402X.2016.1267891. PubMed PMID: 28405494; PubMed Central PMCID: PMC5384386.

150. Ruf P, Gires O, Jager M, Fellinger K, Atz J, Lindhofer H. Characterisation of the new EpCAM-specific antibody HO-3: implications for trifunctional antibody immunotherapy of cancer. British journal of cancer. 2007;97(3):315-21. doi: 10.1038/sj.bjc.6603881. PubMed PMID: 17622246; PubMed Central PMCID: PMC2360319.

151. Strohlein MA, Heiss MM. The trifunctional antibody catumaxomab in treatment of malignant ascites and peritoneal carcinomatosis. Future oncology. 2010;6(9):1387-94. doi: 10.2217/fon.10.111. PubMed PMID: 20919824.

152. Wu Z, Cheung NV. T cell engaging bispecific antibody (T-BsAb): From technology to therapeutics. Pharmacology & therapeutics. 2017. doi: 10.1016/j.pharmthera.2017.08.005. PubMed PMID: 28834699.

153. Stadler CR, Bahr-Mahmud H, Plum LM, Schmoldt K, Kolsch AC, Tureci O, et al. Characterization of the first-in-class T-cell-engaging bispecific single-chain antibody for targeted immunotherapy of solid tumors expressing the oncofetal protein claudin 6. Oncoimmunology. 2016;5(3):e1091555. doi: 10.1080/2162402X.2015.1091555. PubMed PMID: 27141353; PubMed Central PMCID: PMC4839326.

154. Haas C, Krinner E, Brischwein K, Hoffmann P, Lutterbuse R, Schlereth B, et al. Mode of cytotoxic action of T cell-engaging BiTE antibody MT110. Immunobiology. 2009;214(6):441-53. doi: 10.1016/j.imbio.2008.11.014. PubMed PMID: 19157637.

155. Kischel R, Hausmann S, Baeuerle P, Kufer P. Abstract #3252: Effector memory T cells make a major contribution to redirected target cell lysis by T cell-engaging BiTE antibody MT110. Cancer Research. 2009;69(9 Supplement):3252-.

156. Ferrini S, Cambiaggi A, Sforzini S, Marciano S, Canevari S, Mezzanzanica D, et al. Targeting of T lymphocytes against EGF-receptor+ tumor cells by bispecific monoclonal antibodies: requirement of CD3 molecule cross-linking for T-cell activation. International journal of cancer. 1993;55(6):931-7. PubMed PMID: 8253530.

157. Frankel SR, Baeuerle PA. Targeting T cells to tumor cells using bispecific antibodies. Current opinion in chemical biology. 2013;17(3):385-92. doi: 10.1016/j.cbpa.2013.03.029. PubMed PMID: 23623807.

158. Mezzanzanica D, Garrido MA, Neblock DS, Daddona PE, Andrew SM, Zurawski VR, Jr., et al. Human T-lymphocytes targeted against an established human ovarian carcinoma with a bispecific F(ab')2 antibody prolong host survival in a murine xenograft model. Cancer Res. 1991;51(20):5716-21. PubMed PMID: 1833054.

159. Leong SR, Sukumaran S, Hristopoulos M, Totpal K, Stainton S, Lu E, et al. An anti-CD3/anti-CLL-1 bispecific antibody for the treatment of acute myeloid leukemia. Blood. 2017;129(5):609-18. doi: 10.1182/blood-2016-08-735365. PubMed PMID: 27908880; PubMed Central PMCID: PMC5290988.

160. Bi Y, Jiang H, Wang P, Song B, Wang H, Kong X, et al. Treatment of hepatocellular carcinoma with a GPC3-targeted bispecific T cell engager. Oncotarget. 2017. doi: 10.18632/oncotarget.17905. PubMed PMID: 28572527.

161. Eggermont LJ, Paulis LE, Tel J, Figdor CG. Towards efficient cancer immunotherapy: advances in developing artificial antigen-presenting cells. Trends in biotechnology. 2014;32(9):456-65. doi: 10.1016/j.tibtech.2014.06.007. PubMed PMID: 24998519; PubMed Central PMCID: PMC4154451.

162. Kosmides AK, Necochea K, Hickey JW, Schneck JP. Separating T Cell Targeting Components onto Magnetically Clustered Nanoparticles Boosts Activation. Nano letters. 2018;18(3):1916-24. doi: 10.1021/acs.nanolett.7b05284. PubMed PMID: 29488768.

163. Gray HJ, Gargosky SE, Team C-S. Progression-free survival in ovarian cancer patients in second remission with mucin-1 autologous dendritic cell therapy. Journal of Clinical Oncology. 2014;32(15). PubMed PMID: WOS:000358613203489.

164. Yuan JP, Kashiwagi S, Reeves P, Nezivar J, Yang Y, Arrifin NH, et al. A novel mycobacterial Hsp70-containing fusion protein targeting mesothelin augments antitumor immunity and prolongs survival in murine models of ovarian cancer and mesothelioma. J Hematol Oncol. 2014;7. doi: Artn 15

10.1186/1756-8722-7-15. PubMed PMID: WOS:000334632400001.

165. Chiang CL, Kandalaft LE, Tanyi J, Hagemann AR, Motz GT, Svoronos N, et al. A dendritic cell vaccine pulsed with autologous hypochlorous acid-oxidized ovarian cancer lysate primes effective broad antitumor immunity: from bench to bedside. Clinical cancer research : an official journal of the American Association for Cancer Research. 2013;19(17):4801-15. doi: 10.1158/1078-0432.CCR-13-1185. PubMed PMID: 23838316; PubMed Central PMCID: PMC4049094.

166. Sulchek TA, Friddle RW, Langry K, Lau EY, Albrecht H, Ratto TV, et al. Dynamic force spectroscopy of parallel individual Mucin1-antibody bonds. Proceedings of the National Academy of Sciences of the United States of America. 2005;102(46):16638-43. doi: 10.1073/pnas.0505208102. PubMed PMID: 16269547; PubMed Central PMCID: PMC1276867.

167. Pacheco P, White D, Sulchek T. Effects of microparticle size and Fc density on macrophage phagocytosis. PloS one. 2013;8(4):e60989. doi: 10.1371/journal.pone.0060989. PubMed PMID: 23630577; PubMed Central PMCID: PMC3632606.

168. Li Y, Kurlander RJ. Comparison of anti-CD3 and anti-CD28-coated beads with soluble anti-CD3 for expanding human T cells: differing impact on CD8 T cell phenotype and responsiveness to restimulation. Journal of translational medicine. 2010;8:104. doi: 10.1186/1479-5876-8-104. PubMed PMID: 20977748; PubMed Central PMCID: PMC2987859.

169. Lo YC, Edidin MA, Powell JD. Selective activation of antigen-experienced T cells by anti-CD3 constrained on nanoparticles. Journal of immunology. 2013;191(10):5107-14. doi: 10.4049/jimmunol.1301433. PubMed PMID: 24098054; PubMed Central PMCID: PMC3831631.

170. Cui Y, Cui P, Chen B, Li S, Guan H. Monoclonal antibodies: formulations of marketed products and recent advances in novel delivery system. Drug development and industrial pharmacy. 2017;43(4):519-30. doi: 10.1080/03639045.2017.1278768. PubMed PMID: 28049357.

171. Kumar S, Anselmo AC, Banerjee A, Zakrewsky M, Mitragotri S. Shape and size-dependent immune response to antigen-carrying nanoparticles. Journal of controlled release : official journal of the Controlled Release Society. 2015;220(Pt A):141-8. doi: 10.1016/j.jconrel.2015.09.069. PubMed PMID: 26437263.

172. Brewer MG, DiPiazza A, Acklin J, Feng C, Sant AJ, Dewhurst S. Nanoparticles decorated with viral antigens are more immunogenic at low surface density. Vaccine. 2017;35(5):774-81. doi: 10.1016/j.vaccine.2016.12.049. PubMed PMID: 28057386.

173. Lee K, Yu Y. Janus nanoparticles for T cell activation: clustering ligands to enhance stimulation. Journal of Materials Chemistry B. 2017. doi: 10.1039/C7TB00150A.

174. Holt BA, Bellavia MC, Potter D, White D, Stowell SR, Sulchek T. Fc microparticles can modulate the physical extent and magnitude of complement activity. Biomaterials science. 2017;5(3):463-74. doi: 10.1039/c6bm00608f. PubMed PMID: 28067347; PubMed Central PMCID: PMC5330945.

175. Perica K, De Leon Medero A, Durai M, Chiu YL, Bieler JG, Sibener L, et al. Nanoscale artificial antigen presenting cells for T cell immunotherapy. Nanomedicine : nanotechnology, biology, and medicine. 2014;10(1):119-29. doi: 10.1016/j.nano.2013.06.015. PubMed PMID: 23891987; PubMed Central PMCID: PMC4114774.

176. Fadel TR, Steenblock ER, Stern E, Li N, Wang X, Haller GL, et al. Enhanced cellular activation with single walled carbon nanotube bundles presenting antibody stimuli. Nano letters. 2008;8(7):2070-6. doi: 10.1021/nl080332i. PubMed PMID: 18547120.

177. Giannoni F, Barnett J, Bi K, Samodal R, Lanza P, Marchese P, et al. Clustering of T cell ligands on artificial APC membranes influences T cell activation and protein kinase C theta translocation to the T cell plasma membrane. Journal of immunology. 2005;174(6):3204-11. PubMed PMID: 15749850.

178. Shen C, Cheng K, Miao S, Wang W, He Y, Meng F, et al. Latex bead-based artificial antigen-presenting cells induce tumor-specific CTL responses in the native T-cell repertoires and inhibit tumor growth. Immunology letters. 2013;150(1-2):1-11. doi: 10.1016/j.imlet.2013.01.003. PubMed PMID: 23328744.

179. Sunshine JC, Perica K, Schneck JP, Green JJ. Particle shape dependence of CD8+ T cell activation by artificial antigen presenting cells. Biomaterials. 2014;35(1):269-77. doi: 10.1016/j.biomaterials.2013.09.050. PubMed PMID: 24099710; PubMed Central PMCID: PMC3902087.

180. Turtle CJ, Riddell SR. Artificial antigen-presenting cells for use in adoptive immunotherapy. Cancer journal. 2010;16(4):374-81. doi: 10.1097/PPO.0b013e3181eb33a6. PubMed PMID: 20693850; PubMed Central PMCID: PMC2929753.

181. Chen B, Jia Y, Gao Y, Sanchez L, Anthony SM, Yu Y. Janus particles as artificial antigen-presenting cells for T cell activation. ACS applied materials & interfaces. 2014;6(21):18435-9. doi: 10.1021/am505510m. PubMed PMID: 25343426; PubMed Central PMCID: PMC4404154.

182. Lee K, Yi Y, Yu Y. Remote Control of T Cell Activation Using Magnetic Janus Particles. Angewandte Chemie. 2016;55(26):7384-7. doi: 10.1002/anie.201601211. PubMed PMID: 27144475; PubMed Central PMCID: PMC4959603.

183. Gao Y, Yu Y. Macrophage uptake of Janus particles depends upon Janus balance. Langmuir : the ACS journal of surfaces and colloids. 2015;31(9):2833-8. doi: 10.1021/la504668c. PubMed PMID: 25674706.

184. Sanchez L, Yi Y, Yu Y. Effect of partial PEGylation on particle uptake by macrophages. Nanoscale. 2017;9(1):288-97. doi: 10.1039/c6nr07353k. PubMed PMID: 27909711.

185. He W, Frueh J, Wu Z, He Q. How Leucocyte Cell Membrane Modified Janus Microcapsules are Phagocytosed by Cancer Cells. ACS applied materials & interfaces. 2016;8(7):4407-15. doi: 10.1021/acsami.5b10885. PubMed PMID: 26824329.

186. Gao Y, Yu Y. How half-coated janus particles enter cells. Journal of the American Chemical Society. 2013;135(51):19091-4. doi: 10.1021/ja410687z. PubMed PMID: 24308498.

187. Crossland KD, Lee VK, Chen W, Riddell SR, Greenberg PD, Cheever MA. T cells from tumor-immune mice nonspecifically expanded in vitro with anti-CD3 plus IL-2 retain specific function in vitro and can eradicate disseminated leukemia in vivo. Journal of immunology. 1991;146(12):4414-20. PubMed PMID: 1674958.

188. Garlie NK, LeFever AV, Siebenlist RE, Levine BL, June CH, Lum LG. T cells coactivated with immobilized anti-CD3 and anti-CD28 as potential immunotherapy for cancer. Journal of immunotherapy. 1999;22(4):336-45. PubMed PMID: 10404435.

189. Shiheido H, Chen C, Hikida M, Watanabe T, Shimizu J. Modulation of the human T cell response by a novel non-mitogenic anti-CD3 antibody. PloS one. 2014;9(4):e94324. doi: 10.1371/journal.pone.0094324. PubMed PMID: 24710513; PubMed Central PMCID: PMC3978038.

190. Ye Q, Loisiou M, Levine BL, Suhoski MM, Riley JL, June CH, et al. Engineered artificial antigen presenting cells facilitate direct and efficient expansion of tumor infiltrating lymphocytes. Journal of translational medicine. 2011;9:131. doi: 10.1186/1479-5876-9-131. PubMed PMID: 21827675; PubMed Central PMCID: PMC3162913.

191. Finke JH, Rayman P, Alexander J, Edinger M, Tubbs RR, Connelly R, et al. Characterization of the cytolytic activity of CD4+ and CD8+ tumor-infiltrating

lymphocytes in human renal cell carcinoma. Cancer research. 1990;50(8):2363-70. PubMed PMID: 2107973.

192. Levine BL, Bernstein WB, Connors M, Craighead N, Lindsten T, Thompson CB, et al. Effects of CD28 costimulation on long-term proliferation of CD4+ T cells in the absence of exogenous feeder cells. Journal of immunology. 1997;159(12):5921-30. PubMed PMID: 9550389.

193. Kalamasz D, Long SA, Taniguchi R, Buckner JH, Berenson RJ, Bonyhadi M. Optimization of human T-cell expansion ex vivo using magnetic beads conjugated with anti-CD3 and Anti-CD28 antibodies. Journal of immunotherapy. 2004;27(5):405-18. PubMed PMID: 15314550.

194. Perica K, Bieler JG, Schutz C, Varela JC, Douglass J, Skora A, et al. Enrichment and Expansion with Nanoscale Artificial Antigen Presenting Cells for Adoptive Immunotherapy. ACS nano. 2015;9(7):6861-71. doi: 10.1021/acsnano.5b02829. PubMed PMID: 26171764; PubMed Central PMCID: PMC5082131.

195. Mackey D, Kelly E, Nooney R. Modelling random antibody adsorption and immunoassay activity. Mathematical biosciences and engineering : MBE. 2016;13(6):1159-68. doi: 10.3934/mbe.2016036. PubMed PMID: 27775373.

196. Abraham RT, Weiss A. Jurkat T cells and development of the T-cell receptor signalling paradigm. Nature reviews Immunology. 2004;4(4):301-8. doi: 10.1038/nri1330. PubMed PMID: 15057788.

197. Conroy PJ, Law RH, Caradoc-Davies TT, Whisstock JC. Antibodies: From novel repertoires to defining and refining the structure of biologically important targets. Methods. 2017;116:12-22. doi: 10.1016/j.ymeth.2017.01.003. PubMed PMID: 28088364.

198. Jung Y, Jeong JY, Chung BH. Recent advances in immobilization methods of antibodies on solid supports. Analyst. 2008;133(6):697-701. doi: 10.1039/B800014J.

199. Welch NG, Scoble JA, Muir BW, Pigram PJ. Orientation and characterization of immobilized antibodies for improved immunoassays (Review). Biointerphases. 2017;12(2):02D301. doi: 10.1116/1.4978435. PubMed PMID: 28301944.

200. Spitznagel TM, Clark DS. Surface-density and orientation effects on immobilized antibodies and antibody fragments. Bio/technology. 1993;11(7):825-9. PubMed PMID: 7764064.

201. Peretz V, Motiei M, Sukenik CN, Popovtzer R. The Effect of Nanoparticle Size on Cellular Binding Probability. Journal of Atomic, Molecular, and Optical Physics. 2012;2012:7. doi: 10.1155/2012/404536.

202. Mescher MF. Surface contact requirements for activation of cytotoxic T lymphocytes. Journal of immunology. 1992;149(7):2402-5. PubMed PMID: 1527386.

203. Dustin ML, Chakraborty AK, Shaw AS. Understanding the structure and function of the immunological synapse. Cold Spring Harbor perspectives in biology. 2010;2(10):a002311. doi: 10.1101/cshperspect.a002311. PubMed PMID: 20843980; PubMed Central PMCID: PMC2944359.

204. Bjorndahl JM, Sung SS, Hansen JA, Fu SM. Human T cell activation: differential response to anti-CD28 as compared to anti-CD3 monoclonal antibodies. European journal of immunology. 1989;19(5):881-7. doi: 10.1002/eji.1830190515. PubMed PMID: 2544432.

205. Bailey SR, Nelson MH, Majchrzak K, Bowers JS, Wyatt MM, Smith AS, et al. Human CD26(high) T cells elicit tumor immunity against multiple malignancies via enhanced migration and persistence. Nature communications. 2017;8(1):1961. doi: 10.1038/s41467-017-01867-9. PubMed PMID: 29213079; PubMed Central PMCID: PMC5719008.

206. Hickey JW, Vicente FP, Howard GP, Mao HQ, Schneck JP. Biologically Inspired Design of Nanoparticle Artificial Antigen-Presenting Cells for Immunomodulation. Nano letters. 2017;17(11):7045-54. doi: 10.1021/acs.nanolett.7b03734. PubMed PMID: 28994285.

207. Zhang Q, Wei W, Wang P, Zuo L, Li F, Xu J, et al. Biomimetic Magnetosomes as Versatile Artificial Antigen-Presenting Cells to Potentiate T-Cell-Based Anticancer Therapy. ACS nano. 2017;11(11):10724-32. doi: 10.1021/acsnano.7b04955. PubMed PMID: 28921946.

208. Parsons JT, Horwitz AR, Schwartz MA. Cell adhesion: integrating cytoskeletal dynamics and cellular tension. Nature reviews Molecular cell biology. 2010;11(9):633-43. doi: 10.1038/nrm2957. PubMed PMID: 20729930; PubMed Central PMCID: PMC2992881.

209. Thauland TJ, Hu KH, Bruce MA, Butte MJ. Cytoskeletal adaptivity regulates T cell receptor signaling. Science signaling. 2017;10(469). doi: 10.1126/scisignal.aah3737. PubMed PMID: 28270556; PubMed Central PMCID: PMC5854469.

210. Hivroz C, Saitakis M. Biophysical Aspects of T Lymphocyte Activation at the Immune Synapse. Frontiers in immunology. 2016;7:46. doi: 10.3389/fimmu.2016.00046. PubMed PMID: 26913033; PubMed Central PMCID: PMC4753286.

211. Kabanova A, Zurli V, Baldari CT. Signals Controlling Lytic Granule Polarization at the Cytotoxic Immune Synapse. Frontiers in immunology. 2018;9:307. doi: 10.3389/fimmu.2018.00307. PubMed PMID: 29515593; PubMed Central PMCID: PMC5826174.

212. Joseph N, Reicher B, Barda-Saad M. The calcium feedback loop and T cell activation: how cytoskeleton networks control intracellular calcium flux. Biochimica et biophysica acta. 2014;1838(2):557-68. doi: 10.1016/j.bbamem.2013.07.009. PubMed PMID: 23860253.

213. Blas-Rus N, Bustos-Moran E, Sanchez-Madrid F, Martin-Cofreces NB. Analysis of Microtubules and Microtubule-Organizing Center at the Immune Synapse. Methods in molecular biology. 2017;1584:31-49. doi: 10.1007/978-1-4939-6881-7_3. PubMed PMID: 28255694; PubMed Central PMCID: PMC5503130.

214. Negulescu PA, Krasieva TB, Khan A, Kerschbaum HH, Cahalan MD. Polarity of T cell shape, motility, and sensitivity to antigen. Immunity. 1996;4(5):421-30. PubMed PMID: 8630728.

215. Tang JL, Schoenwald K, Potter D, White D, Sulchek T. Bifunctional Janus microparticles with spatially segregated proteins. Langmuir : the ACS journal of surfaces and colloids. 2012;28(26):10033-9. doi: 10.1021/la3010079. PubMed PMID: 22624704; PubMed Central PMCID: PMC3428262.

216. Fooksman DR, Vardhana S, Vasiliver-Shamis G, Liese J, Blair DA, Waite J, et al. Functional anatomy of T cell activation and synapse formation. Annual review of immunology. 2010;28:79-105. doi: 10.1146/annurev-immunol-030409-101308. PubMed PMID: 19968559; PubMed Central PMCID: PMC2885351.

217. Christensen JE, Andreasen SØ, Christensen JP, Thomsen AR. CD11b expression as a marker to distinguish between recently activated effector CD8+ T cells and memory cells. International Immunology. 2001;13(4):593-600. doi: 10.1093/intimm/13.4.593.

218. Berret JF. Local viscoelasticity of living cells measured by rotational magnetic spectroscopy. Nature communications. 2016;7:10134. doi: 10.1038/ncomms10134. PubMed PMID: 26729062; PubMed Central PMCID: PMC4728338.

219. Trickey WR, Vail TP, Guilak F. The role of the cytoskeleton in the viscoelastic properties of human articular chondrocytes. Journal of orthopaedic research : official publication of the Orthopaedic Research Society. 2004;22(1):131-9. doi: 10.1016/S0736-0266(03)00150-5. PubMed PMID: 14656671.

220. Evans EA, Hochmuth RM. Membrane viscoelasticity. Biophysical journal. 1976;16(1):1-11. doi: 10.1016/S0006-3495(76)85658-5. PubMed PMID: 1244886; PubMed Central PMCID: PMC1334809.

221. Pennock ND, White JT, Cross EW, Cheney EE, Tamburini BA, Kedl RM. T cell responses: naive to memory and everything in between. Advances in physiology education. 2013;37(4):273-83. doi: 10.1152/advan.00066.2013. PubMed PMID: 24292902; PubMed Central PMCID: PMC4089090.

222. Rodriguez RM, Pitzalis C, Kingsley GH, Henderson E, Humphries MJ, Panayi GS. T lymphocyte adhesion to fibronectin (FN): a possible mechanism for T cell accumulation in the rheumatoid joint. Clinical and experimental immunology. 1992;89(3):439-45. PubMed PMID: 1387596; PubMed Central PMCID: PMC1554473.

223. Fay ME, Myers DR, Kumar A, Turbyfield CT, Byler R, Crawford K, et al. Cellular softening mediates leukocyte demargination and trafficking, thereby increasing

clinical blood counts. Proceedings of the National Academy of Sciences of the United States of America. 2016;113(8):1987-92. doi: 10.1073/pnas.1508920113. PubMed PMID: 26858400; PubMed Central PMCID: PMC4776450.

224. Bashour KT, Gondarenko A, Chen H, Shen K, Liu X, Huse M, et al. CD28 and CD3 have complementary roles in T-cell traction forces. Proceedings of the National Academy of Sciences of the United States of America. 2014;111(6):2241-6. doi: 10.1073/pnas.1315606111. PubMed PMID: 24469820; PubMed Central PMCID: PMC3926067.

225. O'Connor RS, Hao X, Shen K, Bashour K, Akimova T, Hancock WW, et al. Substrate rigidity regulates human T cell activation and proliferation. Journal of immunology. 2012;189(3):1330-9. doi: 10.4049/jimmunol.1102757. PubMed PMID: 22732590; PubMed Central PMCID: PMC3401283.

226. Saitakis M, Dogniaux S, Goudot C, Bufi N, Asnacios S, Maurin M, et al. Different TCR-induced T lymphocyte responses are potentiated by stiffness with variable sensitivity. eLife. 2017;6. doi: 10.7554/eLife.23190. PubMed PMID: 28594327; PubMed Central PMCID: PMC5464771.

227. Xu W, Mezencev R, Kim B, Wang L, McDonald J, Sulchek T. Cell stiffness is a biomarker of the metastatic potential of ovarian cancer cells. PloS one. 2012;7(10):e46609. doi: 10.1371/journal.pone.0046609. PubMed PMID: 23056368; PubMed Central PMCID: PMC3464294.

228. Huttenlocher A, Lakonishok M, Kinder M, Wu S, Truong T, Knudsen KA, et al. Integrin and cadherin synergy regulates contact inhibition of migration and motile activity. The Journal of cell biology. 1998;141(2):515-26. PubMed PMID: 9548728; PubMed Central PMCID: PMC2148455.

229. Braga V. The crossroads between cell-cell adhesion and motility. Nature cell biology. 2000;2(10):E182-4. doi: 10.1038/35036433. PubMed PMID: 11025678.

230. Hosseini BH, Louban I, Djandji D, Wabnitz GH, Deeg J, Bulbuc N, et al. Immune synapse formation determines interaction forces between T cells and antigen-presenting cells measured by atomic force microscopy. Proceedings of the National Academy of Sciences of the United States of America. 2009;106(42):17852-7. doi: 10.1073/pnas.0905384106. PubMed PMID: 19822763; PubMed Central PMCID: PMC2764924.

231. Zerda Adl, Kratochvil MJ, Suhar NA, Heilshorn SC. Review: Bioengineering strategies to probe T cell mechanobiology. APL Bioengineering. 2018;2(2):021501. doi: 10.1063/1.5006599.

232. Waterman-Storer CM, Salmon WC, Salmon ED. Feedback interactions between cell-cell adherens junctions and cytoskeletal dynamics in newt lung epithelial cells. Molecular biology of the cell. 2000;11(7):2471-83. PubMed PMID: 10888682; PubMed Central PMCID: PMC14933.

233. Shaw AS. T-cell activation and immunologic synapse. Immunologic research. 2005;32(1-3):247-52. doi: 10.1385/IR:32:1-3:247. PubMed PMID: 16106076.

234. Wolfl M, Greenberg PD. Antigen-specific activation and cytokine-facilitated expansion of naive, human CD8+ T cells. Nature protocols. 2014;9(4):950-66. doi: 10.1038/nprot.2014.064. PubMed PMID: 24675735; PubMed Central PMCID: PMC4312138.

235. He W, Frueh J, Wu Z, He Q. Leucocyte Membrane-Coated Janus Microcapsules for Enhanced Photothermal Cancer Treatment. Langmuir : the ACS journal of surfaces and colloids. 2016;32(15):3637-44. doi: 10.1021/acs.langmuir.5b04762. PubMed PMID: 27023433.

236. Leulmi S, Chauchet X, Morcrette M, Ortiz G, Joisten H, Sabon P, et al. Triggering the apoptosis of targeted human renal cancer cells by the vibration of anisotropic magnetic particles attached to the cell membrane. Nanoscale. 2015;7(38):15904-14. doi: 10.1039/c5nr03518j. PubMed PMID: 26364870.

237. Stadler M, Scherzer M, Walter S, Holzner S, Pudelko K, Riedl A, et al. Exclusion from spheroid formation identifies loss of essential cell-cell adhesion molecules in colon cancer cells. Scientific reports. 2018;8(1):1151. doi: 10.1038/s41598-018-19384-0. PubMed PMID: 29348601; PubMed Central PMCID: PMC5773514.

238. Fennema E, Rivron N, Rouwkema J, van Blitterswijk C, de Boer J. Spheroid culture as a tool for creating 3D complex tissues. Trends in biotechnology. 2013;31(2):108-15. doi: 10.1016/j.tibtech.2012.12.003. PubMed PMID: 23336996.

239. Mehta G, Hsiao AY, Ingram M, Luker GD, Takayama S. Opportunities and challenges for use of tumor spheroids as models to test drug delivery and efficacy. Journal of controlled release : official journal of the Controlled Release Society. 2012;164(2):192-204. doi: 10.1016/j.jconrel.2012.04.045. PubMed PMID: 22613880; PubMed Central PMCID: PMC3436947.

240. Carvalho MR, Lima D, Reis RL, Oliveira JM, Correlo VM. Anti-Cancer Drug Validation: the Contribution of Tissue Engineered Models. Stem cell reviews. 2017;13(3):347-63. doi: 10.1007/s12015-017-9720-x. PubMed PMID: 28233276.

241. van den Brand D, Massuger LF, Brock R, Verdurmen WP. Mimicking Tumors: Toward More Predictive In Vitro Models for Peptide- and Protein-Conjugated Drugs. Bioconjugate chemistry. 2017;28(3):846-56. doi: 10.1021/acs.bioconjchem.6b00699. PubMed PMID: 28122451; PubMed Central PMCID: PMC5355905.

242. Hirschhaeuser F, Menne H, Dittfeld C, West J, Mueller-Klieser W, Kunz-Schughart LA. Multicellular tumor spheroids: an underestimated tool is catching up again. Journal of biotechnology. 2010;148(1):3-15. doi: 10.1016/j.jbiotec.2010.01.012. PubMed PMID: 20097238.